DEVELOPMENT OF A BACTERIAL RESPONSIVE ANTIBIOTIC RELEASE SYSTEM

Dissertation zur Erlangung des

naturwissenschaftlichen Doktorgrades

der Julius-Maximilians-Universität Würzburg

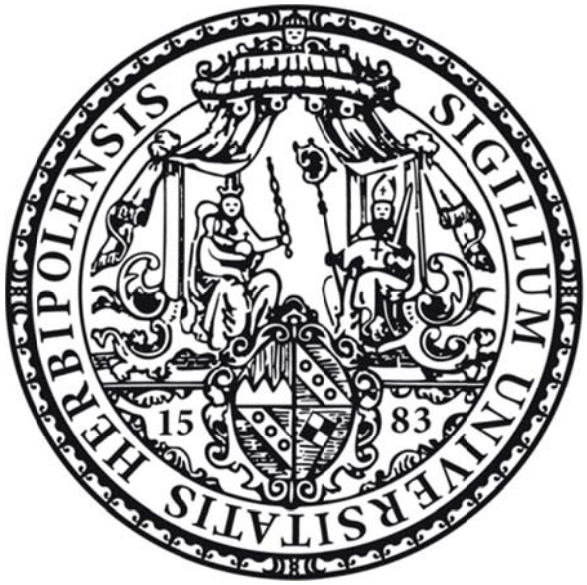

vorgelegt von

Maria Cecilia Krähenbühl Amstalden

aus

Campinas, SP, Brasilien

Würzburg 2018

Eingereicht bei der Fakultät für Chemie und
Pharmazie am: _____

Gutachter der schriftlichen Arbeit

1. Gutachter: _____

2. Gutachter: _____

Prüfer des öffentlichen Promotionskolloquiums

1. Prüfer: _____

2. Prüfer: _____

3. Prüfer: _____

Datum des öffentlichen Promotionskolloquiums: _____

Doktorurkunde ausgehändigt am: _____

Die vorliegende Arbeit wurde in der Zeit von

November 2013 bis November 2017 am

Institut für Pharmazie und Lebensmittelchemie der

Bayerischen Julius-Maximilians-Universität Würzburg

unter der Anleitung von Herrn

Prof. Dr. Dr. Lorenz Meinel

angefertigt.

Table of Content

Table of Content

1. Introduction 1
1.1 Antibiotic resistance crisis 1
1.2 Smart drug release systems 6
2. Aim 13
3. Experimental section 17
3.1 Materials 17
3.1.1 Solid Phase Peptide Synthesis 17
3.1.2 Enzymatic assays 17
3.1.3 Immunoassays 17
3.1.4 Chromatographic characterization and purification of peptides and constructs 17
3.1.5 Construction of PEG-peptide-antibiotic conjugate 18
3.1.6 Hydrogel formulation assays 18
3.1.7 Buffers 18
3.2 Methods 19
3.2.1 Peptide synthesis 20
3.2.2 Preparative peptide and construct purification 21
3.2.3 Analytical high performance liquid chromatography (HPLC) 21
3.2.4 Lyophilization 21
3.2.5 Dynamic Light Scattering (DLS) 21
3.2.6 Mass spectrometry 22
3.2.7 In vitro assays 22
3.2.8 Hydrogel assays 25
3.2.9 Conjugation reactions 26
3.2.10 Statistical analysis 27
4. Results 31
4.1 Search for the best cleavable linker 31
4.1.1 Peptide synthesis and purification 31
4.1.2 Specificity assays ..... Fehler! Textmarke nicht definiert.
4.2 Aureolysin activity determination 41
4.2.1 Azocasein assay 41
4.2.2 Enzyme-linked immunosorbent assay 42
4.2.3 Cleavage assay 43

4.3 Hydrogel formulation assays 46
4.3.1 Physical incorporation of antibiotic into a hydrogel matrix 46
4.3.2 Covalent binding of fluorophore to peptide sequence 55
4.4 Aminopeptidase activity determination 59
4.4.1 Synthesis and characterization of aminopeptidase substrate 59
4.4.2 Determination of aminopeptidase concentrations in human plasma 61
4.4.3 Release assays by aminopeptidase 62
4.5 Construction of a PEGylated chelocardin release system 65
4.5.1 Synthesis of a CHD linker 65
4.5.2 Conjugation of CHD linker to PEG via copper-free click reaction 71
4.5.3 Antibiotic release by aureolysin cleavage 72
4.5.4 Loading optimization of CHD 74
4.5.5 Analysis of aggregates by DLS 78
5. Discussion and outlook 83
6. Summary 93
7. Zusammenfassung 97
8. References 101
9. Appendix 119
9.1 List of abbreviations 119
9.2 List of Figures 120
9.3 List of Tables 122
9.4 Publications and presentations 123
10. Acknowledgements 127

Introduction

1. Introduction

1.1 Antibiotic resistance crisis

The discovery of antimicrobial drugs is considered to be the greatest achievement of modern medicine in the last century. Due to antibiotics, life expectancy was increased by dramatically reducing the lethal outcomes of bacterial infections [1]. In industrialized and highly developed countries like the USA, people had a life expectation of 56 years in 1920, while nowadays the life span is over 80 years [2]. The mortality rate for pneumococcal related bacteremia was lowered from 50–80% to 18% after the discovery of penicillin [3-5]. For staphylococcal pneumonia, the rates decreased from 73% to 13%, respectively [6, 7]. However, the benefits of antibiotics can be observed worldwide. In developing countries, the introduction of antibiotic therapies decreased the mortality and morbidity linked to food-borne diseases, poor sanitary conditions, or tropical infections [8]. Also, antibiotics are applied to support medical care, for example by means of a prophylactic or a post-operative approach to prevent surgical site infections [9, 10], as well as to treat cancer and related opportunistic infections [11, 12].

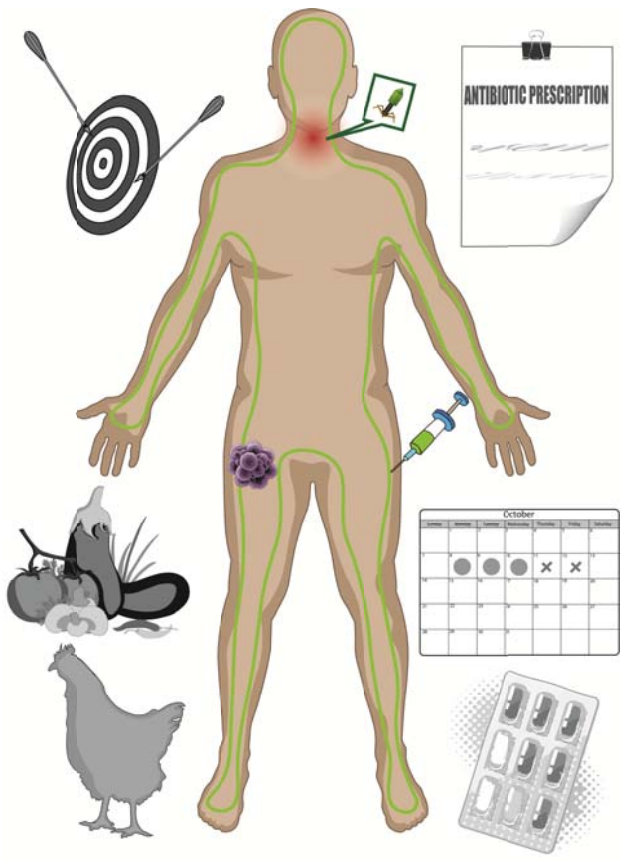

Figure 1 – Main reasons for bacterial antibiotic resistance development: the untargeted mechanism of action of those drugs, misprescription of antibiotic in cases of viral infections, the unnecessary contact of humans with antibiotic via agriculture and animal husbandry and interruption of antibiotic therapy by patients.

However, what initially seemed to be a scientific miracle quickly turned out that it wouldn't last forever. Already in the 1950s, many cases of bacterial resistance to penicillin were reported and the advances accomplished over the preceding decade seemed to be threatened [13]. In 1959, methicillin was introduced to treat infections caused by *Staphylococcus aureus* penicillin resistant strains. Nonetheless, already in 1961 there were reports of methicillin resistance in the United Kingdom, which soon spread through many other European countries and also reached Japan, the United States, and Australia [14, 15]. Current data show that the proportion of β-lactam bacterial resistance meanwhile exceeds 20% in all World Health Organization (WHO) regions [16]. This crisis mainly affects countries with weak health systems and inconsistent treatment policies

where effective regulations for antibiotic use have not been established yet. In Nigeria, for instance, studies revealed that up to 88% of *Staphylococcus aureus* infections cannot be treated with methicillin anymore, also known as "methicillin resistant *Staphylococcus aureus"* (MRSA) strains [17, 18]. This percentage tends to increase over the next years. Currently, 700,000 people die every year due to infections which are resistant to antibiotic therapies. If this trend goes on, by 2050 this number could reach up to ten millions of deaths annually [19]. The main reasons for antibiotic resistance are the emergence of mutations in intrinsic genes or the acquisition of exogenous genetic material bearing single or multiple resistance determinants. While being exposed to antimicrobial drugs, the growth of susceptible strains is inhibited; the resistant bacteria survive and are selected [20, 21]. The rate of antibiotic resistant strains appearance usually is accelerated by the mis- and overuse of antibiotics, resulting in opportunistic pathogens being genetically selected by unnecessary exposure to these drugs (**Figure 1**) [22].

Antibiotics are highly overused as prophylactic in human and animal medicine, as well as in agriculture [23-25]. Studies have shown that no significant differences with regard to complications and implant survival were found when comparing a 1-day single-dose preoperative antibiotic regimen with that following a standard 1-week postoperative antibiotic protocol [26]. Misprescription is a major concern in primary care where a large number of infections is treated with antibacterial compounds though being of viral origin. E.g., 90% of all antibiotic prescriptions in the USA are issued by general practitioners with upper respiratory tract infections representing the leading indication [27-29]. In Europe, even though the prescription rates for antibiotics vary throughout each country, a shift from applying narrow-spectrum to broad-spectrum antibiotics is observed [30]. The lack of sufficient verbal and written information for patients about the necessity of using antibiotics also plays a big role in the development of resistances [31, 32].

However, one frequently neglected aspect is the untargeted mechanism of action of established antibiotics. The mutualistic relationship between host and its microbiota is in a delicate homeostasis which evolved during millennia and can easily be corrupted by administering antibiotic compounds. While this equilibrium is usually restored after the cessation of an antibiotic treatment [33-35], the interactions of microorganisms with the host orient the host's immune system and can easily lead to changes in the dynamics of the innate and adaptive immune system, creating opportunities for pathogens [36-38]. During antibiotic treatment, the colonization pattern of the digestive tract is altered whilst being contaminated with exogenous bacterial species usually persisting much longer and in much higher concentration when compared to individuals not being subject to antimicrobial therapy [39]. Of note, the nasal microflora and thus the respiratory tract can also be affected when systemic antibiotics are administered [40].

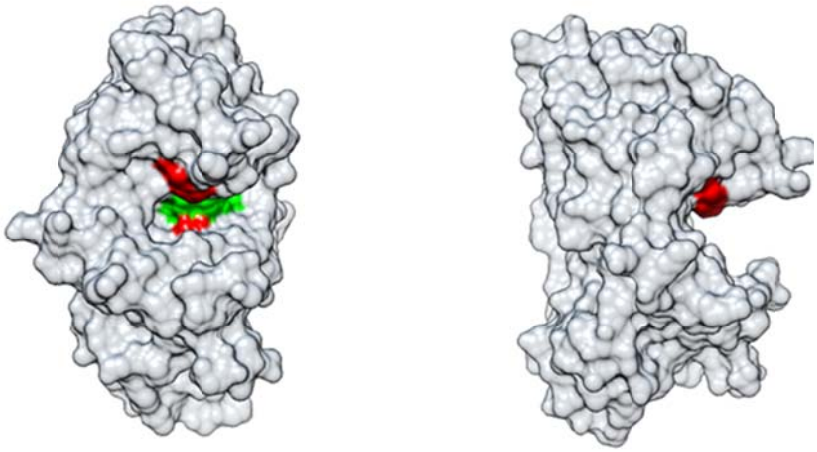

Figure 2 – Tridimensional structure of *S. aureus* zinc metalloproteinase aureolysin. Active site units are depicted in red, while zinc binding sites are depicted in green.

Diseases with many different potential pathogens present different susceptibilities to drugs and are often treated with an indiscriminate antibiotic therapy, which leads to the overgrowth of bacterial resistance [41, 42]. This can be particularly dangerous when commensal bacteria are also opportunistic pathogens. One major example is *Staphylococcus aureus*. These gram-positive bacteria are considered to be "pathobionts", as they can asymptomatically colonize the upper respiratory tract and, at the same time, have the potential of causing a disease if they spread from the initial site of colonization [43-45]. *S. aureus* is one of the most common causes of infective endocarditis and bacteremia. Additionally, it can also be responsible for osteoarticular, dermal, and soft tissue infections, especially after injuries and traumas [46, 47].

The pathogenicity of *Staphylococcus aureus* is a complex process involving a diverse array of extracellular and cell wall components that are expressed during different stages of infection. These different virulence factors help with bacterial colonization, evasion of host defense, growth and cell division, and spread of the infection [48, 49]. One of those several mechanisms of pathogenicity is the expression of a metalloprotease named aureolysin (**Figure 2**), which presents zinc ions as cofactor and belongs to the family of thermolysins [50]. Aureolysin has a molecular weight of 43 kDa and a sequence length of 509 amino acids, whose active site residues are found at E353 and H436.

This enzyme is a potent complement inhibitor which effectively constrains phagocytosis and eradicating bacteria by neutrophils [51]. Usually, the recognition of bacteria via the classical pathway results in the formation of the C3 convertase complex, which cleaves C3 complement protein and leads to the release of anaphylatoxin C3a and deposition of C3b on the bacterial surface. This last molecule is responsible for the opsonization of the pathogen and phagocytosis via recognition of C3b by complement receptors on neutrophils [52]. Aureolysin also capable of cleaving the human bactericidal peptide Cathelicidin LL-37 as a way of evading the host's immunological response [53].

A study conducted by Morgenstern *et al.* showed that about 20 – 30% of the world population have their upper respiratory tract colonized with *Staphylococcus aureus,* of which 2 – 6% are MRSA [54]. In pre-antibiotic eras, the mortality rate of *Staphylococcus aureus* bacteremia (SAB) was around 80%. Even though the discovery and clinical application of antibiotics reduced this rate, the fatalities for SAB have increased from 15 to 50% over the past decades [55-57]. In Denmark, the number of SAB increased from three to 20 per 100,000 inhabitants per year between 1957 and 1990, mainly caused by commensal bacteria having acquired antibiotic resistance [58]. These rates are drastically higher in risk groups; e.g., among elderly, where the incidence rate of MRSA is 127 per 100,000 inhabitants per year [59], or, in case of children, where 51% of all staphylococcal infections was due to MRSA [60]. This worldwide crisis is not only a major concern for public health but also constitutes a serious economic factor. Studies demonstrate that antibiotic resistant infections double the hospitalization and mortality rates when compared to drug-susceptible ones [61], whilst the costs of treating MRSA versus methicillin susceptible strains (MSSA) found out to be 22% more expensive [62]. The estimation of economic costs reaches up to US $30 billion/year, depending on the number of assumed deaths [63].

Methicillin is a narrow spectrum β-lactam antibiotic which exerts its antimicrobial effect by inhibiting the cell wall biosynthesis in gram-positive bacteria, like *S. aureus.* Since cells usually possess a high internal cell turgor, bacteria need a strong cell wall composed of peptidoglycans to keep multiplying in an environment with much lower external pressure. β-lactam antibiotics irreversibly bind to an enzyme called glycosyltransferase (or penicillin binding protein – PBP) and inhibit the linkage of a newly synthesized peptidoglycan to the already existing cell wall [64, 65]. For most bacteria which are β-lactam resistant, the main mechanism of action is the production of β-lactamases. These enzymes quickly cleave the β-lactam ring, thus inactivating the respective compounds by hydrolysis of the pharmacophore [66, 67]. Even though MRSA also expresses β-lactamases, the main mechanism of resistance of these bacteria is expressing the chromosomally localized *mecA* resistance gene [68-71]. *mecA* is responsible for producing the PBP analogue PBP2a, for which β-lactam antibiotics have a much lower affinity, thus allowing the uninterrupted synthesis of the cell wall [72]. Besides, many *Staphylococcus aureus* strains also possess resistance against other classes of antibiotics, like glycopeptides and quinolones [73-75], rendering the respective therapies very difficult.

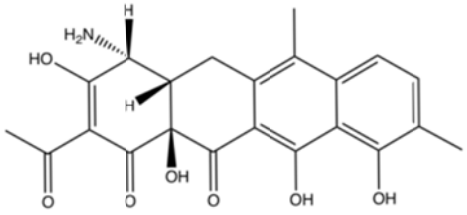

Figure 3 – Chemical structure of the tetracycline analogue chelocardin.

The search for new antibiotics which are active against MRSA is an urgent matter. For that reason, some antimicrobial substances already known for some years but not being fully explored with regard to their pharmacodynamic profile are being revived. A good example is chelocardin (CHD) (**Figure 3**). This antibiotic belongs to the class of atypical tetracyclines which differ from normal tetracyclines due to their mechanism of action [76].

Tetracyclines which are approved for antibiotic therapy target the protein synthesis in bacteria by inhibiting the attachment of aminoacyl-tRNA to the mRNA-ribosome complex. They do so mainly by binding to the 30S ribosomal subunit in the mRNA translation complex. [77]. Cells become resistant to tetracyclines by at least three mechanisms: enzymatic inactivation of tetracycline, efflux, and ribosomal protection [77, 78]. Many studies show that chelocardin has a good activity against tetracycline resistant bacteria [79-81]. This is mainly due to the fact that chelocardin does not only target the biosynthesis of bacterial proteins but also damages the membrane, thus presenting a dual mechanism of action [82, 83]. Chelocardin presents interesting minimum inhibitory concentrations (MIC) for many resistant strains (**Figure 4**) and can therefore be considered a promising candidate for treating MRSA infections.

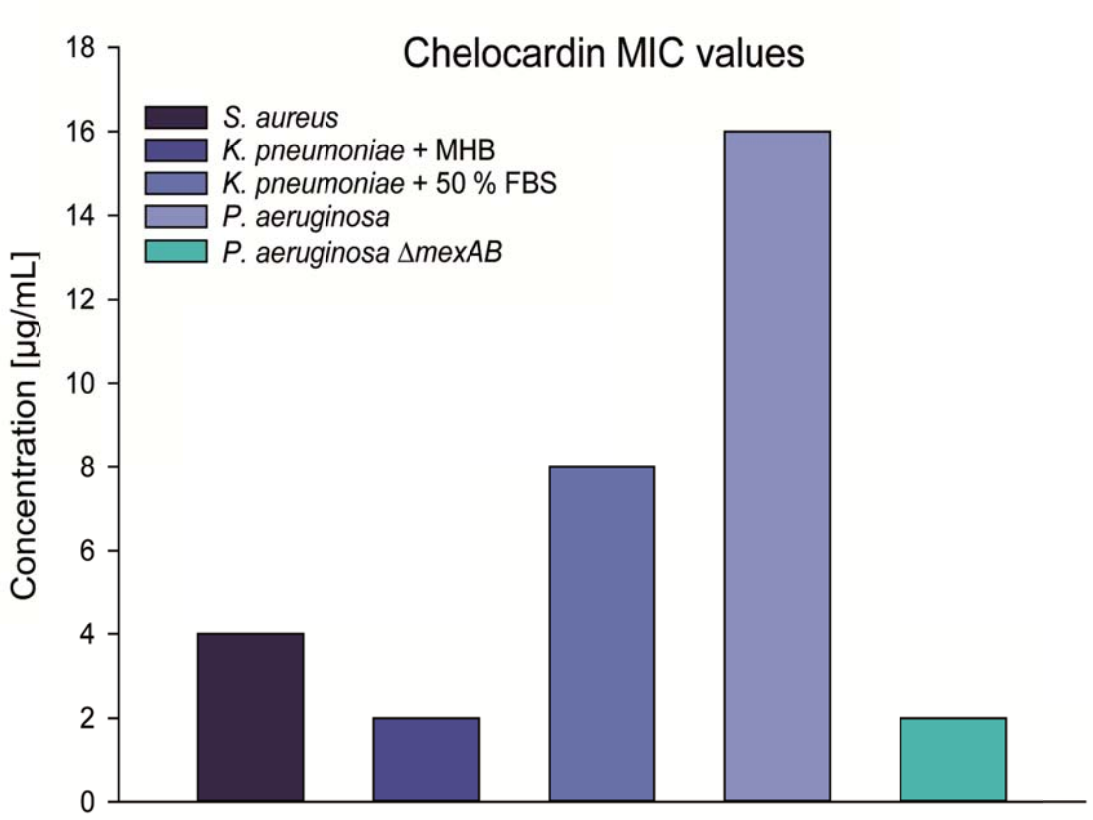

Figure 4 – Minimum inhibitory concentrations for chelocardin against different pathogens. Data kindly provided by Dr. Antoine Abou Fayad, Helmholtz Institute for Pharmaceutical Research.

However, history already showed us that the acquisition of resistance by bacteria against new antimicrobial drugs is only a matter of time. It is our duty to reduce the unnecessary contact of bacteria with antibiotics, and it is useless to keep developing and discovering new antimicrobial substances if we do not change the way of selectively delivering them. Therefore, smart antibiotic delivery ways are needed to avoid the emergence of new resistant and multiresistant strains.

1.2 Smart drug release systems

Drug delivery systems (DDS) are used to improve the pharmacological and therapeutic properties of parenterally administered drugs by altering the pharmacokinetics and biodistribution of their associated active compound, or by serving as a sustained release system. Many undesired properties of a drug candidate such as poor solubility, tissue damage, and lack of selectivity for target tissues can be corrected by using an appropriate delivery system (**Table 1**) [84].

Table 1 – Non-ideal properties of drugs and their therapeutic implications. Adapted from [84].

Problem	Implication/challenges	Effect of DDS
Poor solubility	Difficulty in a proper pharmaceutical format, precipitation in aqueous solutions	DDS that provide both hydrophilic and hydrophobic environments to enhance drug solubility
Tissue damage	Cytotoxic drugs leads to tissue damage, e.g. necrosis	Regulated drug release can reduce or eliminate tissue damage
Poor pharmacokinetics	Quick clearance, requiring higher doses or continuous infusion	DDS protect drugs from premature drug degradation. Lower dosage is required.
Rapid breakdown of drug *in vivo*	Loss of activity after drug administration	DDS substantially alter pharmacokinetics and reduce clearance when compared to free small molecules in circulation
Poor biodistribution	Widespread biodistribution affects normal and healthy tissues, as well as microbiota	DDS lower the volume of distribution and reduce side effects
Lack of selectivity for targeted tissues	Distribution to healthy tissues leads to undesired side effects that restrict the amount of drug considered to be safe to be administered.	DDS increase drug concentration in target tissues

One of the greatest challenges is the tailoring of targeted drug delivery systems. Many drugs do not act exclusively on their supposed target tissue, leading to a variety of undesired side effects. One particularly negative example is in oncological therapy: the majority of antiproliferative chemotherapeutics used at present owe what little selectivity they have for cancer cells to their higher proliferation rates leading to an extremely high toxicity against normal tissue cells, e.g. in the gastrointestinal tract or for hair follicles [85, 86]. In addition, a low bioavailability often limits the use of potential new drug candidates since therapeutic doses become too high and often overlap with the toxic dose range [87, 88].

A targeted antibiotic delivery represents another major challenge. Some infections are difficult to treat due to hard access infection spots or bacterial strategies to defend themselves. Intracellular

infective bacteria are especially difficult to eradicate and the drug activity upon these infections depends on their pharmacokinetics and -dynamics [89, 90]. In those cases, a particular antibiotic needs to satisfy many selection criteria for optimal activity, such as cell penetration, retention, intracellular distribution, and activity towards bacteria in the environment [91]. The ratio of intracellular concentration to the extracellular concentration is the standard parameter to classify the ability for intraphagocytic accumulation of antibiotics; many classic antimicrobial drugs like penicillin and cephalosporins present a low value and consequently a limited activity in those infections.

The same way as in intracellular infections, biofilm formation is also a big concern. Studies show that antibiotic susceptibility decreases 1000 times compared to biofilm formation with bacterial suspension in conventional liquid media [92-94]. The poor drug penetration helps to explain this higher rate of resistance [95, 96]; however, it is shown that naturally selected resistant bacteria tend to express genes related to biofilm formation more than susceptible strains [97-99]. Bone and joint infections are difficult to be treated owing to the anatomical and physiological characteristics of the tissue [100]. The antibiotic penetration is extremely poor, thus requiring much higher doses of the respective compounds [101-103].

However, many advances in drug delivery have been made to help find a solution for these problems. Currently, liposomes are widely being used for antibiotic loading and delivery. Encapsulation of antibiotics is a good solution for designing the desired pharmacokinetics and biodistribution. The liposomal carriers can have their physicochemical properties tailored according to the target tissue requirements and offer the advantage of gradual and sustained drug release while circulating in the body [104]. Studies show that liposomal encapsulated antibiotics significantly reduce the number of microorganisms when compared to the application of the free drug [105-107]. Liposomes are identified by the immunological system as foreign bodies and are therefore opsonized. While this phenomenon is interesting for targeting intracellular infections, it leads to lower blood circulation and fast blood clearance of the respective compounds [108, 109]. Besides, another problem is the loading of the drug. Since most liposomes are composed of fluid bilayers, the loading stability can be poor in some physiological environments [104, 110].

Polymeric nanomaterials have also been extensively studied for the nanoencapsulation of drugs, especially in the field of antibiotics. Novel nanomaterials, nanoparticles (NP) in particular, have unique physicochemical properties (e.g., ultra-small and controllable size, large surface area to mass ratio, high interactions with microorganisms and host cells, structural/functional versatility) and are a promising platform to overcome the limitations of antibiotic targeted delivery [111-113]. Their structural stability provides a low rate of degradation in biological fluids

and when exposed to harsh conditions during their formulation (e.g., spray drying and ultra-fine milling), and storage [114]. Drug delivery profiles can be tuned by manipulating polymer length, surfactants, and monomer chemistry. So far, two main types of polymers have been explored for antibiotic delivery: linear and amphiphilic block polymers. While the linear polymers constituted of NP usually being nanocapsules or solid nanospheres, the second presents itself in self-assembling micelles in which the drug is loaded within the hydrophobic core whilst the hydrophilic corona shields the drug from being opsonized and degraded [111, 115-117]. *In vitro* studies show the enhanced antimicrobial effect of ciprofloxacin and gentamycin loaded poly(lactide-co-glycolic) acid (PLGA) particles against *Pseudomonas aeruginosa* biofilms in comparison to free drugs [118-120]. Carboxymethyl chitosan particles loaded with vancomycin were able to disrupt the cell membrane of *Staphylococcus aureus* in biofilms [121].

In many cases, drugs are unstable and poorly absorbed by the gastrointestinal tract. Some successful efforts have been made in improving the oral administration of antibiotics by using polymeric NPs made of polyethylcyanoacrylate (PECA) [122]. PEGylation of PECA NPs increased half-life in serum and reduced phagocytosis by macrophages [123]. Microencapsulation of gentamycin in PLGA-PEG used as implants was successful in readily releasing the drug into bone tissues and therefore is a promising candidate for post-operative prophylaxis [124]. Many other degradable and non-degradable NP formulations of amino glycosides and β-lactam antibiotics release the drugs at concentrations exceeding the minimal inhibitory concentrations for the most common pathogens involved in osteomyelitis without causing any adverse systemic effects [125].

Conventional drug release systems in which the drug is entrapped within a polymer lattice usually results in an early drug release peak in plasma concentration, followed by a constant, steady linear release. The disadvantage is that local drug concentration and location of delivery cannot be properly controlled. These systems are insensitive towards environmental and metabolic changes in the body and therefore unable of modulating drug release [126]. Thus, the lack of control is the main purpose on seeking bioresponsive controlled release systems. Bioresponsive systems are an innovative way of releasing the drug on site and avoiding side effects. Nanocarriers can be engineered to respond to pH, heat, and magnetic field changes, as well as to chemical and biological triggers [127-129]. The response to stimuli can appear in many ways: chain dimension/size, shape, surface characteristics, secondary or tertiary structure, solubility or degree of intermolecular association [126] and is usually quick, varying from a few minutes to some hours [130, 131].

Among all existing drug delivery strategies, certainly enzyme triggered release systems are an interesting approach. The altered expression of some specific enzymes, like proteases,

phosphatases, and glycosidases during pathological conditions such as cancer, inflammation or infections makes them a valuable trigger for drug release and accumulation of drugs at the desired tissue [129]. In those systems, an essential constituent is the presence of an enzyme-sensitive linker, which responds to the action of the highly expressed enzyme and controllably releases the drug in the specific site.

Studies show the use of short peptide sequences being sensitive for Matrix Metalloproteases (MMP) as a linker between PEG chains to either TAT-functionalized liposomes [132] or CPP-decorated, dextran-coated iron oxide nanoparticles [133]. After MMP cleaved the PEG surface in a tumor environment, the bioactive compounds became exposed and their intracellular penetration was enhanced when compared with other carriers without cleavable linkers. Braun *et al.* were able to design a myostatin inhibitor delivery system responsive to the upregulation of MMP-9 during sarcopenia. This model comprised of a peptide linker sensitive to MMP attached to the myostatin inhibitor and immobilized on a microparticles' surface [134]. This concept can also be used in diagnostics. Ritzer *et al.* developed a concept of a sensory chewing gum which could detect peri-implant inflammations by cleavage of a peptide sequence by MMPs present in oral cavities and subsequent release of a bitter taste molecule, therefore targeting the tongue as a diagnostic sensor [135].

The strategy based upon enzymatic release can be extended to different fields of application with bacterial infection treatments being no exception. For example, regarding the release of antibiotics, Xiong *et al.* successfully accomplished an on-demand release of vancomycin with lipase-sensitive nanogels [136]. However, as discussed by the authors, lipase is abundant in microbial flora since it plays a major role in bacterial metabolism [137, 138]. For that reason, a selective antibiotic delivery system is needed in which the antimicrobial component is only active and released in the presence of virulence factors, thus not afflicting commensal bacteria in the organism and helping to prevent the emergence of new multiresistant strains.

Aim

2. Aim

The aim of this work was to develop an antibiotic delivery system whose release would only be triggered by proteases being expressed during the virulent state of bacteria. We focused on targeting *Staphylococcus aureus* methicillin resistant strains mainly for two reasons: (i) this bacterium is one of the most dangerous pathogens in the world being responsible for an enormously high mortality rate as well as resistance mechanisms against many antibiotics, and (ii) it is a commensal bacterium for humans, asymptomatically colonizing the upper respiratory tract and the skin. Of note, as already discussed, *S. aureus* can be an opportunistic pathogen.

The developed delivery system consists of three parts: the main focus of this work, a short peptide sequence acting as cleavable linker (CL); a polymer linked to its *N*-terminus in order to enhance the pharmacokinetic and half-life of the antibiotic during circulation; and attached to the *C*-terminus, the antibiotic itself. The antibiotic of choice acting as a prototype for our release system was the atypical tetracycline chelocardin (CHD), synthesized at the Helmholtz Institute for Pharmaceutical Research Saarland (Saarbrücken, Germany) in the research group of Prof. Dr. Rolf Müller.

The peptide sequence representing the cleavable linker is selectively recognized by aureolysin, a 43 kDa protease which is expressed during the virulent state of *S. aureus*, primarily attacking the C3 complement protein and inactivating it [51]. Once the sequence is cleaved, the antibiotic is partially released; however, carrying four remaining amino acids attached to it. Once again, we use a bioresponsive tool from the human organism to completely release the antimicrobial substance: aminopeptidases are a class of enzymes which catalyze the cleavage of amino acids at the *N*-termini of peptides and proteins, respectively, and which are abundantly present in the human plasma [139]. These proteases would also be able to cleave the remaining amino acids which are attached to the antibiotic, thus fully releasing it and exposing its antimicrobial activity against the pathogenic *S. aureus*.

The first challenge was to find a suitable peptide sequence which would only be sensitive towards the bacterial protease and not against any human proteases. After this, a meticulous study of *in vitro* antibiotic release was performed with both aureolysin and aminopeptidase enzymes, in order to better understand the kinetics and the action of our chosen biotriggers. Finally, formulation experiments were performed to determine the best way to incorporate and release chelocardin. Hence, this work was subdivided into four phases (**Figure 5**).

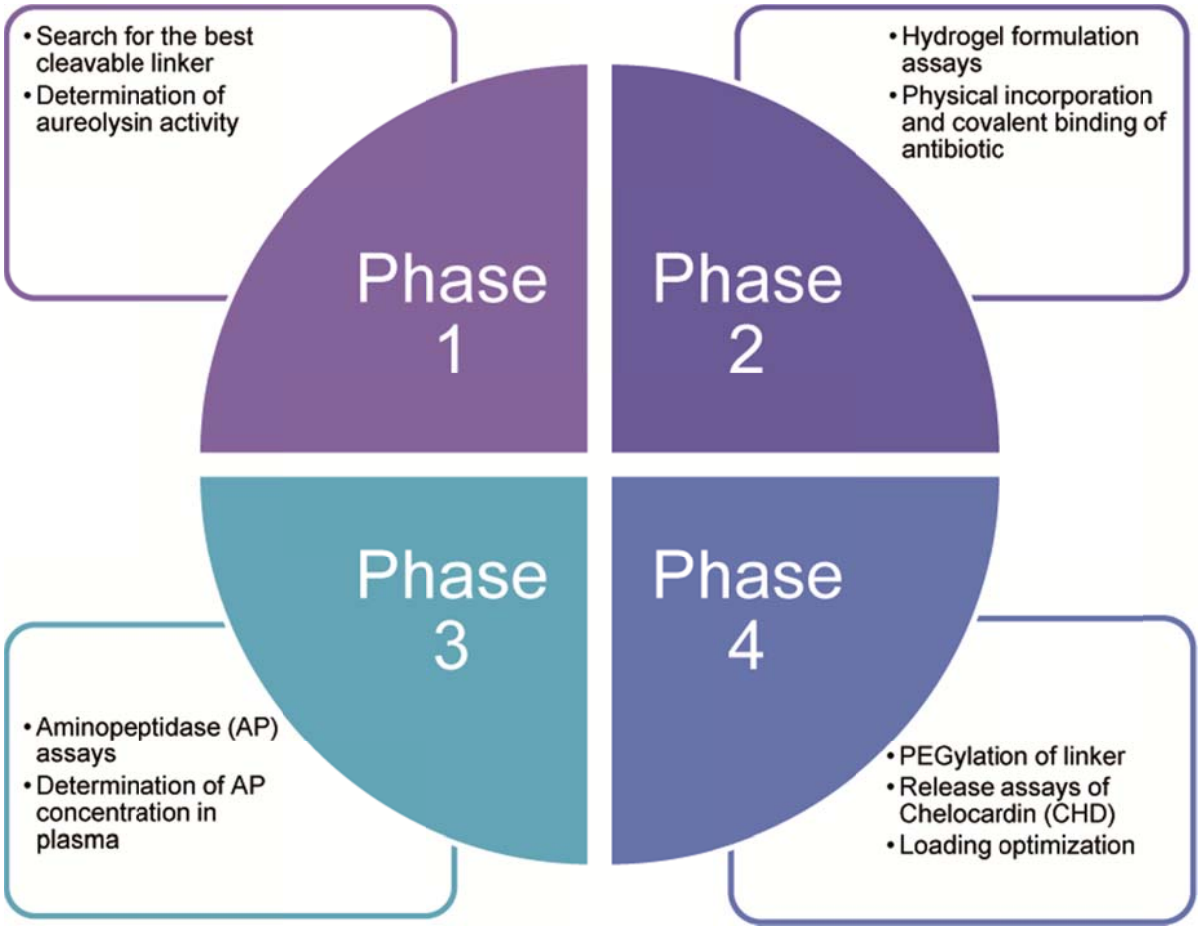

Figure 5 – Study design for the development of a bioresponsive antibiotic release system.

Experimental section

3. Experimental section

3.1 Materials

3.1.1 Solid Phase Peptide Synthesis

FMOC-protected amino acids	Novabiochem Merck-Millipore (Darmstadt, Germany)
Chlorotrityl Chloride Resin (CTC)	Chem-Impex Wood (Dale, IL, USA)
2-Azidoacetic acid	Carbosynth (Berkshire, UK)
2-(1*H*-benzotriazol-1-yl)-1,1,3,3-tetramethyluronium hexafluorophosphate (HBTU)	Chem-Impex Wood (Dale, IL, USA)
1-Hydroxybenzotriazole hydrate (HOBt)	Sigma-Aldrich Chemie (Schnelldorf, Germany)
Piperidine	Sigma-Aldrich Chemie (Schnelldorf, Germany)
N,*N*-Diisopropylethylamine (DIPEA)	Carl Roth GmbH (Karlsruhe, Germany)
Diisopropylcarbodiimide (DIC)	Fluka (Buchs, Switzerland)
Dimethylformamide (DMF)	Fisher Scientific (Schwerte, Germany)
Dichloromethane (DCM)	Fisher Scientific (Schwerte, Germany)
Methanol	Fisher Scientific (Schwerte, Germany)
Trifluoroacetic acid (TFA)	VWR (Radnor, Pennsylvania, USA)
1-[Bis(dimethylamino)methylene]-1*H*-1,2,3-triazolo=[4,5-b]pyridinium 3-oxid hexafluorophosphate (HATU)	ChemPep, Inc (Wellington, USA)

3.1.2 Enzymatic assays

Human neutrophil matrix metalloproteinases (MMPs)	EMD Millipore Corporation (Billerica, MA)
Metalloproteinase from *Staphylococcus aureus* (Aureolysin)	BioCentrum Ltd. (Cracow, Poland)
Leucine Aminopeptidase	Sigma-Aldrich Chemie (Schnelldorf, Germany)
L-Leucin-*p*-nitroanilide	Sigma-Aldrich Chemie (Schnelldorf, Germany)
Sulfanilamide-azocasein	Sigma-Aldrich Chemie (Schnelldorf, Germany)
Tris-HCl base	Sigma-Aldrich Chemie (Schnelldorf, Germany)
APMA	Sigma-Aldrich Chemie (Schnelldorf, Germany)
NaCl	Sigma-Aldrich Chemie (Schnelldorf, Germany)
$CaCl_2$	Sigma-Aldrich Chemie (Schnelldorf, Germany)
$ZnCl_2$	Sigma-Aldrich Chemie (Schnelldorf, Germany)
Brij 35	Sigma-Aldrich Chemie (Schnelldorf, Germany)

3.1.3 Immunoassays

96-well ELISA plate	(Immuno-Plate; Nunc, Denmark)
α-Aureolysin antibody (murine, serum)	Kindly provided by Dr. Knut Ohlsen, Institute for Molecular Infection Biology (IMIB), University of Würzburg
Rabbit IgG α-mouse IgG	Dianova (Hamburg, Germany)
Peroxidase Substrate Kit TMB	Vector Laboraties (Burlingname, California)
Tween-20	Sigma-Aldrich Chemie (Schnelldorf, Germany)
0.2 µm cellulose acetate membrane sterile filter bottles	Fisher Scientific (Schwerte, Germany)

3.1.4 Chromatographic characterization and purification of peptides and constructs

Acetonitrile (HPLC grade)	VWR (Radnor, Pennsylvania, USA)
Trifluoroacetic acid (TFA) (HPLC grade)	VWR (Radnor, Pennsylvania, USA)
Methanol (HPLC grade)	VWR (Radnor, Pennsylvania, USA)
Ultra-pure water for Chromatography	Prepared by a water purification system (Merck Millipore (Darmstadt, Germany))

3.1.5 Construction of PEG-peptide-antibiotic conjugate

1-Ethyl-3-(3-dimethylaminopropyl)carbodiimide (EDC)	Sigma-Aldrich Chemie (Schnelldorf, Germany)
***N*-Hydroxysuccinimide (NHS)**	Fisher Scientific (Schwerte, Germany)
4arm-PEG10K-NH_2	Sigma-Aldrich Chemie (Schnelldorf, Germany)
DBCO-PEG4-NHS ester	Jena Bioscience (Jena, Germany)
DBCO-PEG 10 kDa	Jena Bioscience (Jena, Germany)
DMF (water free)	Sigma-Aldrich Chemie (Schnelldorf, Germany)

3.1.6 Hydrogel formulation assays

3-D Life Maleimide-Dextran thiol-reactive polymer	Cellendes GmbH (Tübingen, Germany)
3-D Life PEG-Link	Cellendes GmbH (Tübingen, Germany)
Fluorescein isothiocyanate–dextran 20 kDa	Sigma-Aldrich Chemie (Schnelldorf, Germany)
Fluorescein isothiocyanate–dextran 40 kDa	Sigma-Aldrich Chemie (Schnelldorf, Germany)

3.1.7 Buffers

All substances were obtained from Sigma-Aldrich Chemie (Schnelldorf, Germany)

Buffer system	**Composition**
Human Matrix Metalloproteinase MMP-8 buffer (pH 6.8-7.0)	200 mM NaCl 50 mM Tris-HCl 5 mM $CaCl_2$ 1 µM $ZnCl_2$ 0.05% Brij 35
Metalloproteinase from *Staphylococcus aureus* (pH 7.8)	20 mM Tris-HCl 5 mM $CaCl_2$
Leucine aminopeptidase buffer (pH 7.0)	50 mM Tris-HCl 1 mM $CaCl_2$ 150 mM NaCl
PBS (pH 7.4)	137 mM KCl 2.69 mM KCl 4.3 mM Na_2HPO_4 1.5 mM KH_2PO_4

3.2 Methods

All experimental work described in the following was performed by me, except for:

- MALDI-TOF

  All experiments were planned by me in collaboration with Prof. Dr. Dr. Lorenz Meinel and PD Dr. Tessa Lühmann. Sample preparation was performed by me, the technical work was done either by Dr. Jennifer Ritzer (peptide analysis) or Dr. Michael Büchner and his team (Institute for Organic Chemistry, University of Würzburg) (PEGylated peptides).

- LC-MS/MS analysis

  All strategies were planned by me in collaboration with Prof. Dr. Dr Lorenz Meinel and PD Dr. Tessa Lühmann. Sample preparation was undertaken by me, the technical work and data analysis was performed by Dr. Jennifer Ritzer, Katharina Dodt, or Johanna Siehler.

- ELISA

  The assay was planned by me in collaboration with Martina Selle and PD Dr. Knut Ohlsen (Institute for Molecular Infection Biology (IMIB), University of Würzburg). Bacterial supernatants and antibodies were provided by their research group. Experiments were performed by me in collaboration with Martina Selle.

3.2.1 Peptide synthesis

Peptides were manually synthesized by Solid Phase Peptide Synthesis (SPPS) using FMOC amino acid coupling strategy. The FMOC-protected amino acids were coupled to an acid labile Chlorotrityl Chloride resin (CTC – loading 1.0 meq/g) in a 5 molar excess compared to the resins' loading capacity. The resin was swollen by incubating it with DCM at room temperature under agitation for at least 30 min. The first amino acid was dissolved in a mixture of DCM and DMF with one equivalent of DIPEA and was added to the swollen resin. The coupling reaction was incubated under agitation at room temperature for at least 1 h. Afterwards, methanol was added in a final concentration of 0.1 mL/g of resin to block eventual remaining free binding sides of the resin and again incubated for 15 min. The resin was washed three times with DCM and another three times using methanol.

The FMOC group was cleaved by incubating the sequence with a mixture of piperidine in DMF; first at a concentration of 40% (v/v) for 3 min followed by 20% (v/v) for 10 min. The resin was washed four times with DMF and the subsequent amino acid was coupled using a 0.2 M solution of HBTU in DMF and 500 µL of DIPEA. The reaction was again incubated for at least 1 h under agitation at room temperature. Those steps were repeated until the synthesis of the desired peptide sequence was completed. For sequence 3g (**Table 2**), after the cleavage of the last FMOC protecting group, 2-azidoacetic acid was coupled overnight in a 3 molar excess in 0.5 M HOBt solution in DMF with 80 µL of DIC and 88 µL of DIPEA. The resin was dried by washing it three times with DMF and three times using diethyl ether.

Table 2 – Peptide sequences synthesized in this work.

Peptide (*N*-*C* termini)	Identification number	Mass Calculated [Da]	Mass Identified [Da]
Cf-GARSNLDEDG	1a	1519	1519.489
Cf-GVNQHLCGSG	2a	1457	1457.583
Cf-GLFEKKVYLG	3a	1511	1511.681
C-PEG6-GLFEKKVYL-C	3b	1639	1639.0
C-PEG6-GLFEKKVYLG-C	3c	1696	1696.0
Cf-PEG3-LFEKKVYL-PEG3-C	3d	1908.95	1908.009
N_3-LFEKKVYL (with protect. groups)	3e	1434.35	1433.903
KVYL-Af	4a	851	851.35
KVYL	4b	522	522.30

To cleave the peptide from the resin, solutions of TFA in DCM having different concentrations were prepared depending on whether the amino acids' side chain protecting groups should be detached or not. The peptide sequences that should have their side chains protected were incubated with a 10% (v/v) solution of TFA in DCM, while the ones whose protecting groups should be detached were incubated with a 95% (v/v) solution. The incubation was performed under agitation for at least 1 h followed by precipitation using ice cooled diethyl ether. The

suspension was centrifuged for 5 min at 3000 g (Sigma 3K12 centrifuge, Sigma Laborzentrifugen GmbH, Osterode am Harz, Germany), the supernatant was discarded, and the pellet was washed three times using diethyl ether.

3.2.2 Preparative peptide and construct purification

Peptides and constructs were purified by FPLC on a GE ÄKTA Explorer system (GE Healthcare, Chalfont St Giles, UK) with a Jupiter 15u C18 300 A column (21.2 mm internal diameter, 250 mm length) (Phenomenex Inc., Torrance, CA), with eluent A being 0.1% (v/v) of TFA in water and eluent B being 0.1% (v/v) of TFA in acetonitrile. The purity of each fraction was analyzed by HPLC and their correct mass was confirmed by MALDI-MS or LC-MS, respectively. Samples were lyophilized later.

3.2.3 Analytical high performance liquid chromatography (HPLC)

HPLC analysis was performed using a VWR Hitachi Elite LaChrom HPLC (Autosampler L-2200; Pump L-2130; Column Oven L-2300; UV detector L-2400) as well as an Hitachi LaChrom Ultra UHPLC system (Autosampler L-2200U; Pump L-2160U; Column Oven L-2300; Diode Array Detector L-2455U) (both VWR International GmbH, Darmstadt, Germany). A ZORBAX Eclipse XDB-C18 column (4.6 mm internal diameter, 150 mm length) (Agilent, Santa Clara, CA) was utilized; the mobile phase consisted of eluent A (0.1% (v/v) TFA in water and eluent B (0.1% (v/v) TFA in acetonitrile). Column oven temperature was kept at 25 °C and the absorbance was monitored at a wavelength of λ = 214 nm, unless specified otherwise.

3.2.4 Lyophilization

Lyophilization was carried out utilizing a laboratory freezing dryer (Christ alpha 1-4, Martin Christ Gefriertrocknungsanlagen GmbH, Osterode am Harz, Germany). After purification, peptide and PEGylated samples were put under a nitrogen atmosphere prior to lyophilization in order to evaporate any acetonitrile residues in the sample. Samples were stored at –80 °C overnight.

3.2.5 Dynamic Light Scattering (DLS)

Particle size distributions of the PEGylated samples were measured using a Delsa™ Nano HC Particle Analyzer (Beckman Coulter® Inc., Fullerton, CA, USA) at 25 °C. Each measurement consisted of three individual runs comprising 70 accumulations. 1 mL of each individual sample was subject to analysis in a disposable cuvette. Values for intensity distribution, hydrodynamic

diameter, and polydispersity index (PdI) were obtained and compared to potential aggregates formed during incubation.

3.2.6 Mass spectrometry

MALDI-MS

Samples were desalted using ZipTip$_{C18}$ tips, following the manufacturer's instructions. Afterwards, samples were mixed 1:1 to the appropriate matrixes and applied to the MTP 384 target plate.

Matrix assisted laser desorption ionization (MALDI)-MS spectra were acquired in linear positive mode by using an Autoflex II LRF instrument (Bruker Daltonics, Billerica, USA). Mass spectra were calibrated externally using a peptide standard (Bruker Daltonics, Billerica, USA).

Liquid chromatography–mass spectrometry (LC-MS)

The LC-MS system from Shimadzu contained a DGU-20A3R degassing unit, a LC20AB liquid chromatograph, and a SPD-20A UV/Vis detector (Shimadzu Scientific Instruments, Columbia, MD, USA). Mass spectra were obtained with an LC-MS 2020. A Synergi 4u fusion-RP column (150 x 4.6 mm) (Phenomenex Inc., Torrance, CA) was used, as well as eluent A (0.1% (v/v) TFA in water) and eluent B (0.1% (v/v) TFA in methanol) as mobile phases. The detection range was set to 60 – 1000 (m/z). A wavelength of λ = 214 nm was used for detection after loading 30 µL of the respective sample. The gradient was set as (i) linear gradient from 5 to 90% eluent B in 8 min, (ii) flushing at 90% eluent B for 5 min, (iii) linear gradient to 5% eluent B in 1 min, and (iv) rinsing the column with 5% of eluent B for 4 min.

3.2.7 In vitro assays

Enzymatic digestion of azocasein

This assay was based on the protocol established by Chavira *et al.*, applying the following modifications [140]: 0.1 g of azocasein was added to 20 mL of aureolysin buffer (final concentration: 5 mg/mL) and stirred under magnetic agitation for 2 h. The suspension was centrifuged for 20 min at 4500 g. The supernatant containing potential peptide residues was discarded. The pellet was suspended in the same buffer volume and stirred for another 2 h. A stable suspension was formed. 300 µL of substrate was transferred to a 1.5 mL reaction tube (Eppendorf GmbH, Hamburg, Germany) and 1 µg of aureolysin or 1µg of trypsin, respectively, was added. The mixture was incubated in a ThermoMixer (Eppendorf GmbH, Hamburg, Germany) at

37 °C for 1, 2, 3, 4, 6, 8, and 10 h under 1300 rpm of agitation. The reaction was stopped by the addition of a solution of 100 µL of 10% trichloroacetic acid (TCA) in appropriate buffer. The digested sample was further centrifuged for 10 min at 13000 g and the TCA supernatant was subsequently transferred to 700 µL of 525 mM NaOH. Absorption was determined using a plate reader (Tecan SpectraMax250, Molecular Devices, CA, USA) applying a wavelength of λ = 442 nm. A sample without the presence of proteases was used as a negative control. The specific activity unit (SAU) was calculated as:

$$SAU = \frac{\text{Absorption}_{[442\ nm]}}{\text{mg (enzyme)} * \text{min}}$$

Cleavage assays by aureolysin

1 mg of purified lyophilized peptide was diluted into 2 mL of aureolysin buffer, resulting in a final concentration of 0.5 mg/mL of the substrate. To analyze the impact of aureolysin concentration on peptide cleavage, a logarithmic screening of aureolysin concentration from 10^{-1} to 10^{4} ng/mL was performed, followed by a narrower screening from 3 to 1000 ng/mL. For both concentration assays, the samples were incubated under agitation for 1 h at 37 °C. Protease activity was interrupted by incubating the sample at 95 °C for 15 min. Afterwards, peptides were again incubated under the same conditions as already described for the aureolysin concentration which resulted in 50% cleavage of the substrate within 1 h. Samples were taken after 5, 10, 30, 60, 120, 180, and 360 min. The relative decrease of the PCL main peak was analyzed by RP-HPLC, applying a determination wavelength of λ = 214 nm and loading 30 µL of the sample. The gradient was set as (i) equilibration of the column at 5% eluent B for 3 min, (ii) linear gradient from 5 to 100% eluent B in 32 min, (iii) flushing at 100% eluent B for 2 min, (iv) linear gradient to 5% eluent B within 4 min, and (v) re-equilibration at initial conditions.

Cleavage assays by human proteases

Pro-MMPs (e.g. MMP-8, MMP-1, or MMP-9; adapted to 0.1 mg/mL and › 100.0 mU/mg based on the manufacturer certificate if applicable) were activated with 4-aminophenylmercuric acetate (APMA) as described before [141]. 1 mg of purified lyophilized peptide was diluted into 2 mL of MMP buffer, resulting into a final concentration of 0.5 mg/mL of the substrate. The substrates were incubated using 900 ng/mL of different MMPs for 1 h at 37 °C. Enzymatic activity was stopped by adding 4 µL of a 250 mM EDTA solution. The relative decrease of PCLs' main peak was analyzed by RP-HPLC as mentioned before.

Enzyme-linked immunosorbent assays

Preparation of a standard curve

The 96-well ELISA plate was coated overnight with a solution of 1 µg/mL aureolysin in PBS at 4 °C. The liquid was discarded and the plate was washed three times with PBS-T (PBS + 0.1% (w/v) Tween-20). To block any possible remaining binding sites of the plate, a solution of PBS + 5% BSA was added to each well and incubated for 1 h at 37 °C. The reaction was again washed three times with PBS-T. A serial dilution of 1:2 (first dilution 1:100) of the detection antibody (α-aureolysin) was performed in PBS + 5% BSA. The dilutions were added onto the plate and incubated for 1 h at room temperature. The plate was washed three times and incubated with the HRP conjugated secondary antibody (diluted 1:10000 in PBS + 5% BSA) at room temperature for 1 h. After washing the plate three times, the chromogenic substrate was added and incubated for 15 min, followed by the adding of a stop solution (H_2SO_4 diluted 1:2 (v/v) in H_2O), turning the solution from blue to yellow. The quantification was performed using a plate reader and a detection wavelength of λ = 450 nm.

Detection of aureolysin in bacterial supernatants

Staphylococcus aureus strains 8325, MA12, and Newman (all *Δspa*) were cultivated in either LB medium or fetal bovine serum (FBS) until their stationary growing phase was reached, followed by sterile filtration with a 0.22 µm cellulose acetate membrane of the supernatants. Similar to the previously described method, the 96-well ELISA plate was coated overnight with the supernatants at 4 °C. The liquid was discarded and washed three times with PBS-T (PBS + 0.1% (w/v) Tween). To block possible remaining binding sites of the plate, a solution of PBS + 5% BSA was added to each well and incubated for 1 h at 37 °C. The reaction was again washed three times with PBS-T. The detection antibody was diluted 1:1600 and added to each well. The plate was incubated for 1 h at 37 °C, washed three times, and incubated with the HRP conjugated secondary antibody (diluted 1:10000 in PBS + 5% BSA) at room temperature for 1 h. After washing the plate three times, the chromogenic substrate was added and incubated for 15 min, followed by the adding of a stop solution (H_2SO_4 diluted 1:2 (v/v) in H_2O), turning the solution from blue to yellow. The quantification was performed using a plate reader and a detection wavelength of λ = 450 nm.

Aminopeptidase (AP) assays

1 mg of purified lyophilized peptide was diluted into 2 mL of AP-buffer, resulting into a final concentration of 0.5 mg/mL of substrate. L-Leucine-*p*-nitroanilide was used as control substrate.

To analyze the impact of AP concentration on peptide cleavage, AP was added at concentrations of 0 (negative control), 0.18, 0.36, 0.72, 1.8, and 3.6 µg/mL, and the samples were shaken at 37 °C for 1 h. For analysis of the impact of AP incubation time, AP concentration of 0.72 µg/mL was incubated with the substrate under the same conditions and analyzed after 10 and 20 min, and after 1, 2, 3, and 4 h. Enzymatic activity was stopped by incubating the samples at 95 °C for 15 min. The relative decrease of the PCL main peak was analyzed by RP-HPLC as described before.

Determination of AP concentration in human plasma

The determination of AP concentration in human plasma samples was performed based on a protocol established by Pfleiderer [142]. The AP specific substrate L-Leucine-*p*-nitroanilide was dissolved in AP buffer (concentration 0.5 mg/mL) obtained from the Institute for Transfusion Medicine and Haemotherapy, Würzburg. Linearity was observed by serially diluting AP from porcine kidney dissolved in AP and adding it to the substrate. After incubating the plate at 37 °C for 30 min, a plate reader set at a wavelength of $\lambda = 405$ nm was used for absorbance measurement. The concentration for each plasma sample was calculated from the standard curve using linear regression analysis.

3.2.8 Hydrogel assays

Fluorophore diffusion assay

The diffusion assay was based on a protocol established by Vigen *et al.* [143] with some modifications. Each system was prepared by incorporating 7 µg of each fluorophore in 50 µL hydrogel, with polymeric concentrations varying from 5 to 10 mM. Hydrogels were incubated in 100 µL PBS, the supernatant was collected and replaced with fresh PBS after 1, 3, 6, 24, 48, 72, 168, 336, and 504 h after polymerization. The supernatants from each time point and the exact initial masses were determined on an LS 50 B fluorescence spectrophotometer (Perkin Elmer, Waltham, USA) at an excitation wavelength of $\lambda = 490$ nm and an emission wavelength of $\lambda = 514$ nm for FITC-dextran and $\lambda = 489$ nm (excitation) and $\lambda = 509$ nm (emission) for eGFP, respectively. The fluorophore mass in each sample was determined in comparison to a standard curve in PBS. Rate constants *K* were determined by fitting the release profiles to a first-order exponential approximation. Each assay was performed in triplicate.

Hydrogel incubation with aureolysin

Hydrogels were prepared as described above (formulations described in **Table 3**) and incubated in 100 µL of aureolysin buffer containing 0.5 µg of aureolysin. The supernatant was collected and replaced with fresh buffer and enzyme every 30 min for a total of 4 h. Samples without the addition of aureolysin were used as a negative control. The supernatants from each time point and the exact initial masses were measured with an LS 50 B fluorescence spectrophotometer at an excitation wavelength of $\lambda = 489$ nm an emission wavelength of $\lambda = 509$ nm for GFP. The mass of fluorophore in each sample was determined by comparison to a standard curve in PBS. Rate constants, K, were determined by fitting release profiles to a first-order exponential approximation. Each assay was performed in triplicate.

Table 3 – Hydrogel formulations.

Formulation ID	Polymer concentration [mM]	Fluorophore	Peptide:thiol-PEG ratio	Peptide isometry
5FD20	5	FITC-Dex 20kDa	0:10	-
10FD20	10	FITC-Dex 20kDa	0:10	-
5FD40	5	FITC-Dex 40kDa	0:10	-
10FD40	10	FITC-Dex 40kDa	0:10	-
5GFP	5	GFP	0:10	-
10GFP	10	GFP	0:10	-
5GFP10L	5	GFP	1:9	L
5GFP10D	5	GFP	1:9	D
10GFP10L	10	GFP	1:9	L
10GFP10D	10	GFP	1:9	D
5GFP20L	5	GFP	2:8	L
5GFP20D	5	GFP	2:8	D
10GFP20L	10	GFP	2:8	L
10GFP20D	10	GFP	2:8	D
5GFP30L	5	GFP	3:7	L
5GFP30D	5	GFP	3:7	D
10GFP30L	10	GFP	3:7	L
10GFP30D	10	GFP	3:7	D
3CfL	3	Cf	1:6	L

3.2.9 Conjugation reactions

EDC/NHS reaction

The coupling of a carboxyl group to an amino group was performed based on the protocol described by Sakurai *et al.* [144]. Briefly, the activation of the carboxylic group at the *C*-terminus of the peptide was performed by mixing equal volumes of side-chain protected peptide (250 mM in DMF), EDC (250 mM in DMF), and NHS (250 mM in DMF), and incubating it under shaking at 25 °C for 1 h. The NHS ester was added in two portions to a solution containing the amine molecule (200 mM in DMF) and the mixture was incubated overnight under the same conditions as described above. The resulting product was analyzed by MALDI-TOF.

HATU/HOBt coupling

Boc alanine, 2 equimolars of DIPEA, and 1.2 equimolar of a HATU: HOBt mixture (1:0.2 proportion) were stirred in THF at room temperature for 10 min. 1.1 equimolar of CHD. HCl with 1 equimolar of DIPEA was dissolved in THF and added dropwise into the mixture. The solution was left stirring overnight at room temperature. For workup, the reaction was diluted in 80 mL of ethyl acetate and washed with brine four times. Sodium sulphate was added and the suspension was filtered using glass wool. The organic phase was removed *in vacuo* using a rotary evaporator (Heidolph, Schwabach, Germany).

Copper free click chemistry

The respective azide containing peptide was dissolved in 50 µL of DMSO and diluted to 1.0 mL with PBS pH 7.4. The solution was added to DBCO functionalized PEG (Molecular weight: 10 kDA) in a molar ratio of 1:1.2 and incubated for 48 h at 25 °C while shaking. The product was analyzed by means of MALDI-MS and UHPLC.

3.2.10 Statistical analysis

All data are reported as mean ± standard deviation of at least three independent measurements, unless specified otherwise. Statistical significance was calculated by one-way ANOVA with an overall significance level of 0.05 using Minitab® version 17.2.1.

Results

4. Results

4.1 Search for the best cleavable linker

4.1.1 Peptide synthesis and purification

The first step was to find a suitable peptide sequence being suitable as a cleavable linker. The linker should be cleaved only by the bacterial virulence protease and not by human ones. Thus, it is inevitable that the peptide sequence constitutes a natural substrate of aureolysin. We entered the MEROPS Sanger Peptidase database in order to find a suitable candidate (https://www.ebi.ac.uk/merops). MEROPS is an on-line database for peptidases and their inhibitors [145]. The three sequences which were identified as potential candidates for cleavable linkers are depicted in **Table 4**.

Table 4 – Peptide sequences as candidates for aureolysin dependent cleavable linker.

Substrate	P4'	P3'	P2'	P1'	P1	P2	P3	P4	Reference
Complement C3 alpha chain	A	R	S	N	L	D	E	D	[51]
Insulin	V	N	Q	H	L	C	G	S	[146]
Plasminogen	L	F	E	K	K	V	Y	L	[147]

Sequences 1a, 2a, and 3a (**Table 2**) were synthesized by Solid Phase Peptide Synthesis, adding glycine as a spacer on each side and a carboxyfluorescein to the *N*-terminus, acting as a prototype for the potential antibiotic linked to the peptide chain.

The successful synthesis of each sequence was confirmed by MALDI-TOF (**Figures 5-7**). They were purified by Äkta using a mixture of H_2O + 0.1% TFA as eluent A and ACN + 0.1% TFA as eluent B. A wavelength of 214 nm was applied.

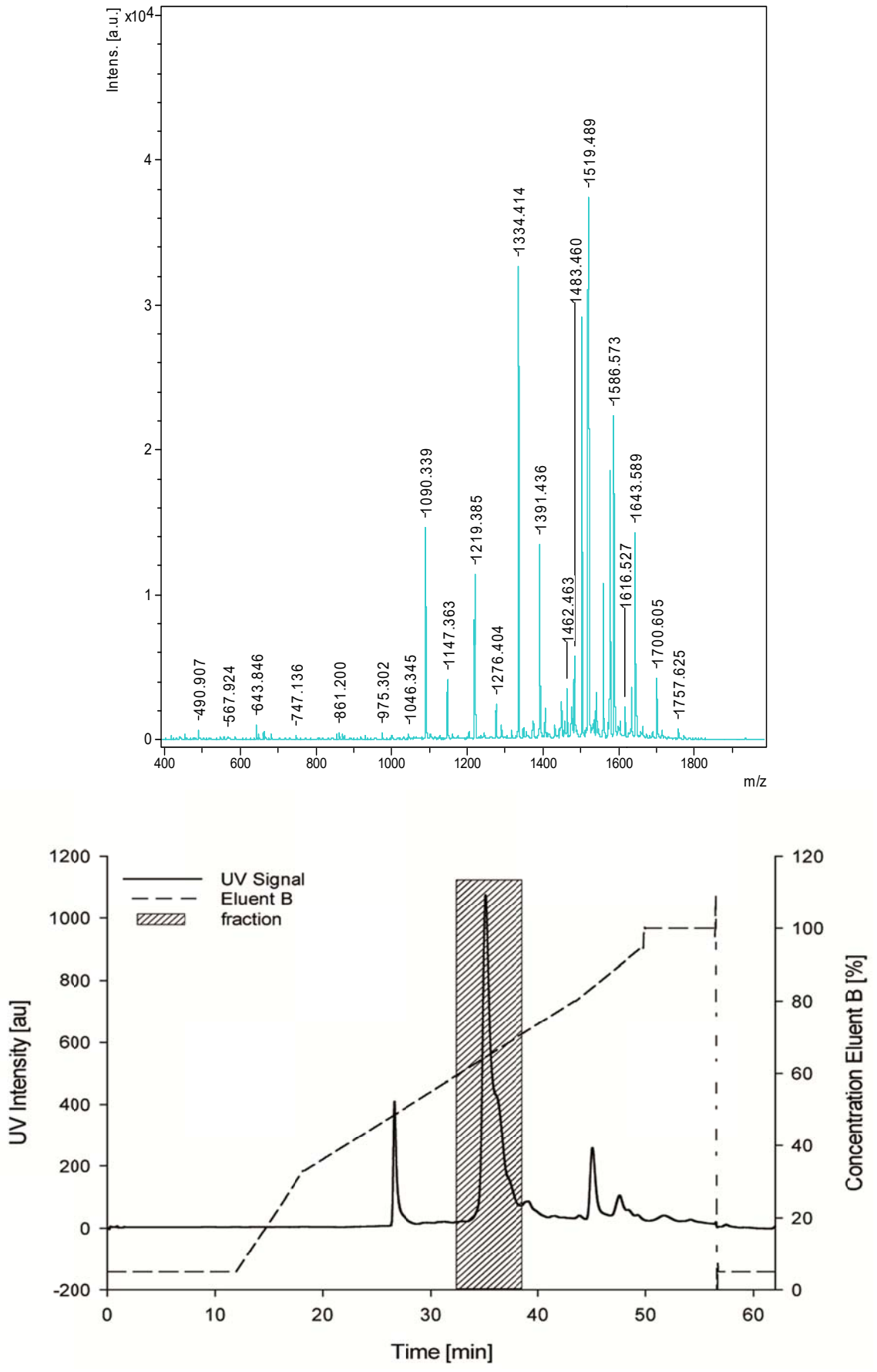

Figure 6 – Mass spectrum of C3 protein originated peptide sequence (above). Below, ÄKTA chromatogram of peptide purification.

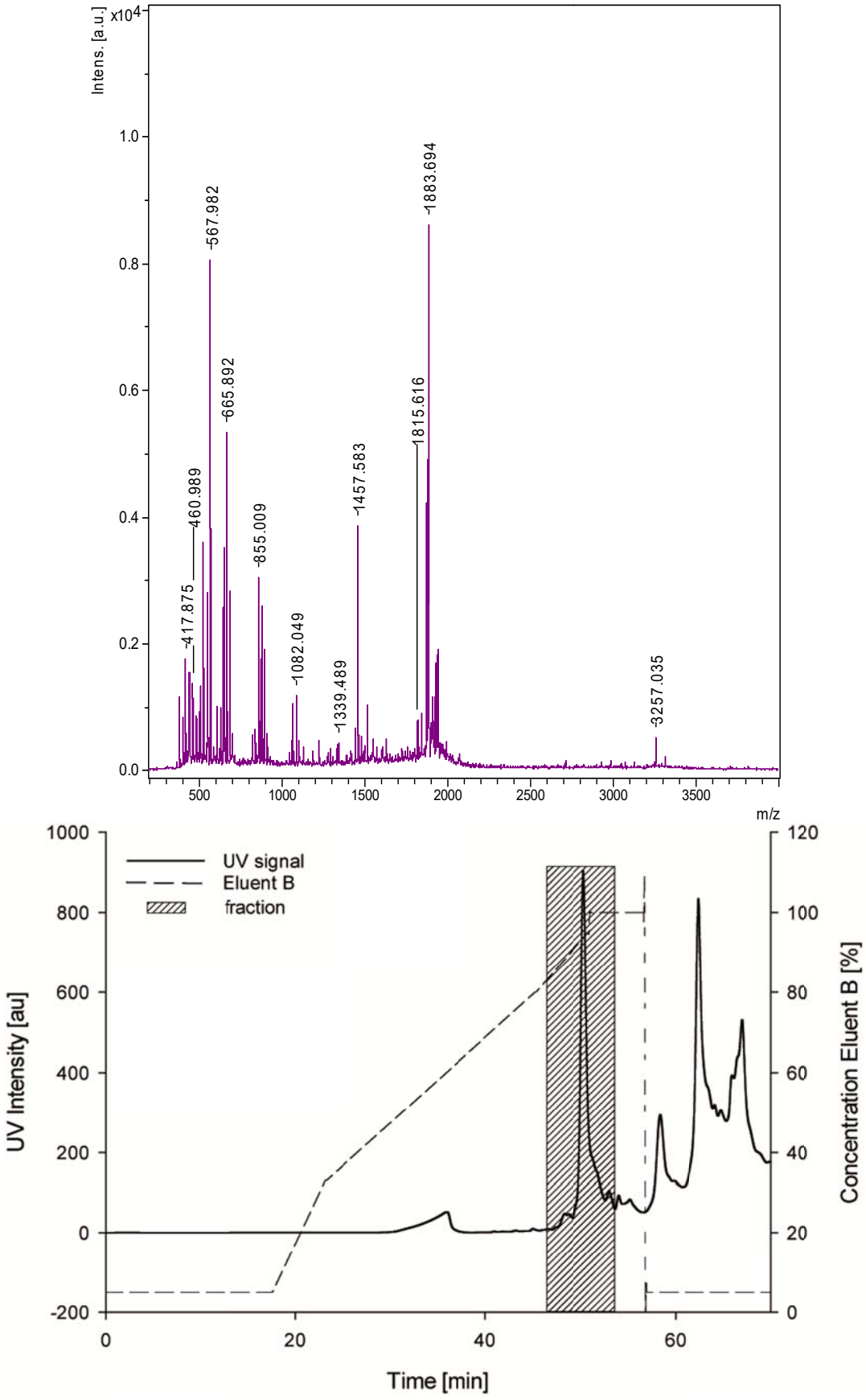

Figure 7 – Mass spectrum of insulin originated peptide sequence (above). Below, ÄKTA chromatogram of peptide purification.

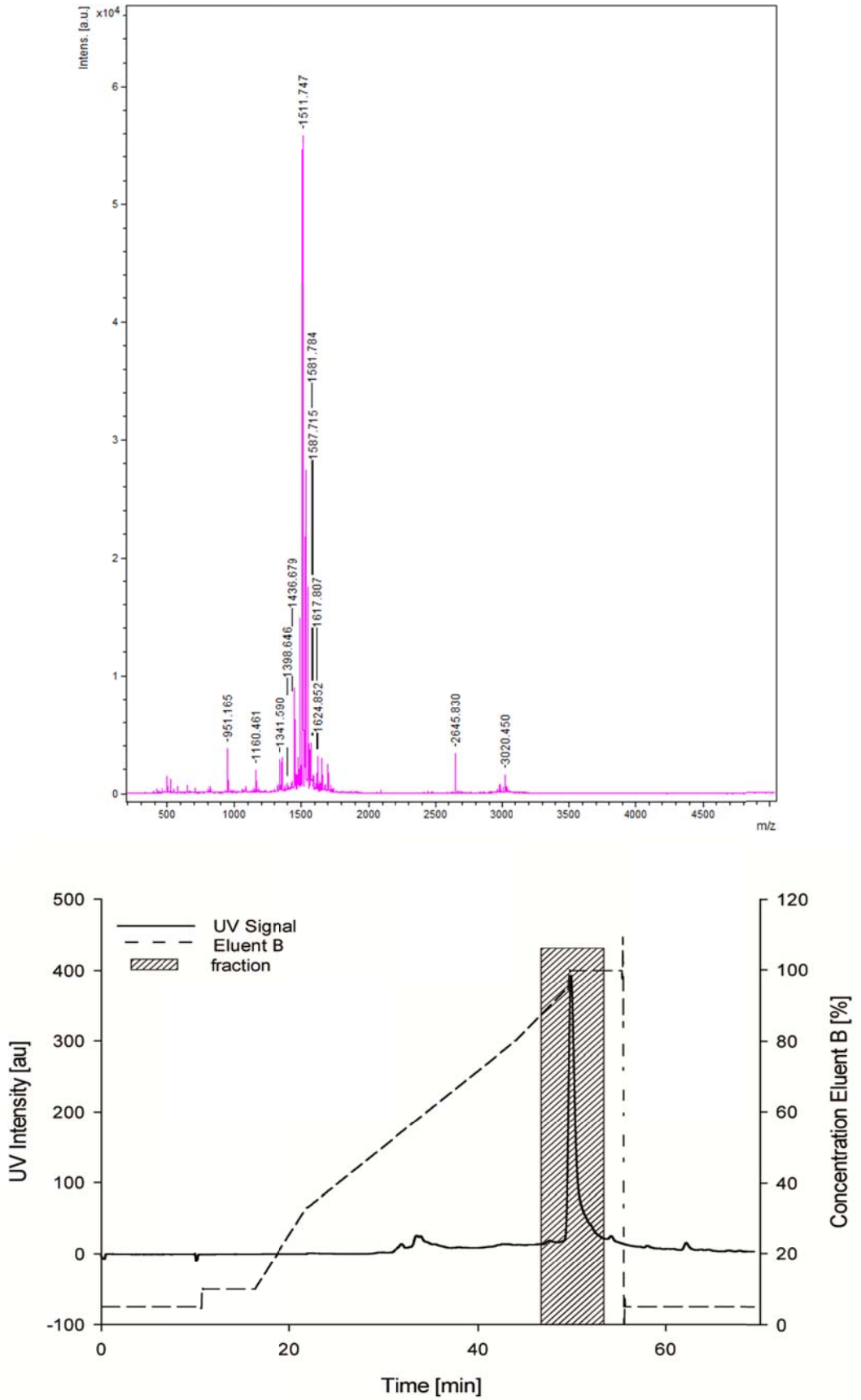

Figure 8 – Mass spectrum of plasminogen originated peptide sequence (above). Below, ÄKTA chromatogram of peptide purification.

4.1.2 Specificity assays

The three sequences were incubated with the bacterial virulence protease aureolysin as well as with human metalloproteases fibroblast collagenase (MMP-1), neutrophil collagenase (MMP-8), 92 kDa type IV collagenase (MMP-9), and collagenase 3 (MMP-13) [148-151]. In order to guarantee the controlled release of the drug, the cleavable linker should only be sensitive towards the specific bacterial virulence protease and not towards any human proteases.

For this study, an arbitrary concentration of 10 ng/mL was chosen. For MMPs, a concentration of 900 ng/mL was chosen as established by Ritzer *et al.* [135]. The quantification of enzymatic activity was determined as the decrease of peptide main peak in relation to the emerged fragment peaks after one hour of incubation (**Figures 9-17**).

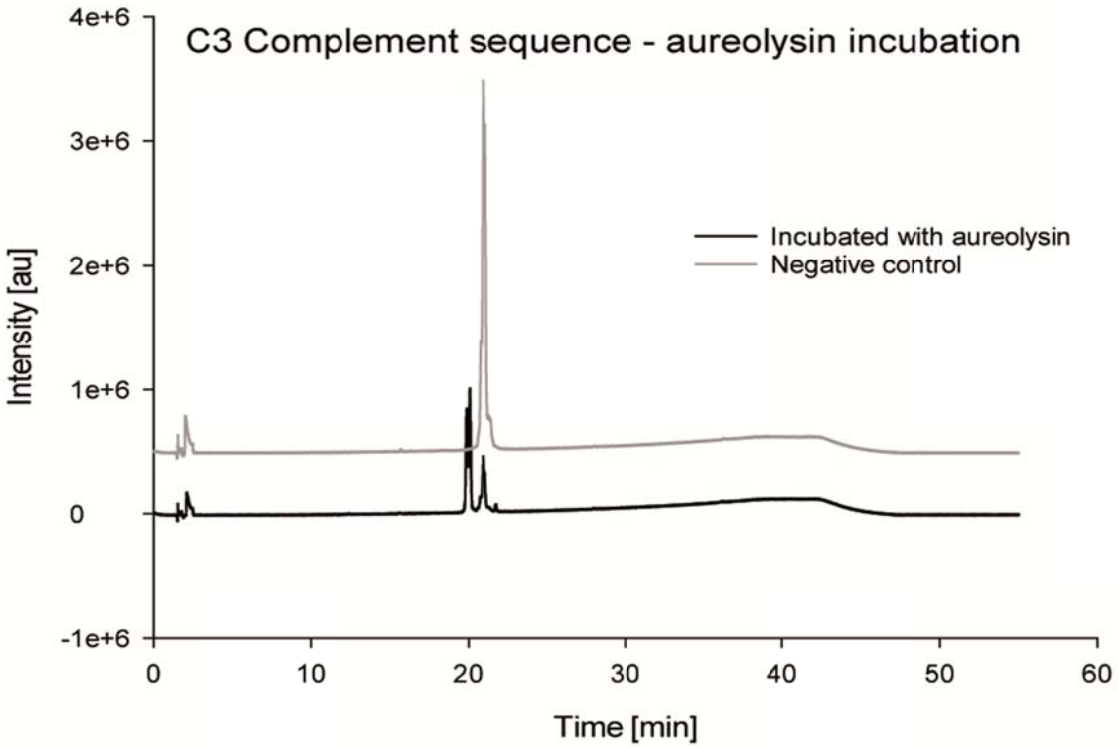

Figure 9 – HPLC chromatogram of C3 complement sequence cleavage assay when incubated for 1 h at 37 °C with aureolysin.

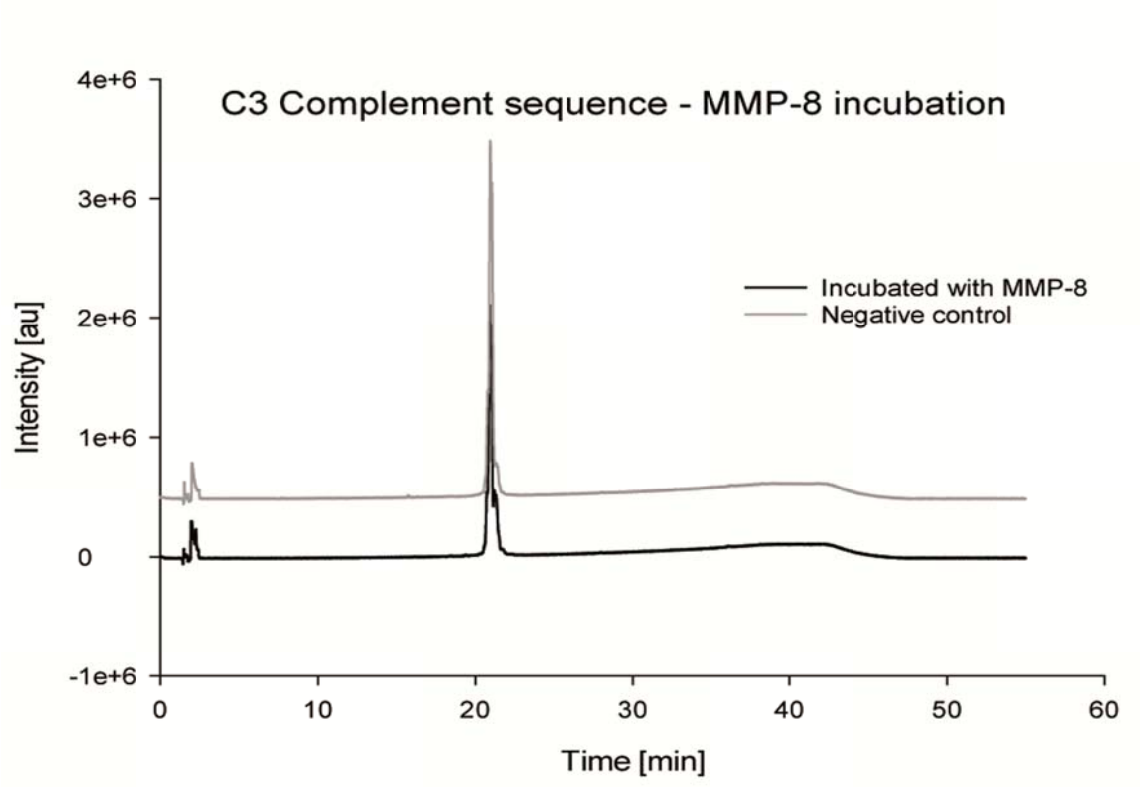

Figure 10 – HPLC chromatogram of C3 complement sequence cleavage assay when incubated for 1 h at 37 °C with MMP-8.

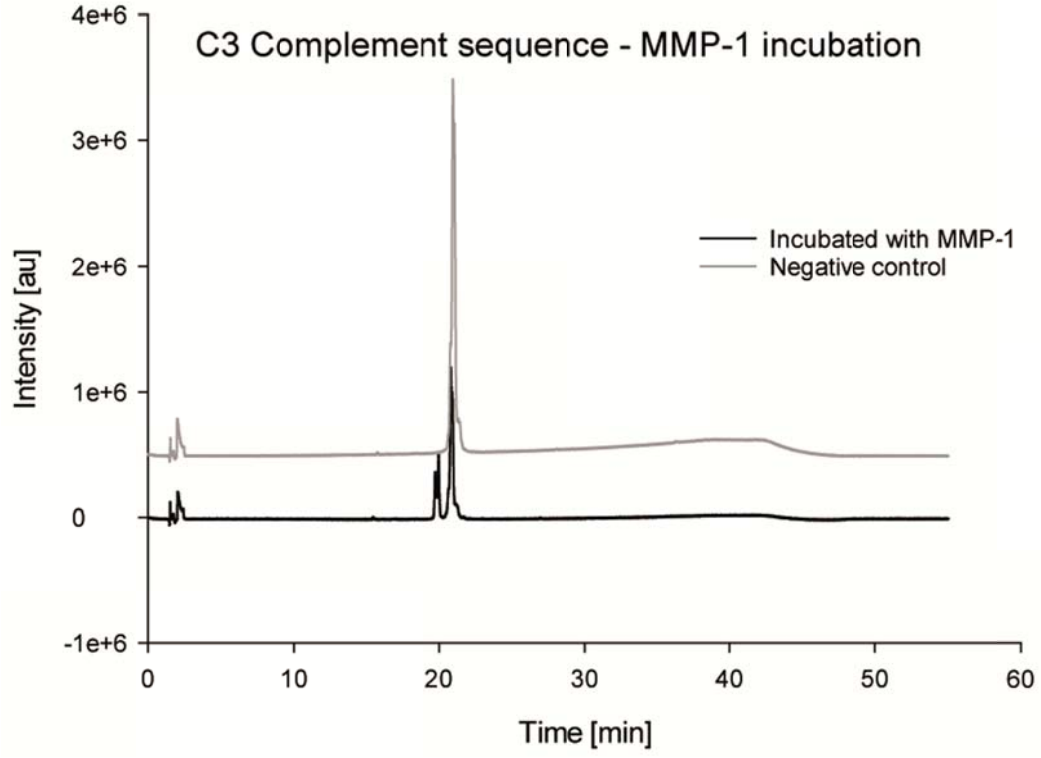

Figure 11 – HPLC chromatogram of C3 complement sequence cleavage assay when incubated for 1 h at 37 °C with MMP-1.

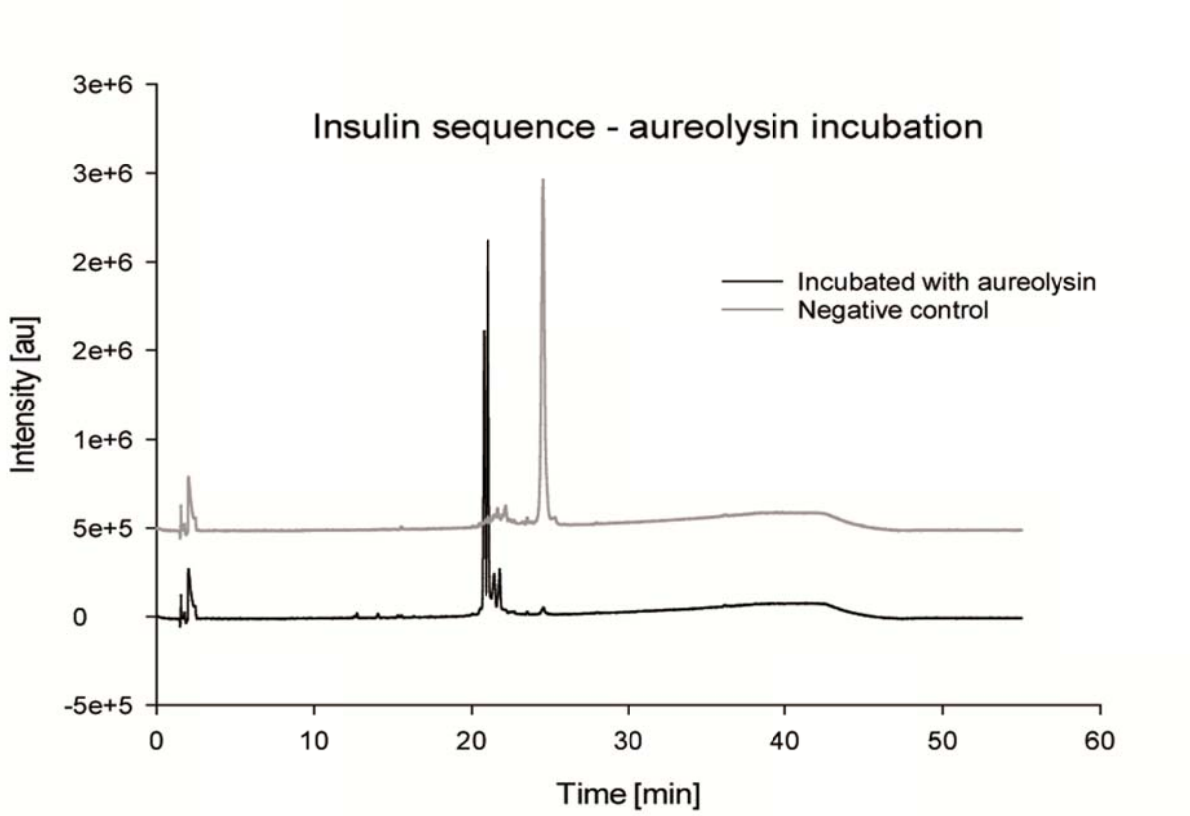

Figure 12 – HPLC chromatogram of insulin sequence cleavage assay when incubated for 1 h at 37 °C with aureolysin.

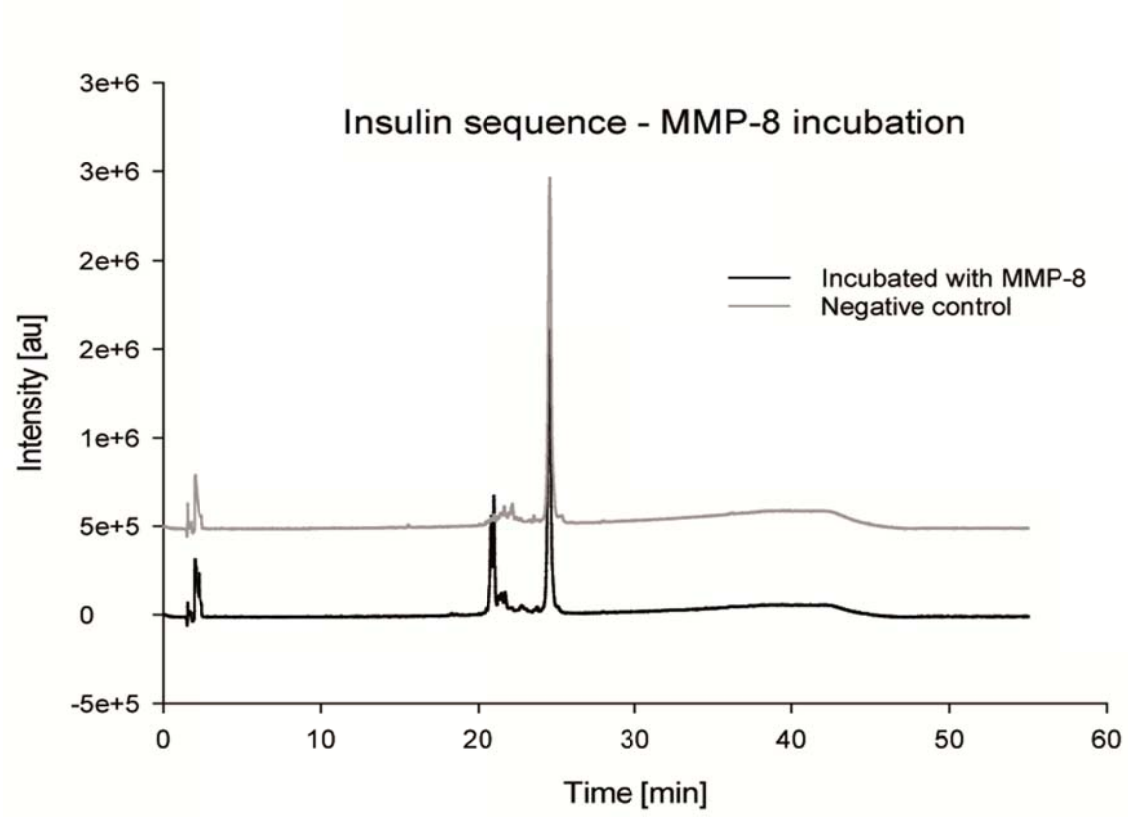

Figure 13 – HPLC chromatogram of insulin sequence cleavage assay when incubated for 1 h at 37 °C with MMP-8.

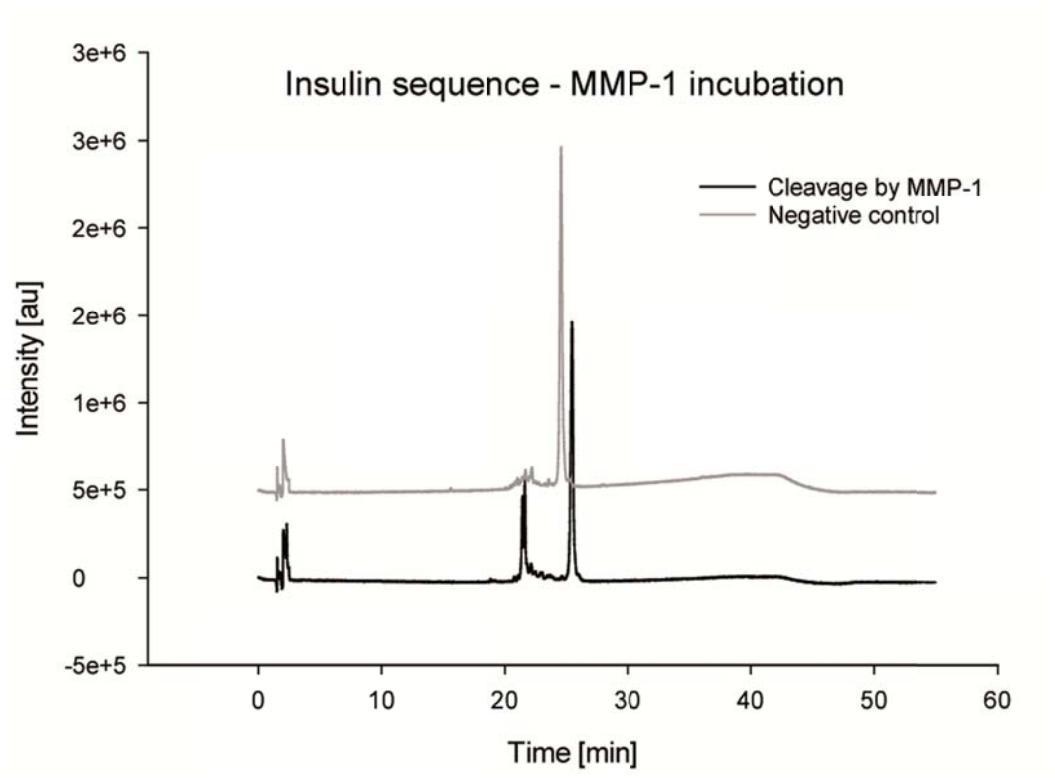

Figure 14 – HPLC chromatogram of insulin sequence cleavage assay when incubated for 1 h at 37 °C with MMP-1.

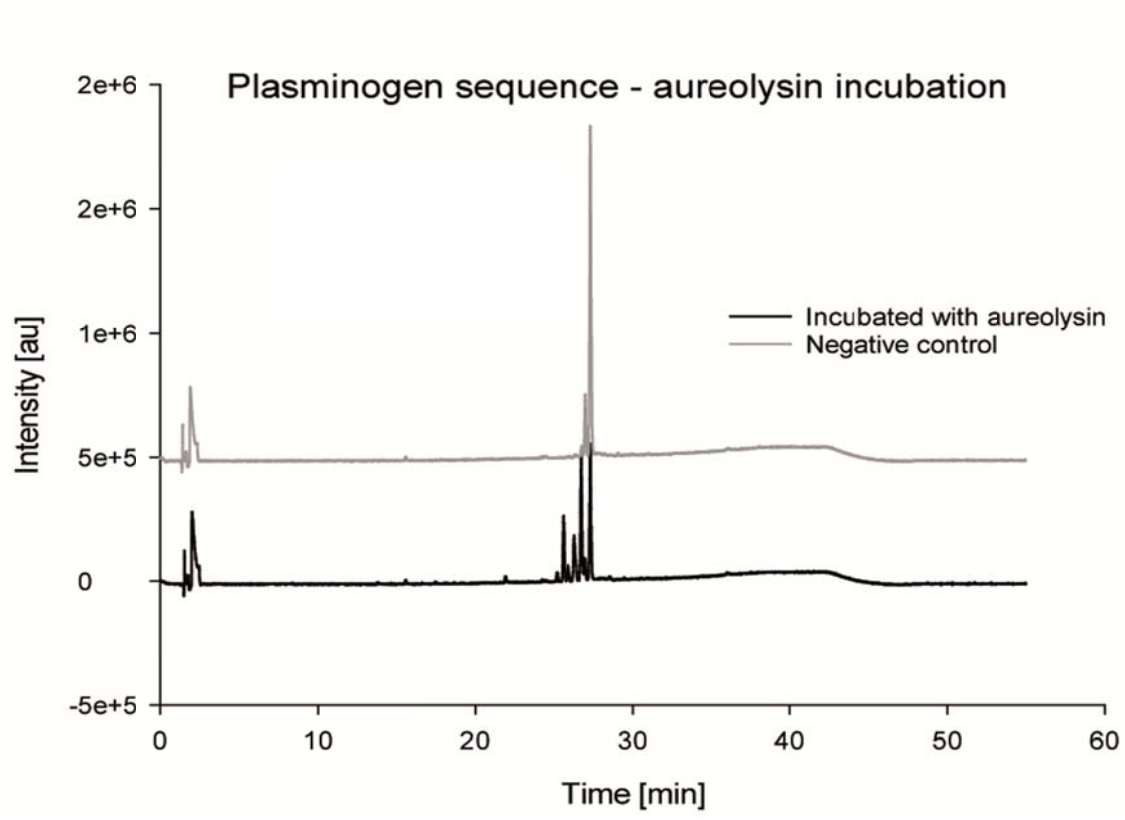

Figure 15 – HPLC chromatogram of plasminogen sequence cleavage assay when incubated for 1 h at 37 °C with aureolysin.

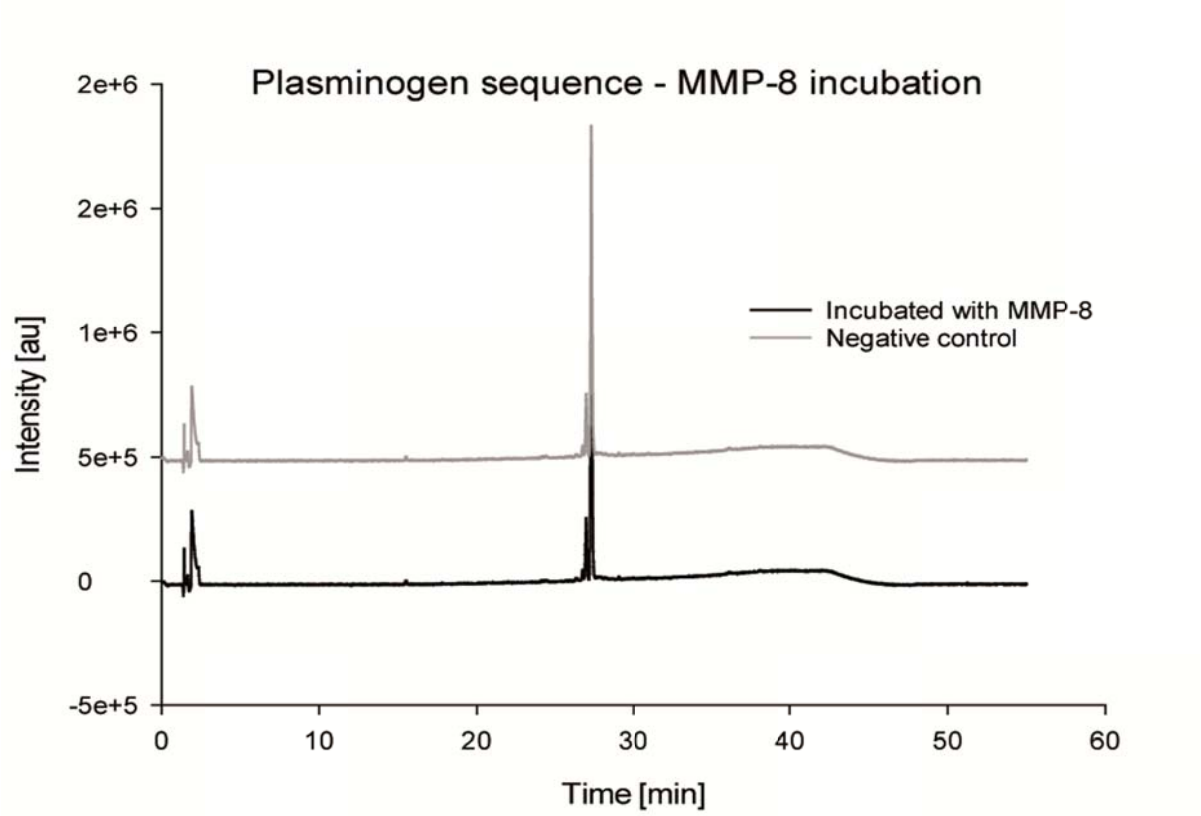

Figure 16 – HPLC chromatogram of plasminogen sequence cleavage assay when incubated for 1 hour at 37 °C with MMP-8.

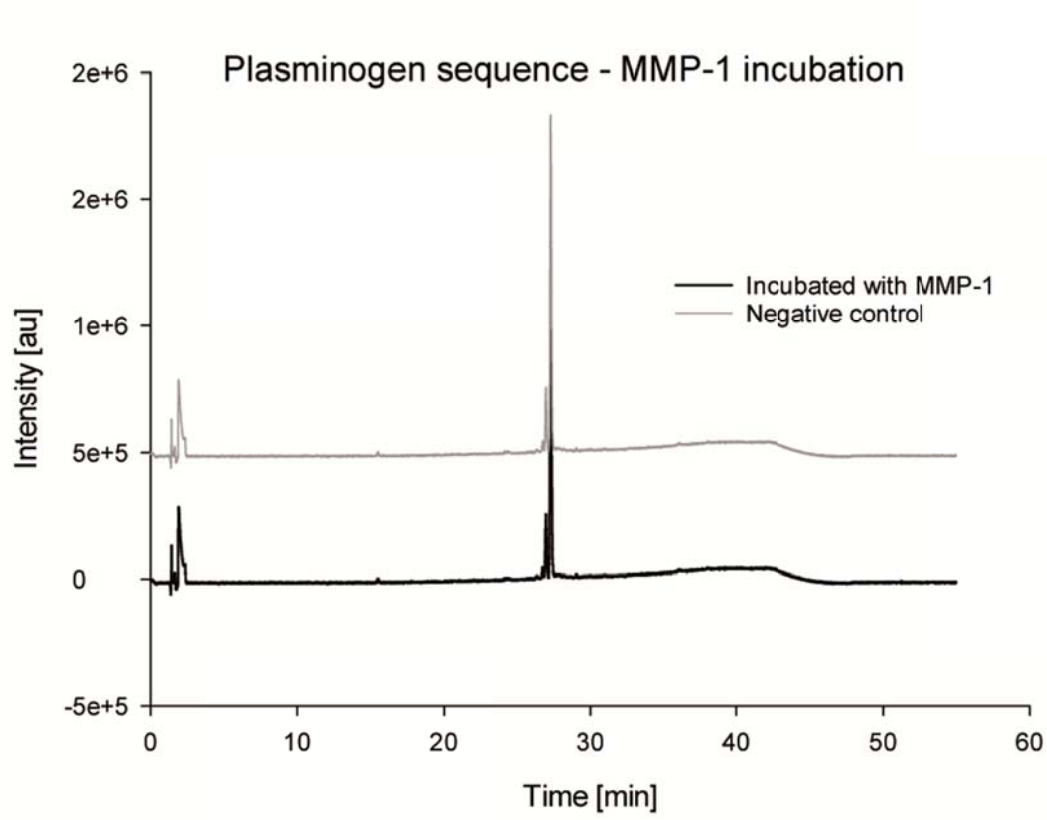

Figure 17 – HPLC chromatogram of plasminogen sequence cleavage assay when incubated for 1 hour at 37 °C with MMP-1.

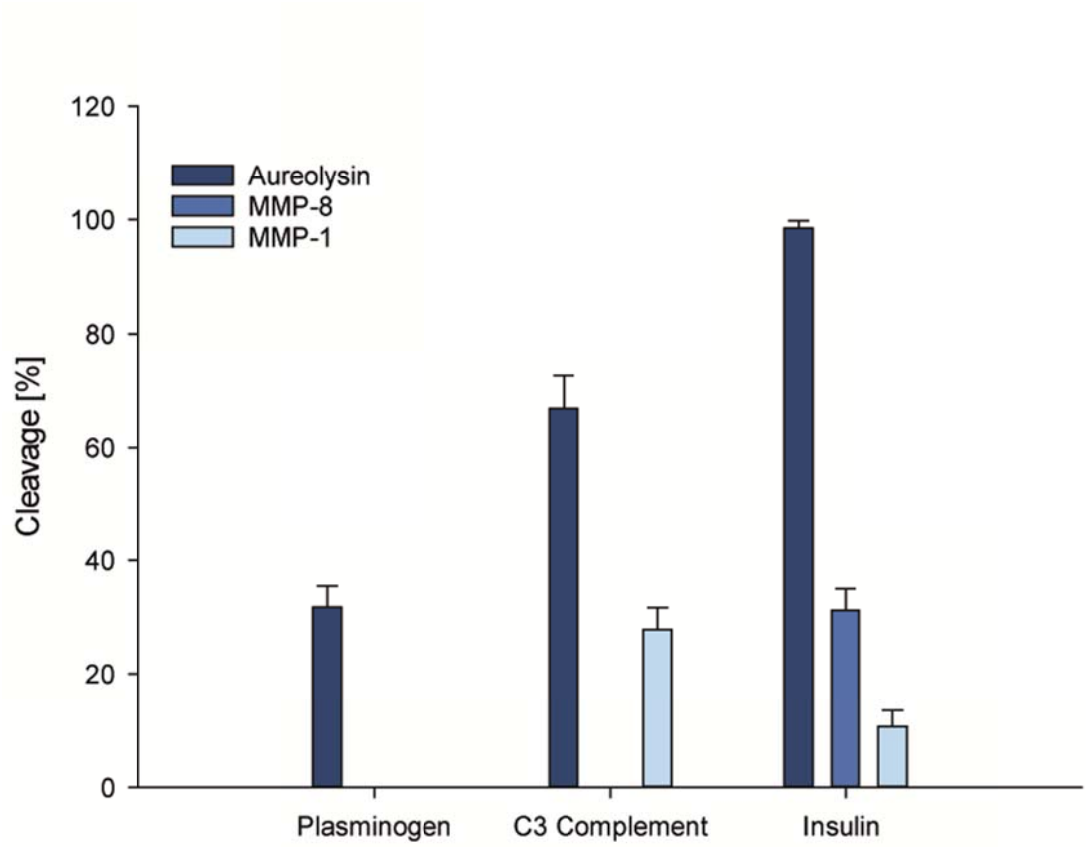

Figure 18 – Cleavage percentage of synthesized peptide sequences after one hour incubation with aureolysin and metalloproteases MMP-8 and MMP-1.

After incubating the three linker prototype sequences with aureolysin and with different types of MMPs, all sequences were cleaved by the bacterial protease as expected (**Figure 18**). The insulin originated sequence presented the best cleavage rate of 98% within one hour, whereas the C3 complement was 65% cleaved, and plasminogen only 35%. However, insulin was also cleaved by MMP-8 and MMP-1, and C3 was sensitive towards MMP-1. No cleavage was observed when incubating any of the sequences with either MMP-9 or MMP-13.

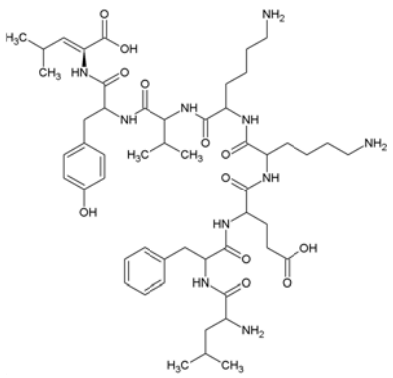

Figure 19 – Structure of plasminogen originated peptide sequence

Even though the plasminogen originated sequence (**Figure 19**) presented the lowest cleavage rate among all tested sequences, it was the only prototype which showed specificity and sensitivity only towards the bacterial protease. Thus, it was chosen to serve as a cleavable linker prototype for the antibiotic delivery system.

4.2 Aureolysin activity determination

After successfully showing that the bacterial protease aureolysin was able to cleave all three sequence prototypes, the next step was to quantify its activity. For that, different methods were used which are described in the following sections.

4.2.1 Azocasein assay

Azocasein is a nonspecific protease substrate. The method comprises of incubating the azo dye containing casein protein with proteases and the subsequent release of soluble peptides, which cannot be precipitated nor filtered. In the absence of the protease, azocasein remains intact. It precipitates as a macromolecule insoluble in acid when TCA is added to the buffer and can be removed by centrifugation, while the supernatant remains uncolored. By the action of a protease, azocasein is cleaved in small soluble peptides and the supernatant becomes colored yellow.

For this assay, we incubated the substrate with aureolysin and, in comparison, with trypsin. Azocasein was prepared in the buffer of both enzymes.

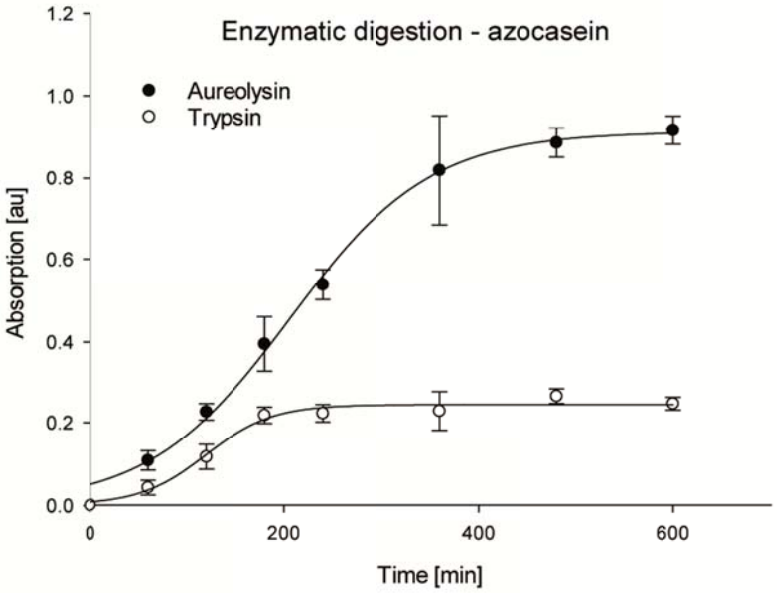

Figure 20 – Time course of aureolysin and trypsin activity. Enzyme activities are the mean values of three independent digestions.

First, the mean absorption values were plotted against the time (**Figure 20**). It is possible to observe that trypsin reached a steady state in absorption after only three hours, whereas for aureolysin, this was the case after more than six hours. As the enzyme loses its activity after some time, azocasein is not cleaved into soluble peptides anymore and the absorption remains constant for the rest of the time monitored during the assay.

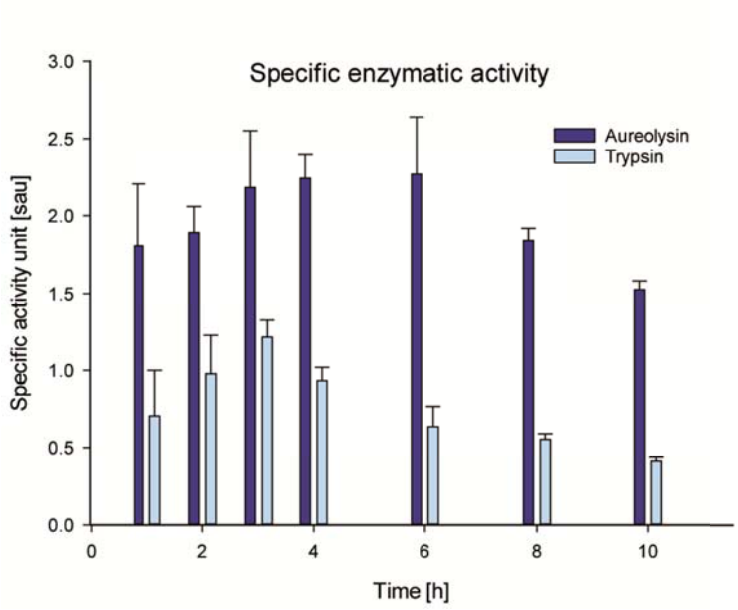

Figure 21 – Specific enzymatic activity comparison for aureolysin (dark blue) and trypsin (light blue).

The specific activity unit was also determined and should remain constant during the period in which each enzyme was active (**Figure 21**). The specific activity units corroborate with previous data; they remain constant during the active enzymatic period and decrease when protease stops cleaving the azocasein substrate. In comparison to trypsin, aureolysin presented a better activity towards azocasein which lasted longer. We now investigated the cleavage activity having our specific cleavable linker as a substrate.

4.2.2 Enzyme-linked immunosorbent assay

In order to quantify the expression of aureolysin by *S. aureus*, we performed an indirect ELISA assay using α-aureolysin as the detection antibody (kindly provided by PD Dr. Knut Ohlsen, Institute for Molecular Infection Biology (IMIB), University of Würzburg). In this variant of the standard ELISA methods, the antigen is adsorbed to the microplate followed by its detection in a two-step process. First, an unlabeled primary antibody binds to the specific antigen. Secondly, an enzyme conjugated secondary antibody that is directed against the host species of the primary antibody is applied (**Figure 22**).

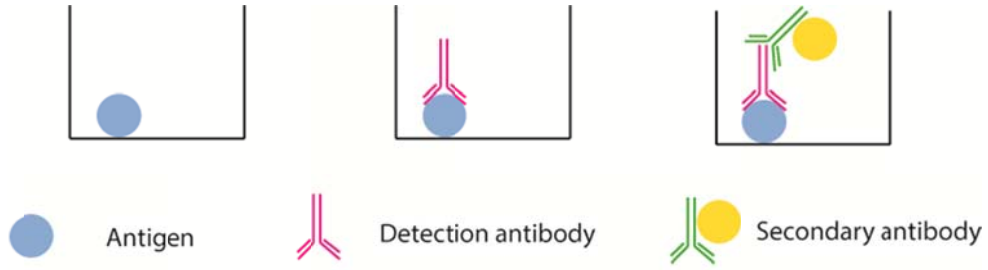

Figure 22 – Overview of indirect ELISA. The antigen (blue) is adsorbed to the surface of the microplate, followed by the binding of the detection antibody (pink). Finally, the secondary antibody conjugated with HRP (green and yellow) binds to the primary antibody.

First, we constructed a detection curve using aureolysin as antigen. Our purpose was to (i) validate the use of this method for the detection of aureolysin and (ii) establish the detection range of the antigen by α-aureolysin. As already described, each well of the ELISA plate was filled with 50 µL of the aureolysin solution in PBS (concentration 1 µg/mL). On the next day, we performed a serial dilution with the α-aureolysin antibody, starting with a 1:100 dilution and following with 1:2 each.

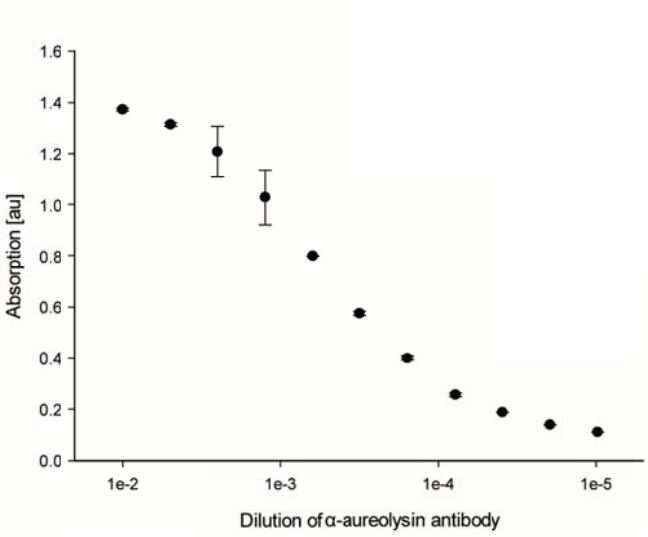

Figure 23 – Standard curve of aureolysin detection by serial dilution of α-aureolysin primary antibody.

As can be seen in **Figure 23**, a dilution of 1:1600 provided a mean absorption value of 0.8, which was chosen as the proper primary antibody dilution for the following assays regarding bacterial supernatants.

In order to detect the expression of aureolysin in bacterial cultures, *Staphylococcus aureus* was cultivated in either LB medium or FBS. We chose three different mutant strains 8325, MA12 and Newman, all Δ*spa*. This gene is responsible for the expression of protein A, an important virulence factor which enables *Staphylococcus aureus* to evade host immune responses [152]. This protein could interfere with the detection of aureolysin through a cross reaction, thus the choice of working with mutant strains in which the gene was abolished. However, no aureolysin could be detected in neither of the samples, independent from the bacterial strain or the culture medium.

4.2.3 Cleavage assay

Since aureolysin is the main trigger for our antibiotic release system, it is necessary to characterize its activity towards our cleavable linker for better understanding of the whole process. For this assay, peptide sequence 3b (**Table 2**) was used.

A big challenge is finding a suitable aureolysin concentration range. As there is no data available in the literature for the amount of aureolysin expressed and released by *S. aureus* during infections, nor could we quantify its expression and release by ELISA, we firstly performed a logarithmic screening in order to find the concentration range in which aureolysin cleaves our linker from 0 to 100% within one hour. Concentration levels of aureolysin from 10^{-1} to 10^{4} ng/mL were tested.

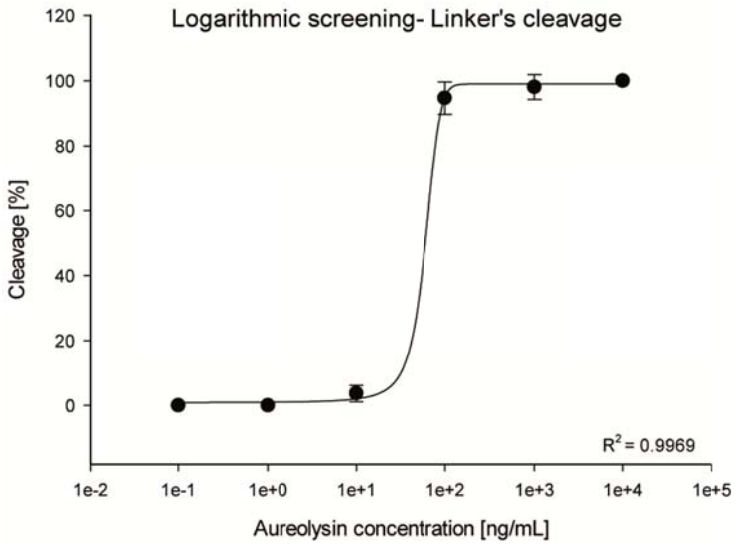

Figure 24 – Plasminogen cleavage by aureolysin. Cleavable linker was incubated with logarithmic concentration of protease in order to find the best range of activity.

As shown in **Figure 24**, aureolysin has a proteolytic activity starting at a minimum concentration of 10 ng/mL (0.23 nM) and reaching full substrate cleavage at around 1000 ng/mL (23 nM). However, since the logarithmic range did not provide a more detailed pattern, the assay was repeated in a narrower concentration range representing the cleavage range only (**Figure 25**).

By analyzing the percent cleavage rate by aureolysin concentrations within the established range, it is possible to obtain a better understanding of how fast the designed linker would be cleaved and, therefore, release the antibiotic into the medium. The next step was to unravel the cleavage kinetics of aureolysin during incubation. For that, an enzyme concentration of 50 ng/mL was chosen since this concentration corresponds to the cleavage of 50% of the initial substrate concentration within one hour.

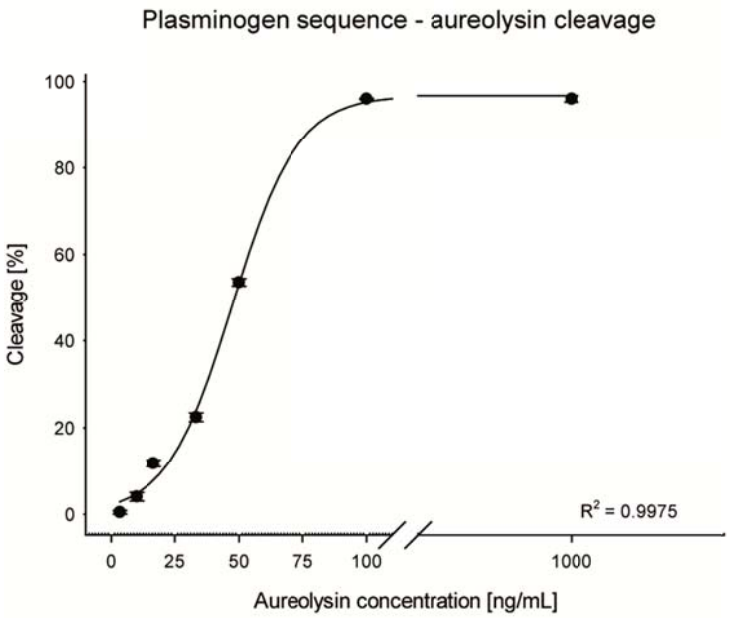

Figure 25 – Plasminogen sequence cleavage efficiency [%] as a function of aureolysin concentration. Enzymatic range: 0 to 1000 ng/mL.

We incubated the peptide sequence again at the same concentration of 0.5 mg/mL and samples were taken at previously established time points. The assay was

concluded after six hours of incubation since, after this time, aureolysin is no longer active as observed during the azocasein digestion assay. We observe in **Figure 26** that during the time one major product is formed with a retention time of 19.2 min for the corresponding signal and two double fragment peaks at 16.1 and 17.5 min, respectively. The major product peak is due to the cleavage fragment KVYLG, which has a molar mass of 578 Da and was confirmed by LC-MS (**Figure 28**). The other formed fragments were not investigated further. Evaluation of the cleavage performance was based on the area percentage decrease of the main peak, whose retention time is 20.1 min. The peptide sequence was entirely cleaved within two hours and the percent cleavage rates could be fitted in a hyperbolic non-linear correlation (**Figure 27**).

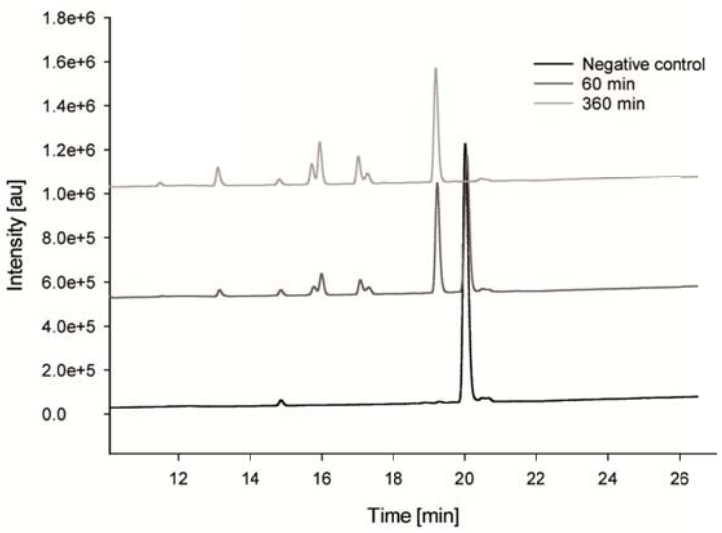

Figure 26 – Overlay of chromatograms of plasminogen linker, before, after 60 min and 360 min of aureolysin incubation. The peptide linker presents a retention time of 20.1 min (black line), which is 50% cleaved after 60 min (dark grey line) and completely cleaved after 360 min (light grey line).

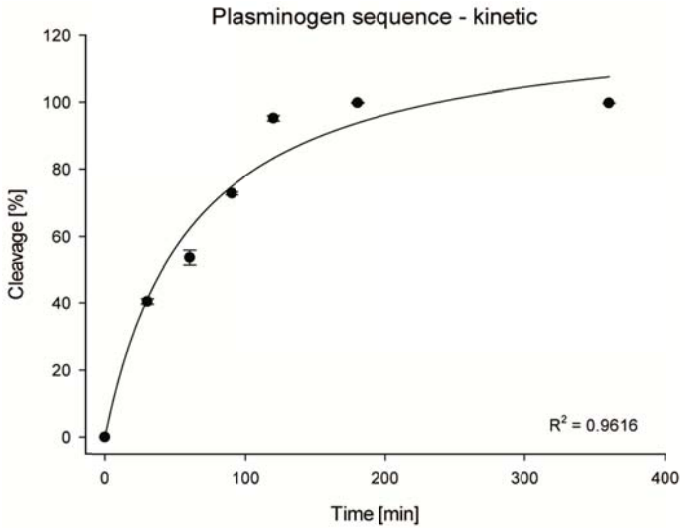

Figure 27 – Plasminogen sequence cleavage as a function of time. Aureolysin concentration: 50 ng/mL.

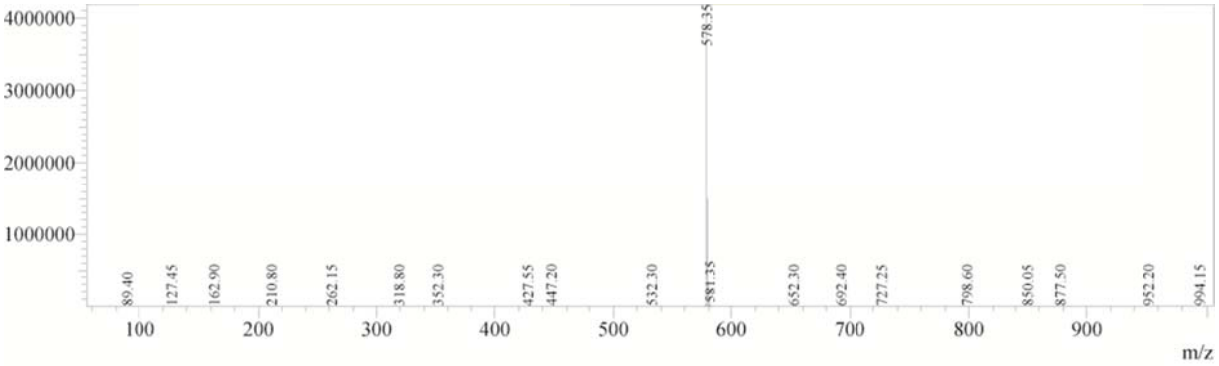

Figure 28 – Mass spectrum of resulted fragment after incubation of plasminogen based linker sequence with aureolysin.

4.3 Hydrogel formulation assays

After characterizing the cleavage assets of our designed peptide linker by the bacterial virulence protease aureolysin, the next step was to develop a suitable pharmaceutic formulation in order to incorporate our release system.

4.3.1 Physical incorporation of antibiotic into a hydrogel matrix

The first approach for this study was a physical incorporation of the active compound into a hydrogel matrix in which peptide linkers would serve as crosslinkers. The strategy is mantaining the biomolecule entrapped in the hydrogel pores and, having the action of aureolysin during a staphylococcal infection, the peptide crosslinkers would be cleaved, leaving the hydrogel matrix and releasing the antibiotic (**Figure 29**).

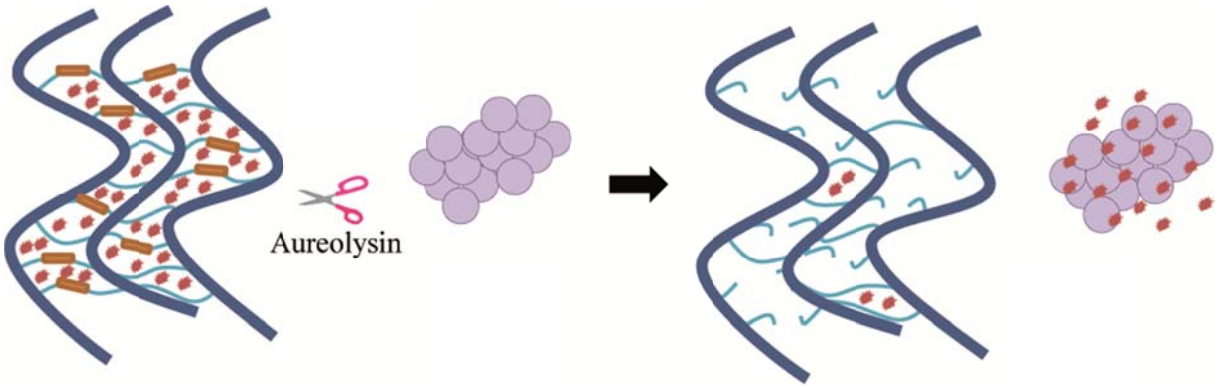

Figure 29 – Strategy of antibiotic physical incorporation into hydrogel. Bacterial protease aureolysin, only released when *S. aureus* is on their virulent state, would cleave the peptide linkers (depicted as orange rectangles) which are helping to maintain the active compound (depicted as red stars) entrapped to the hydrogel matrix, releasing it to the medium.

For this purpose we used the commercially available *3-D life* hydrogel kit for cell culture from Cellendes GmbH (Reutlingen, Germany). This system is comprised of a polyvinyl alcohol (PVA) polymer functionalized with numerous maleimide scaffolds along the backbone and a PEG crosslinker functionalized with thiol groups at each end (**Figure 30**).

Figure 30 – Structures of PVA functionalized with maleimide groups (left) and PEG-link (right).

Before we started adding the thiol-functionalized peptide into the formulation as a bioresponsive crosslinker, we evaluated the hydrogel concentrations in which the fluorophores would not diffuse into the medium. For this part, two different concentrations of 5.0 and 10.0 mM of hydrogel matrix were tested. Fluorescein isothiocyanate (FITC) dextrans with molecular weights of 20 and 40 kDa as well as Green Fluorescent Protein (GFP) with a molecular weight of 27 kDa were chosen as fluorophores.

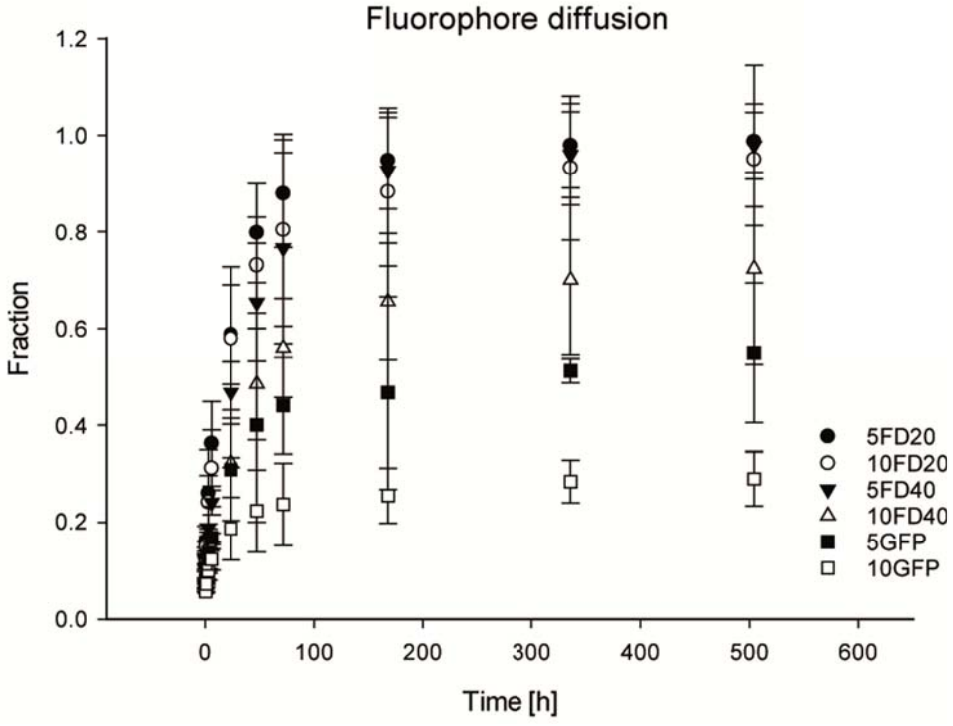

Figure 31 – Fluorophore diffusion fractions over the time for hydrogel formulations.

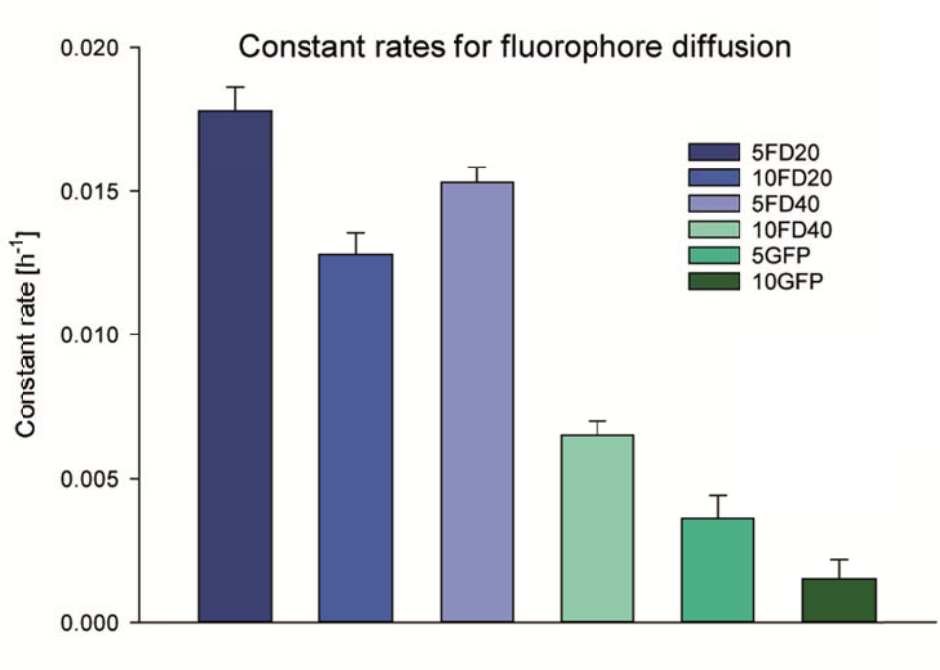

Figure 32 – Constant rates for fluorophore diffusion from different formulations of hydrogel. The values were determined by fitting release profiles to a first-order exponential approximation.

For diffusion assays only regarding PVA-maleimide polymer and PEG-thiol cross linker, without functionalizing the system with peptide linkers it was observed that all FITC-Dex formulations presented a rapid diffusion, with formulations 5FD20, 10FD20, and 5FD40 releasing more than 80% of their initial fluorophore content within 72 hours, while formulation 10FD40 showed a diffusion percentage of 70% within three weeks (**Figure 31**). On the other hand, both GFP containing formulations 5GFP and 10GFP presented low constant rates (**Figure 32**) and diffusion fractions of 54% and 28% after 3 weeks, respectively.

Thus, for a further diffusion assay with hydrogel formulations functionalized with peptide linkers, we chose to continue using only GFP as fluorophore and active compound prototype. Before incubating the peptide linker functionalized system with the bacterial protease aureolysin, we first decided to confirm whether it would retain the fluorophore as efficiently as the primary formulation with only the provided PEG-thiol working as cross linkers. The designed peptide linker for this step was peptide 3b (**Table 2**), which contains the plasminogen originated sequence, as well as cysteine at each terminus to provide the required thiol group being necessary for the crosslinking reaction with the maleimide groups present at the PVA matrix. Besides, a spacer containing six units of PEG was introduced in order to increase its solubility (**Figures 33, 34**).

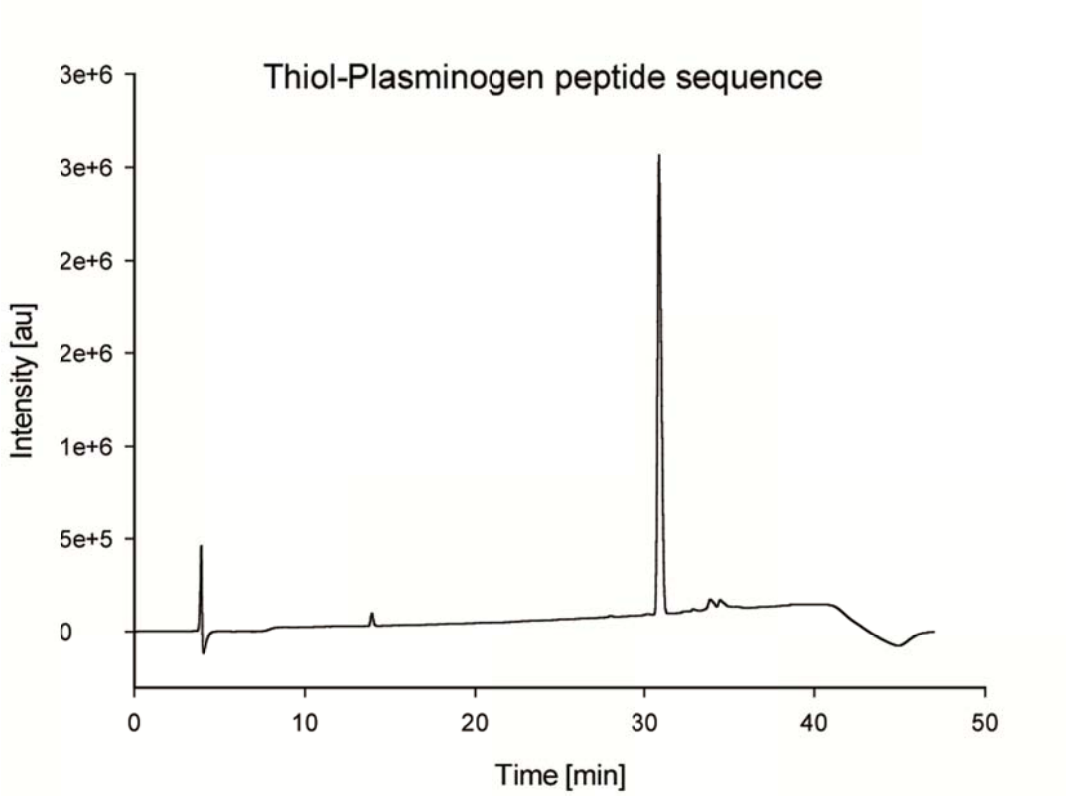

Figure 33 – Chromatogram of L-thiol-Plasminogen peptide sequence (ID 3b).

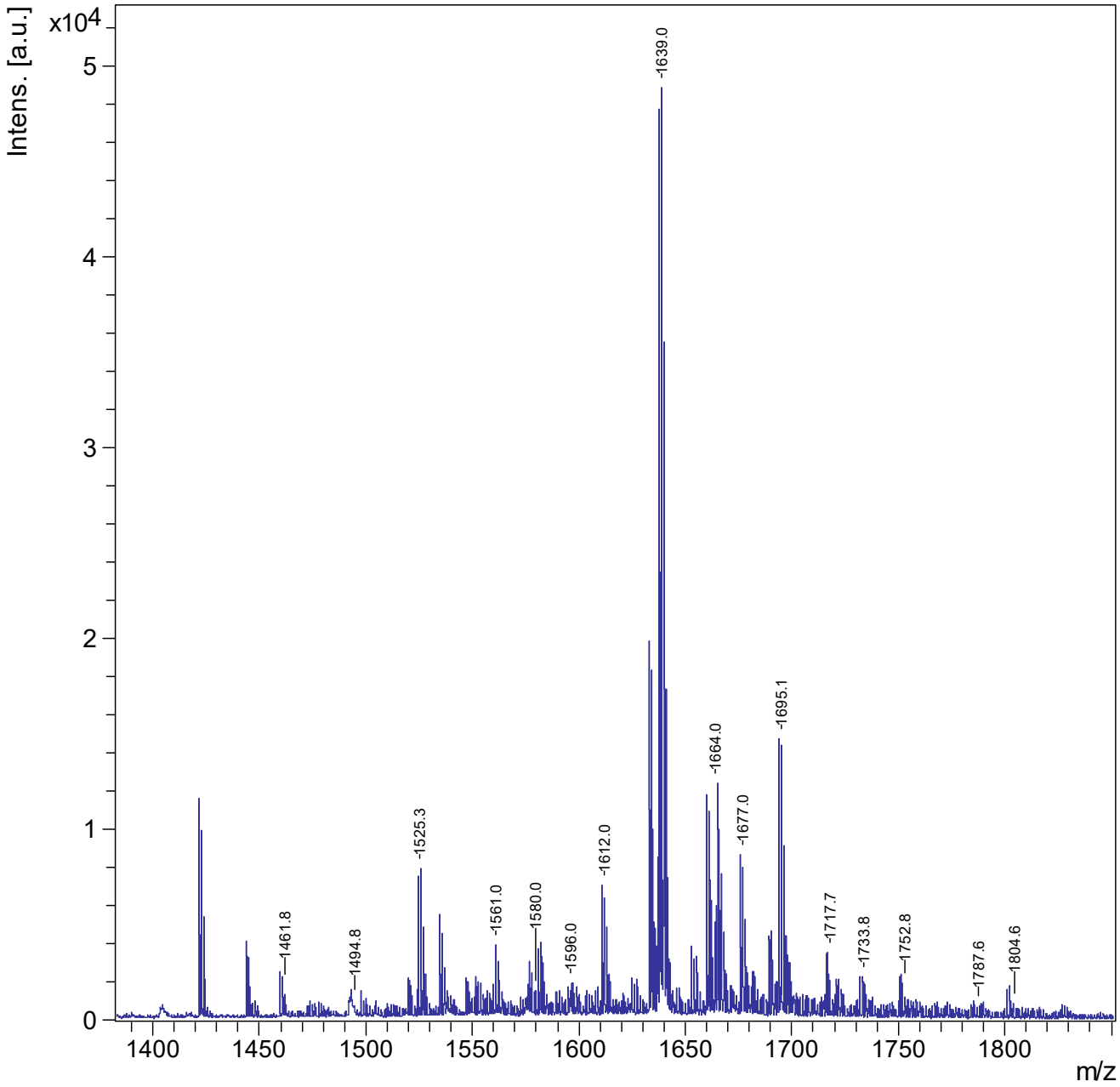

Figure 34 – Mass spectrum of L-thiol-plasminogen peptide sequence (ID 3b)

For a negative control, i.e. a peptide sequence which is not usually cleaved by aureolysin, we synthesized the same sequence but used D-amino acids which are not cleaved by proteases. An additional glycine was incorporated to the sequence in order to differentiate its mass from the L-isomer (**Figure 36**). In order to confirm the suitability of this sequence, the peptide was incubated with aureolysin and no cleavage was observed (**Figure 35**).

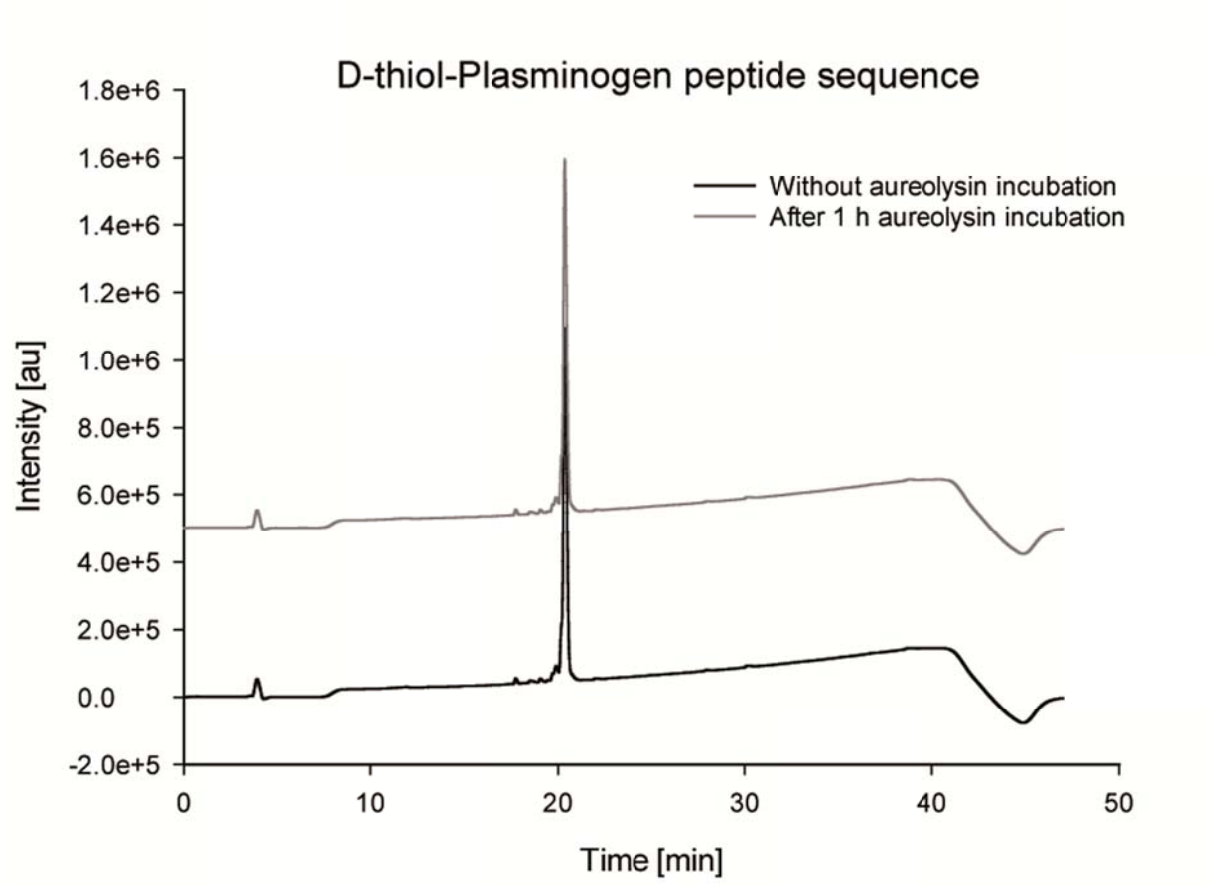

Figure 35 – Chromatogram of D-thiol plasminogen peptide (ID 3c) sequence without aureolysin incubation (black line) and after one hour incubation (grey line). The sequence was not cleaved by the bacterial protease, indicating its suitability as a negative control of the hydrogel release system.

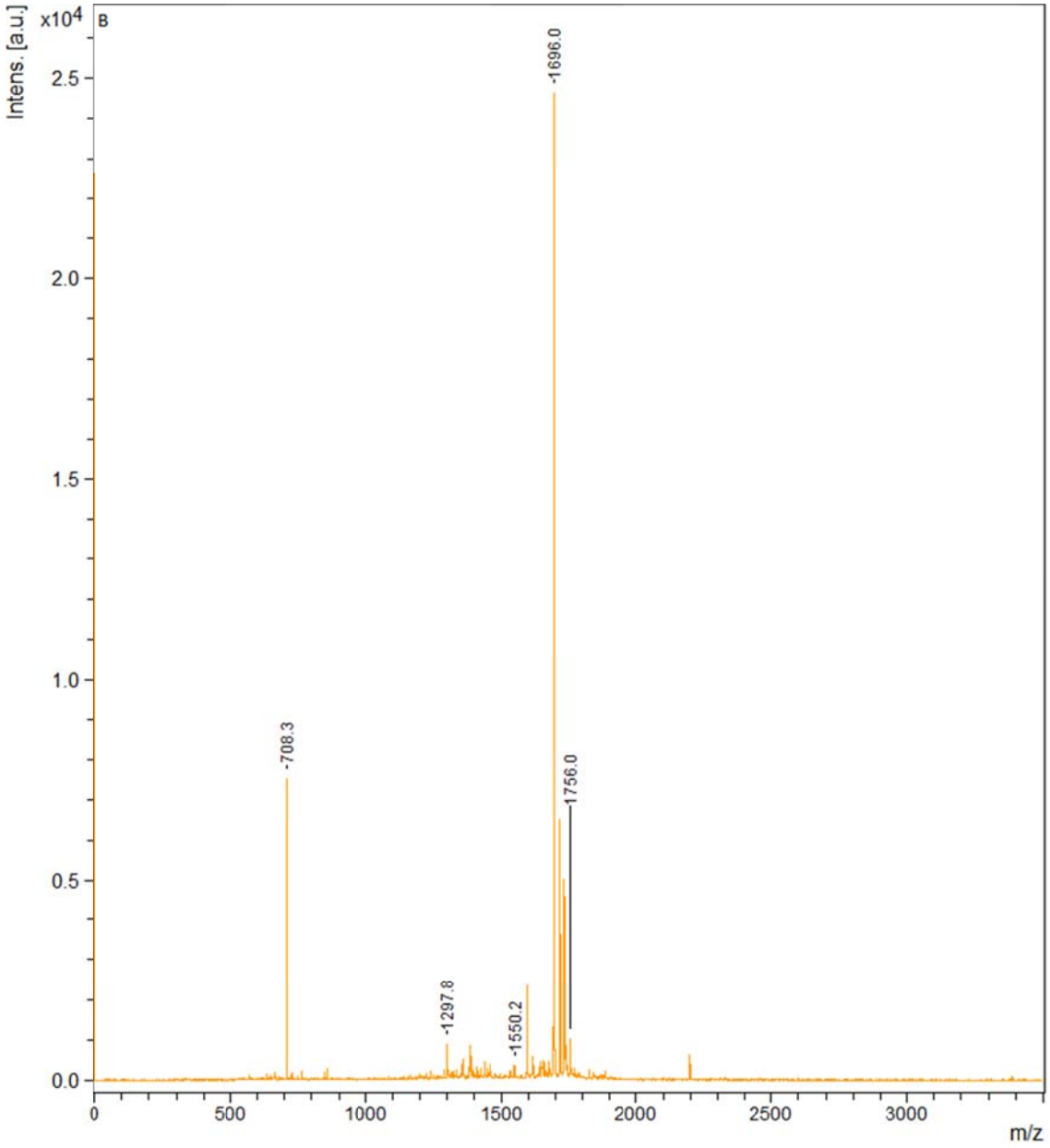

Figure 36 – Mass spectrum of D-thiol-plasminogen peptide sequence (ID 3c)

For this assay we prepared formulations in which the provided thiol-PEG crosslinkers were partially replaced by the synthesized peptide sequences in ratios of 3:7, 2:8, and 1:9 (peptide:PEG linker) with polymeric concentrations of 5 and 10 mM, respectively.

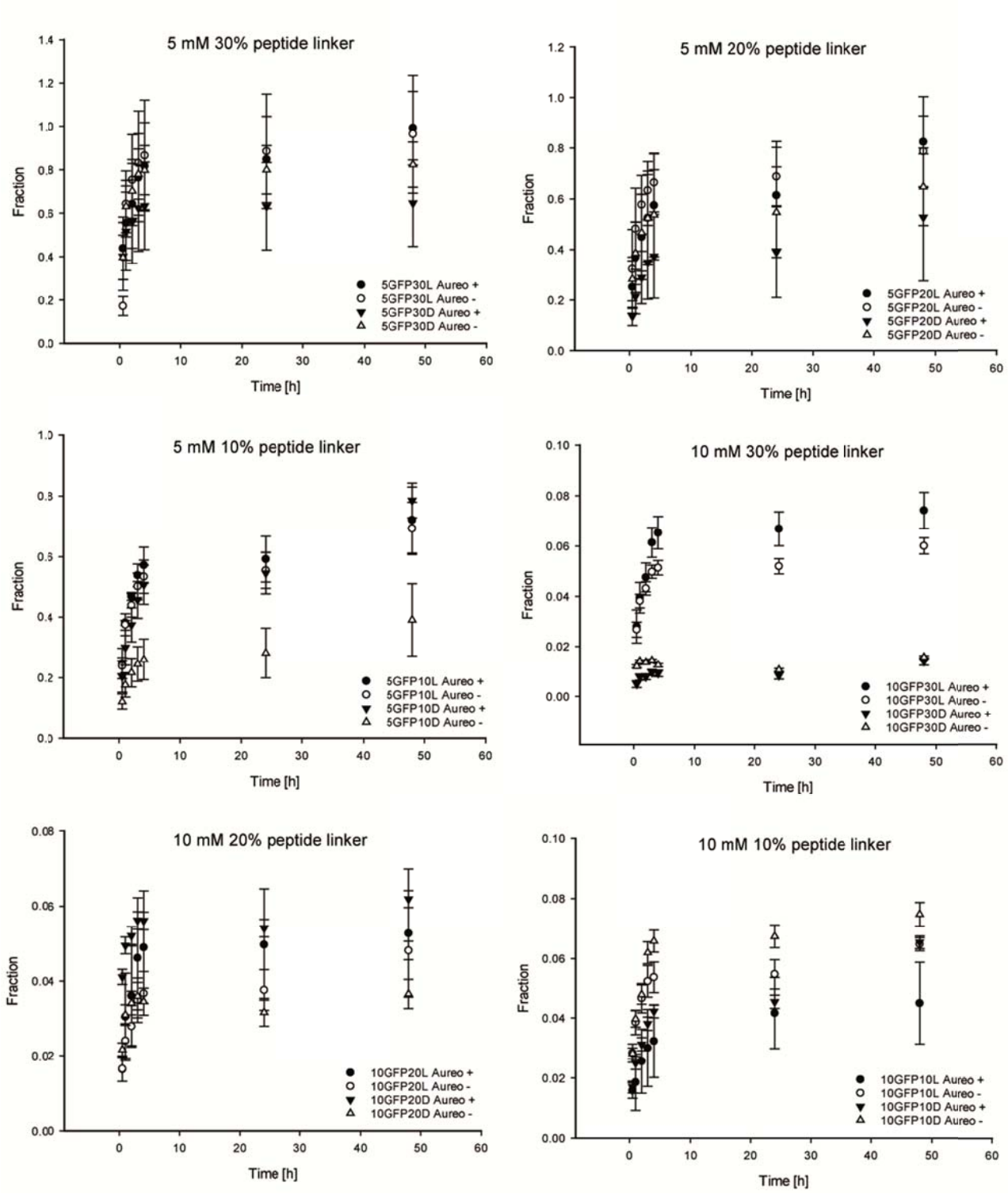

Figure 37 – Fluorophore diffusion fractions over the time for hydrogel formulations.

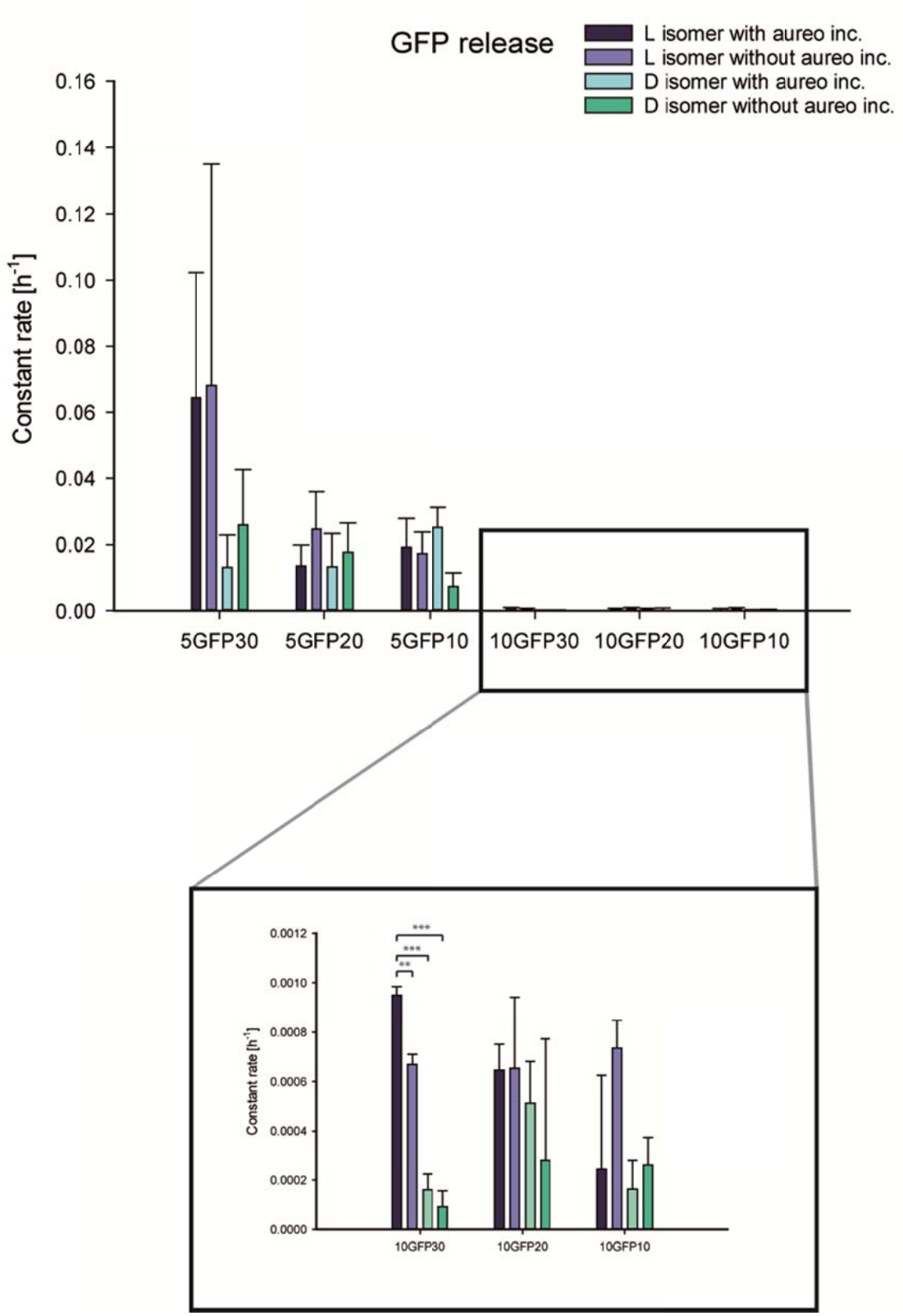

Figure 38 – GFP release over time of different hydrogel formulations. 10GFP30 was the only formulation in which the fluorophore release was faster in comparison to the three negative controls (formulation with D-amino acids and without and/or without aureolysin incubation). One-way ANOVA showed that the constant rate differences are statistically very significant ($p < 0.01$ – marked as **) and extremely significant ($p < 0.001$ – marked as ***).

All formulations with a polymer concentration of 5 mM rapidly released up to 100% of the fluorophore to the medium (**Figure 37**). The systems formulated with the L-isomeric cleavable linker as crosslinkers and incubated with aureolysin did not present a faster release constant when compared to their respective negative controls, I.e. without incubation with aureolysin and/or formulated with non-cleavable D-amino acid isomers). A statistical analysis for those would be not applicable (**Figure 38**).

On the other hand, the 10 mM formulations presented a much lower release due to their increased stiffness reaching only 10% after two days of incubation. Of those hydrogels only the 10GFP30 formulation showed a faster release into the sample which was statistically significant compared to all negative controls. However, the released fraction is still very low and therefore, the strategy of using hydrogels as a polymeric matrix for antibiotic release was changed.

4.3.2 Covalent binding of fluorophore to peptide sequence

A second strategy for the use of a hydrogel system as the polymeric matrix for a bioresponsive antibiotic release system was covalently binding the bioactive compound to the peptide cleavable linker, which would be directly attached to the PVA backbone as previously seen and described in the first strategy (**Figure 39**).

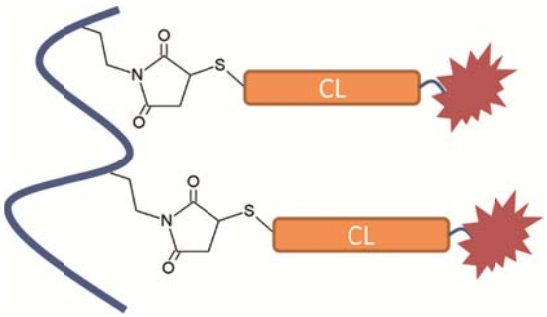

Figure 39 – Schematic depiction of the new strategy. Cleavable peptide sequence is linked by C-terminus cysteine thiol group via cross-linking reaction to hydrogel matrix maleimide molecule.

For this approach, a new linker was synthesized (sequence ID **3d**), containing a cysteine amino acid at the *C*-terminus to provide the thiol group necessary for performing the crosslinking reaction and carboxyfluorescein attached to the *N*-terminus which would be used as an active compound prototype. A PEG spacer containing three ethylene glycol units was also added to each side of the main peptide sequence (**Figures 40 and 41**).

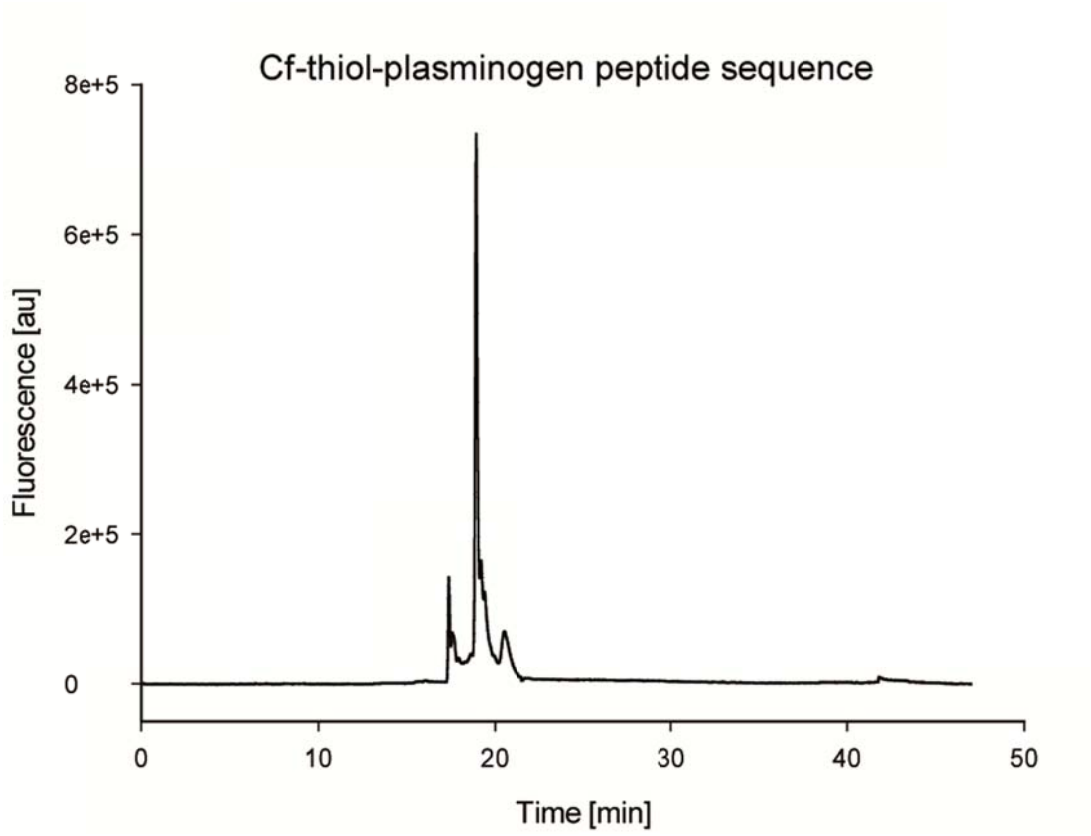

Figure 40 – Chromatogram of L-thiol-Plasminogen peptide sequence (ID 3d). Analyzed with fluorescence detection (Ex/Em: 492/517 nm).

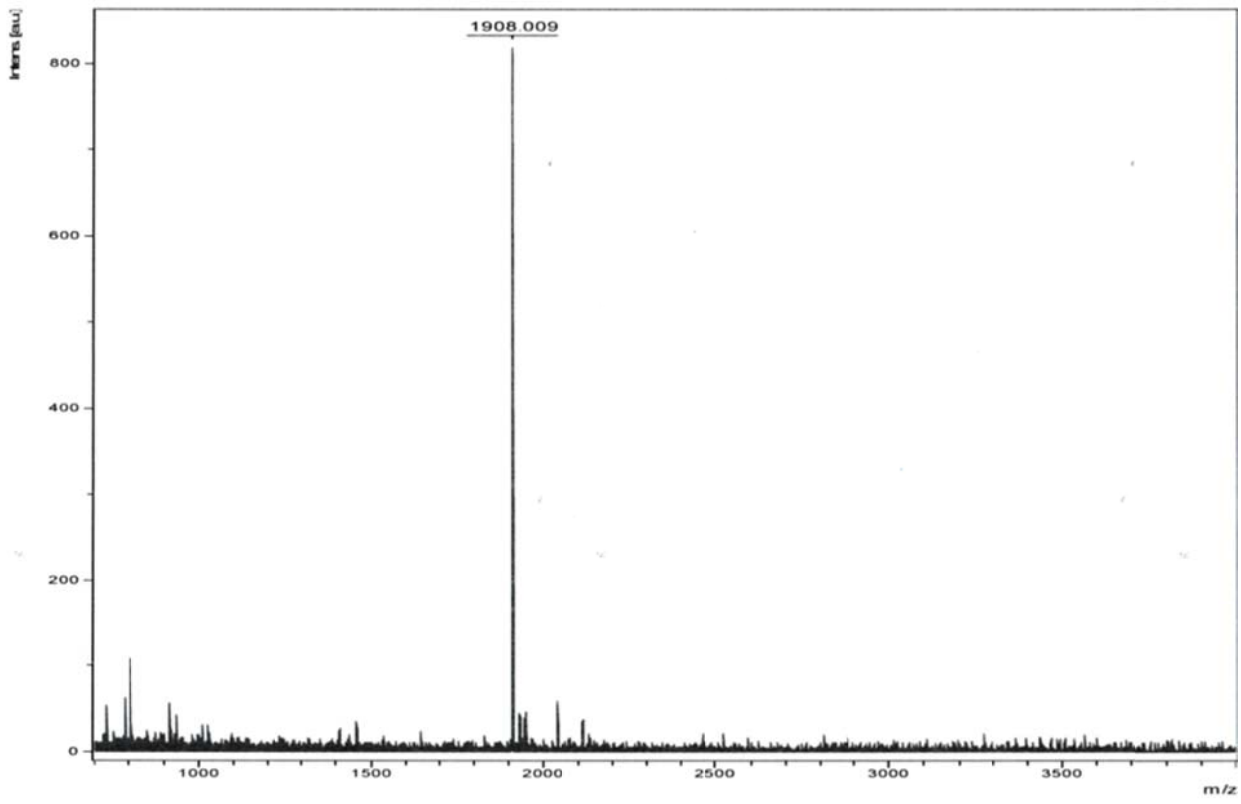

Figure 41 – Mass spectrum of Cf-thiol-plasminogen peptide sequence (ID 3f)

After successfully synthesizing and characterizing the linker, we incubated it with the previously determined optimal aureolysin concentration of 50 ng/mL and analyzed its cleavage profile by UHPLC using a fluorescence detector (Excitation/Emission wavelengths: 492/517 nm) (**Figure 42**) in order to characterize the resulting fragment.

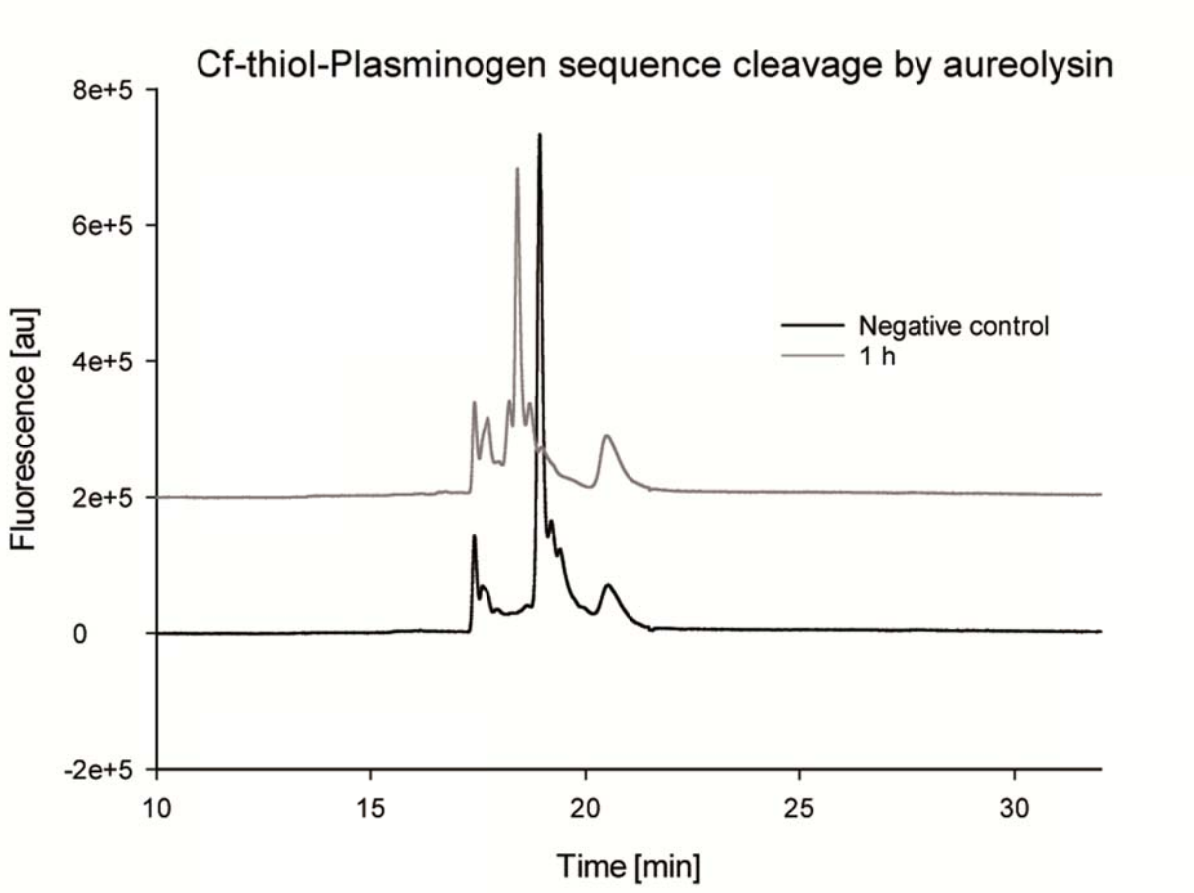

Figure 42 – Overlay of Cf-thiol plasminogen sequences chromatograms before and after 1 h incubation of aureolysin. Analyzed with fluorescence detection (Ex/Em: 492/517 nm).

A mean cleavage rate of 64% could be found which is similar to those observed for the unmodified sequence under the same conditions. The non-cleaved sequence has a retention time of 18.9 min, whereas the main peak resulting from aureolysin incubation appears after 18.4 min.

The next step was to incorporate our peptide linker-carboxyfluorescein system into the hydrogel matrix. For that, a low polymeric concentration of 3 mM was chosen in order to allow the aureolysin enzyme to penetrate into the gel and cleaving the peptide sequences. A peptide:PEG linker ratio of 1:5 was used. After formulating the hydrogel, it was washed with PBS buffer several times to remove any unattached peptide linkers. The system was then incubated with 50 ng/mL aureolysin for one hour. The negative control was not incubated with the target protease. The analysis of the supernatant was performed by UHPLC, again using a fluorescence detector

(excitation/emission wavelengths: 492/517 nm). Even though some additional signals due to impurities are present in the chromatogram, it is possible to observe that the hydrogel formulation incubated with aureolysin presented a peak with a retention time of 18.4 min, which corresponds to the exact time observed for the free linker not appearing for the negative control (**Figure 43**).

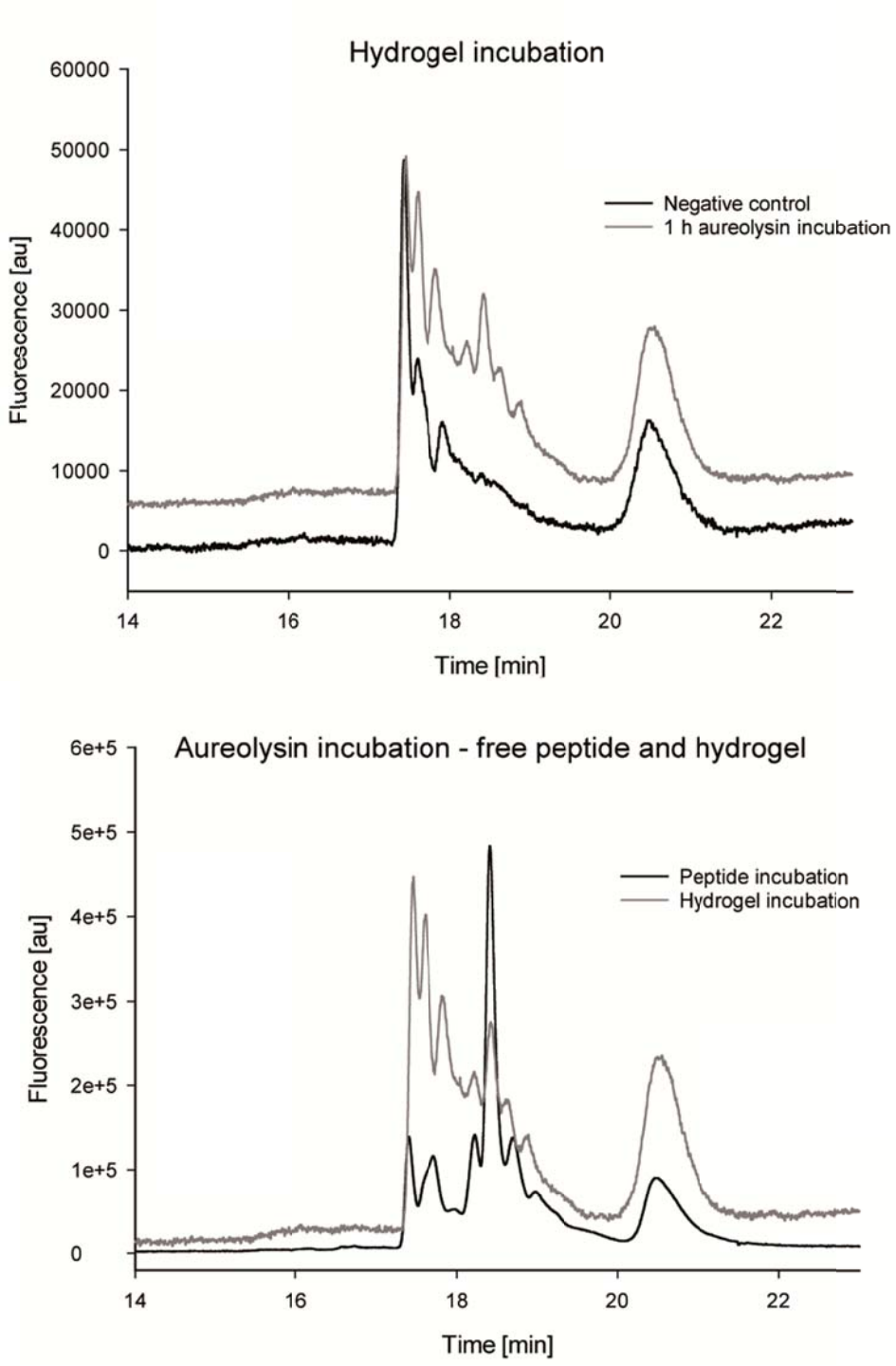

Figure 43 –Chromatograms hydrogel incubation with and without aureolysin (above) and peptide incubation and hydrogel incubation with aureolysin (below).

4.4 Aminopeptidase activity determination

4.4.1 Synthesis and characterization of aminopeptidase substrate

Aminopeptidases are a class of exopeptidases being abundantly present in humans. Their ability of cleaving amino acids from the *N*-terminus of a peptide sequence makes them a useful bioresponsive tool for fully releasing the active compound once the intact linker is cleaved by the staphylococcal metalloprotease aureolysin (**Figure 44**). Aminopeptidases are not supposed to have an effect upon the intact linker since its *N*-terminus would be covalently attached to a polymer in order to enhance its pharmacokinetic profile.

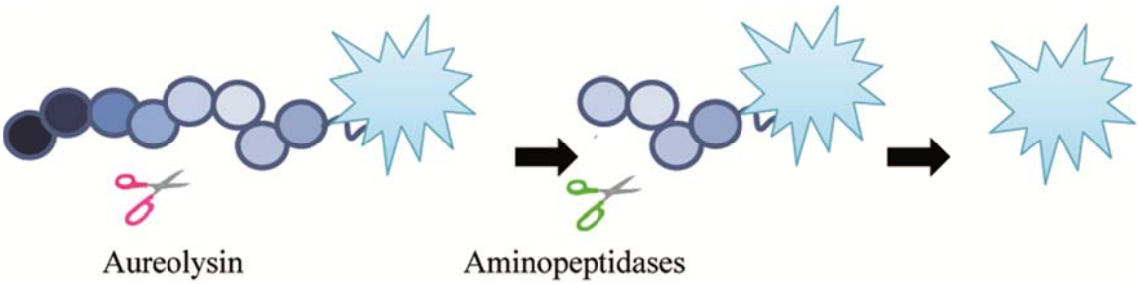

Figure 44 – Representation of using plasmatic aminopeptidases as a bioresponsive tool for the complete release of antibiotic in case of a bacterial infection. The virulent protease aureolysin (depicted as the pink scissors) would cleave the linker and partially release the antibiotic, which would still have at least 4 amino acids covalently bound to an amine group. Aminopeptidases (depicted as the green scissors) present in plasma would cleave each *N*-termini attached amino acid until completely releasing the active compound (depicted as the blue star).

For this step we synthesized the resulted fragment after aureolysin cleavage with a fluorophore attached to its *C*-terminus (peptide 4a). We firstly synthesized tetrapeptide **4b** via SPPS. After cleaving the sequence from the resin, its *C*-terminus was conjugated to the primary amino group present in the prototype compound. The chosen fluorophore for this step was aminofluorescein (Af), since it has a free primary amino group enabling the conjugation with the peptide fragment.

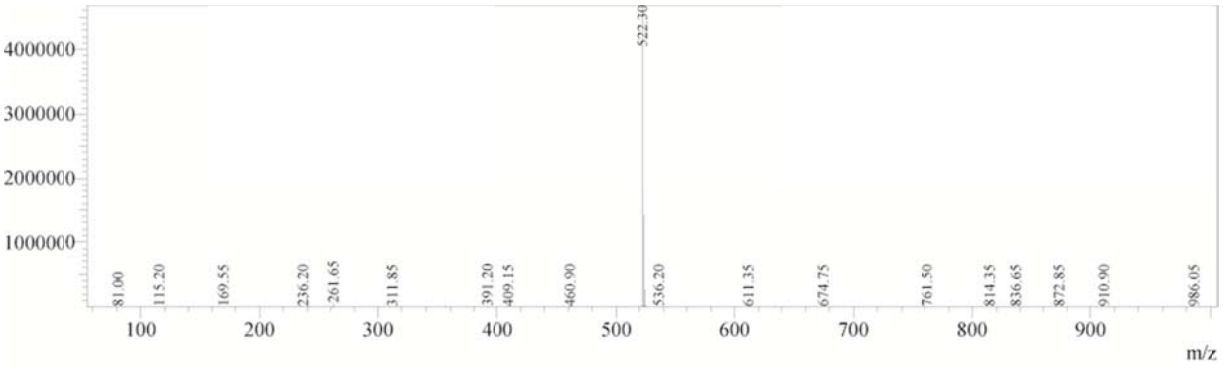

Figure 45 – Mass spectrum of KVYL peptide. Calculated mass: 522 m/z.

After the successful synthesis of KVYL peptide (**Figure 45**) was confirmed, it was coupled to the amino group of aminofluorescein by its *C*-terminal carboxyl group by EDC/NHS conjugation reaction. This reaction was performed using DMF as solvent since the intermediary product is very unstable in water and hydrolyzes quickly, thus becoming inactive and not allowing both components to couple.

The resulting product **4a** was confirmed by mass spectrometry (**Figure 46**) and its purity was characterized by UHPLC applying fluorescence detection (excitation/emission wavelengths: 492/510 nm (**Figure 47**).

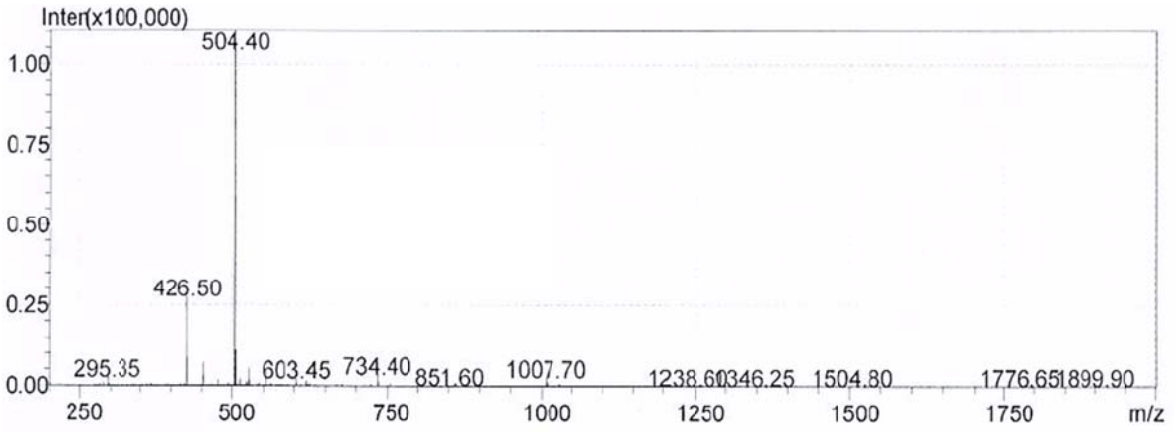

Figure 46 – Mass spectrum of KVYL-Af peptide. Calculated mass: 851 m/z. It is possible to identify the single charged mass of 851.60 and the double charged of 426.50 m/z.

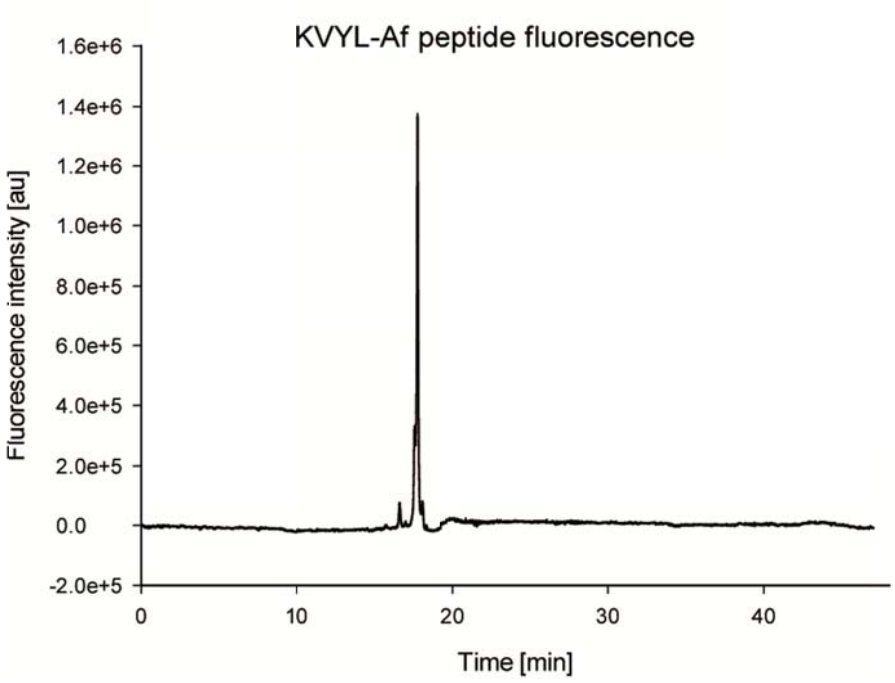

Figure 47 – Chromatogram of KVYL-Af peptide (ID 4a). Analyzed with fluorescence detection (Ex/Em: 492/517 nm).

4.4.2 Determination of aminopeptidase concentrations in human plasma

Before we performed any aminopeptidase activity assays, the basal concentration of these enzymes in human plasma was investigated by using L-leucine-*p*-nitroanilide (0.5 mg/mL) as a substrate being specific for AP. A linear standard curve was established by serially diluting AP from porcine kidney dissolved in AP buffer and adding to the substrate. Using the results obtained after establishing a linear correlation, it was possible to calculate the concentration of the aminopeptidase based on the absorption obtained after incubating the plasma samples with L-leucine-*p*-nitroanilide (**Figure 48**). Basal AP concentration was determined in plasma samples ranging from 0.72 to 3.6 µg/mL (n = 7) obtained from the Institute for Transfusion Medicine and Haemotherapy in Würzburg.

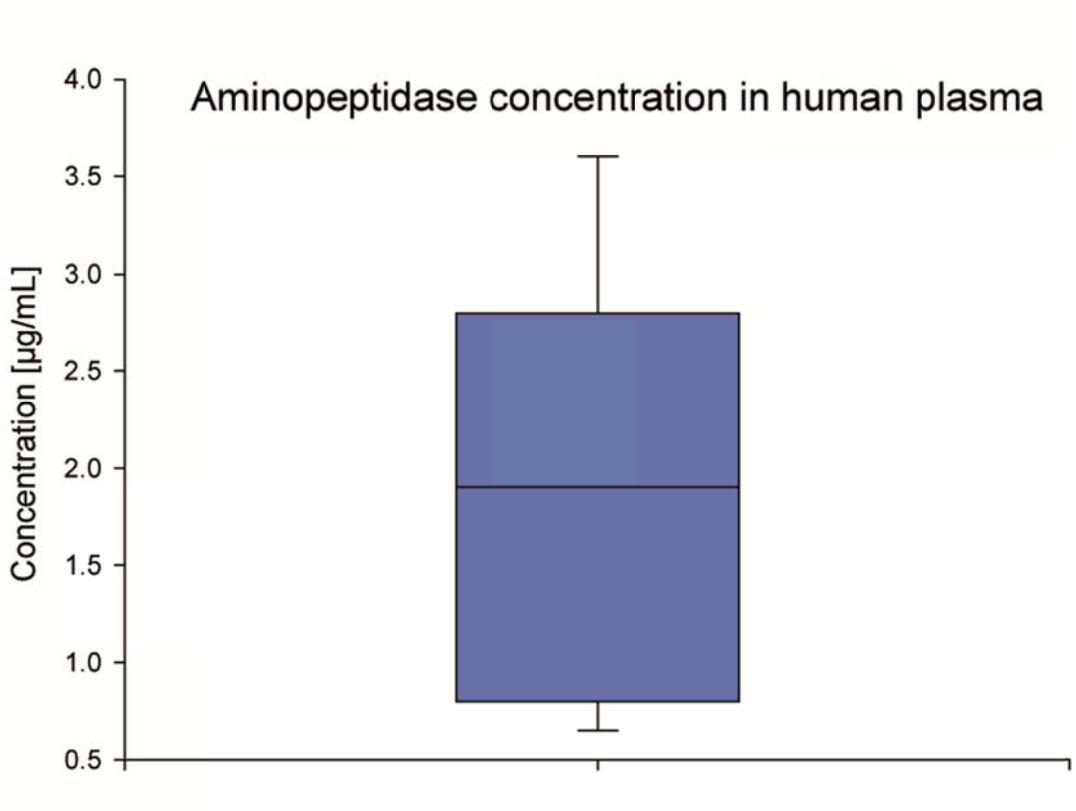

Figure 48 – Basal aminopeptidase concentrations in human plasma. Box-and-whisker plots show the median (solid line), the box contains the middle 50% of values and the whiskers show the lower and upper 25 percent of the data, respectively.

4.4.3 Release assays by aminopeptidase

In order to analyze the impact of AP concentration on peptide cleavage and fluorophore release, we incubated the substrate (concentration 0.5 mg/mL) with 3.6, 1.8, 0.72, 0.36, and 0.18 µg/mL of AP dissolved in an appropriate buffer. These values were chosen to be the highest values within the measured plasma concentrations. The reaction was incubated under conditions previously described. Release was quantified by determining the relative increase of the peak area corresponding to the signal due to the fluorophore during the assay (**Figure 49**).

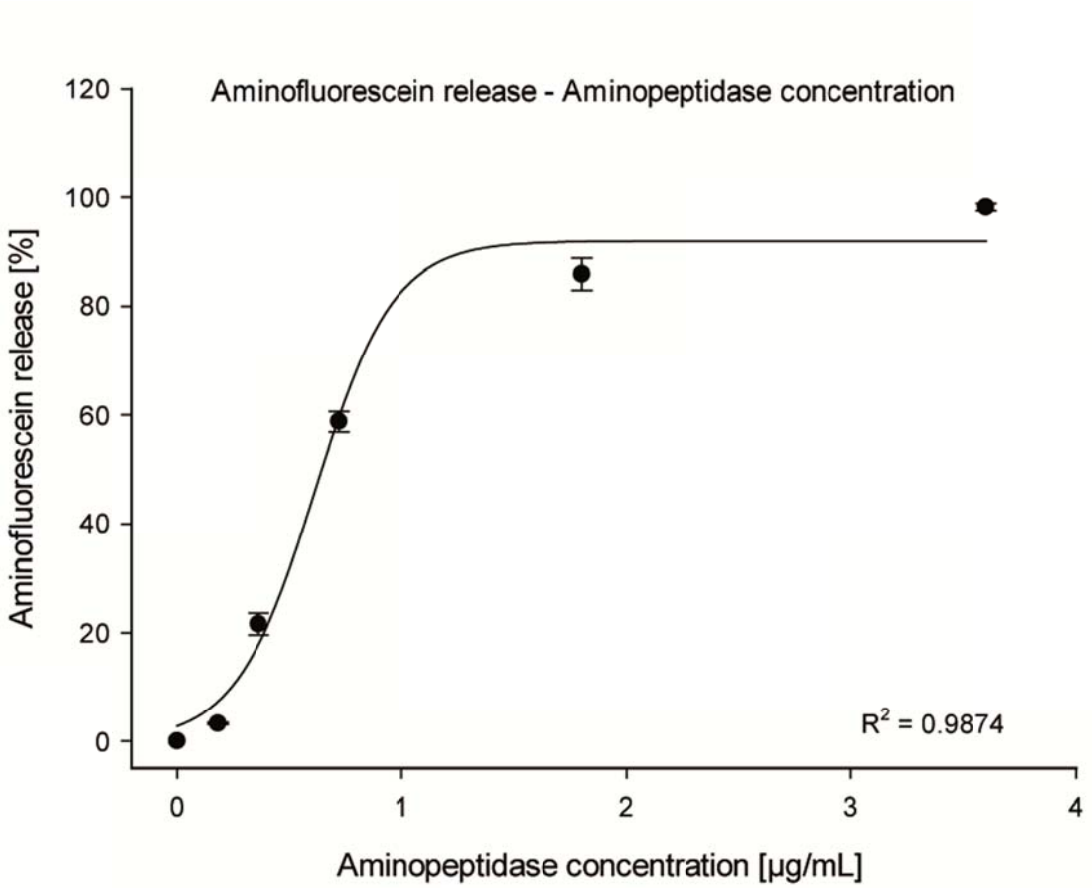

Figure 49 – Complete release of the fluorophore by aminopeptidase.

Within the measured AP plasma concentration range, at least 60% of the fluorophore was completely released after one hour of incubation. It is essential that this release occurs in a very fast manner, since once the peptide sequence was cleaved by the bacterial protease, this means that the bacteria are in their virulent state and therefore, the antibiotic should be available to act on site as quickly as possible.

However, a "worst case scenario" should preferably be presumed, in which the plasmatic AP concentration is very low. Thus, in order to evaluate the impact of AP release over time, we decided to perform the assay at an AP concentration of 0.72 µg/mL. This was not only the lowest concentration measured in human plasma samples, but also represents the concentration corresponding to 60% of complete release of the fluorophore within one hour (**Figure** 50).

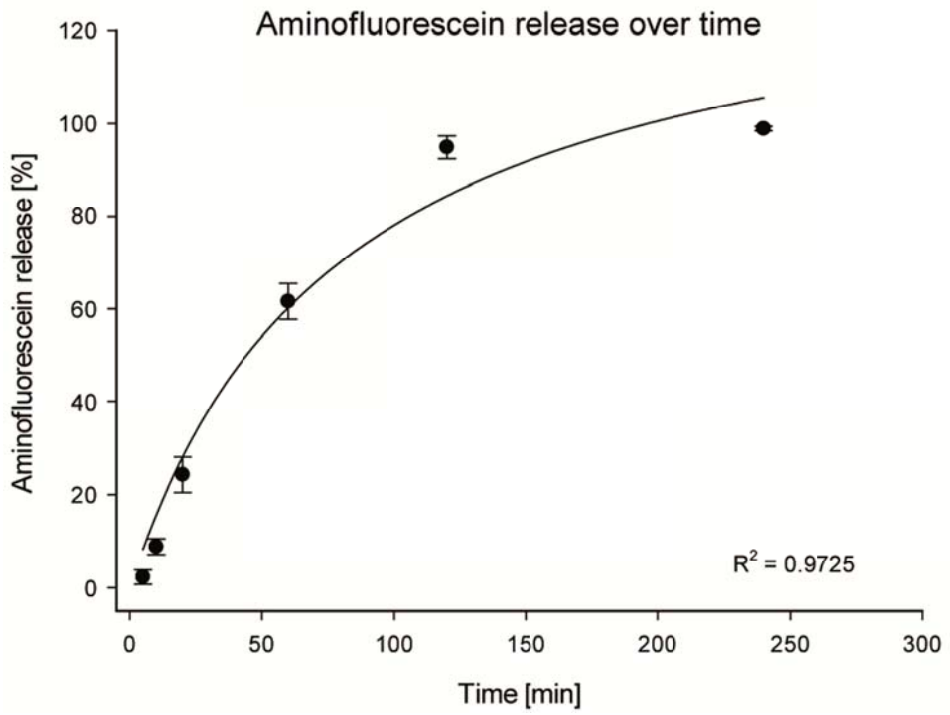

Figure 50 – Aminofluorescein release over time by aminopeptidase digestion at a concentration of 0.72 µg/mL.

Within two hours at the lowest AP concentration measured in human plasma, already 100% of the fluorophore was released, evidencing the rapid mechanism of action of aminopeptidases and corroborating to our strategy of using this human protease as a bioresponsive tool for the controlled release of antibiotic compounds.

By incubating the peptide sequence utilizing the determined mean AP concentration of 1.7 µg/mL, we observed the cleavage of each *N*-terminal amino acid and identified each resulting fragment by LC-MS with respect to their molar masses (**Table 5**).

Table 5 – Intermediate amino acids - aminofluorescein fragments formed by aminopeptidase activity, until the complete release of the fluorophore.

Fragment	Molar mass [Da]
KVYL-Af	851
VYL-Af	724
YL-Af	624
L-Af	462
Af	347

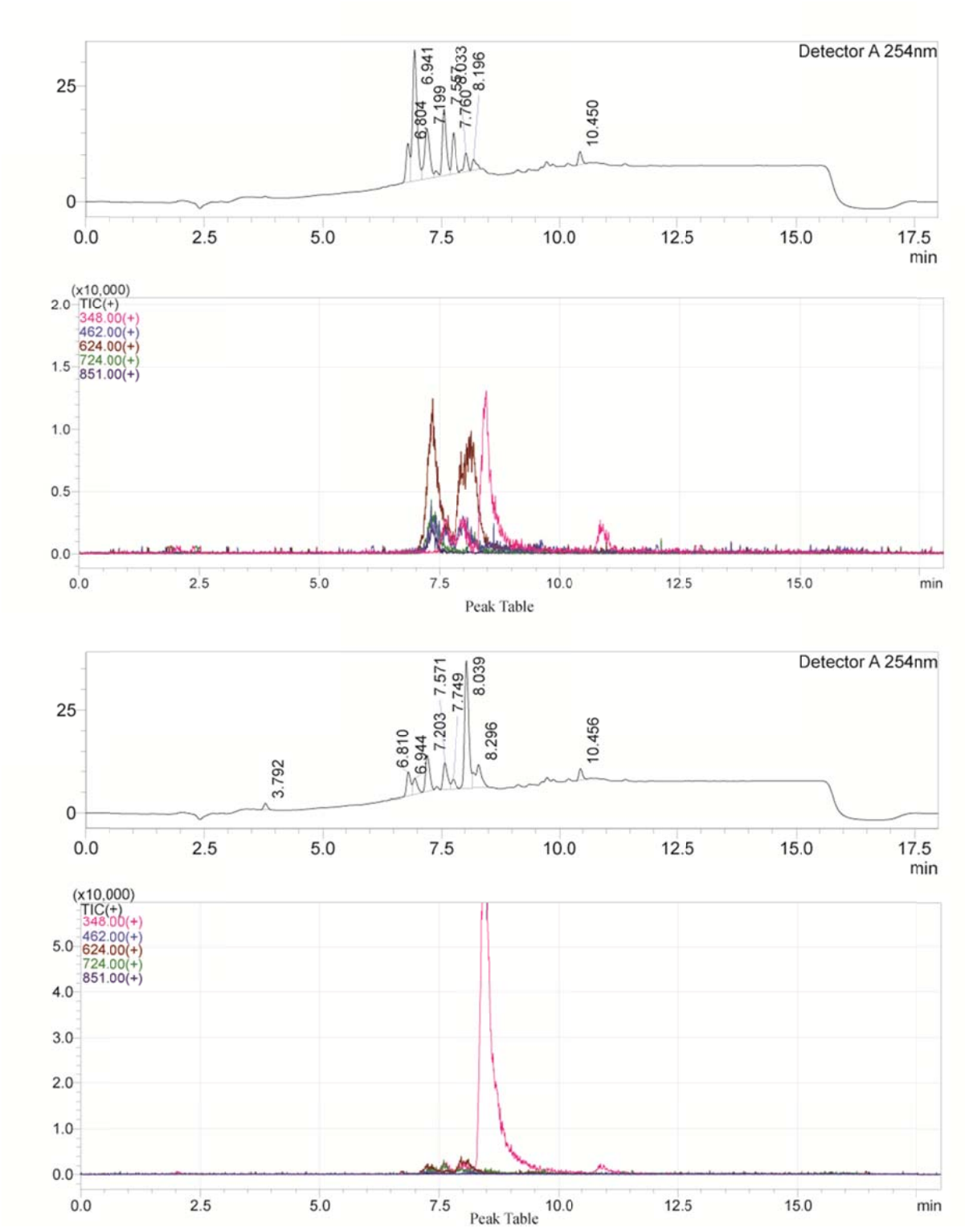

Figure 51 – Chromatograms for full release of Af after 15 (above) and 30 min (below) incubation.

After 15 minutes, it is possible to observe the masses of both resulting fragments and the free fluorophore. After 30 minutes, almost all intermediate fragments were digested by the aminopeptidase and only the mass corresponding to Af is found (**Figure 51**).

The rapid and complete release of the fluorophore, which is serving as a substitute for potential antibiotics, is an indicative of success for using aminopeptidase as a secondary bioresponsive tool. The first cleavage of the intact peptide linker would indicate the presence of virulent *S. aureus*, therefore the full release of the antibiotic by the secondary bioresponsive action of plasmatic aminopeptidases should occur as quickly as possible.

After fully characterizing the kinetic parameters for cleavage of the designed linker as well as the complete release of the antibiotic prototype, our next and final step was to find a suitable formulation and a polymer carrier or matrix, respectively, to accommodate our release system.

4.5 Construction of a PEGylated chelocardin release system

4.5.1 Synthesis of a CHD linker

Having the linker fully characterized as a bioresponsive release strategy, the next step was to design a suitable carrier in order to allow a systemic distribution of the compound and to have a broader field of application for fighting possible opportunistic infections. Besides, we wanted to identify a distinct antibiotic during this step so that the system could be tested in *in vitro* assays. The tetracycline derivative chelocardin was chosen and synthesized at the Helmholtz Intitute for Pharmaceutic Research (HIPS) (Saarbrücken, Germany). The molecule carries a primary amino group at the C4 position which is necessary for sucessfully achieving a coupling reaction to our peptide linker.

In general, a conjugation reaction between an amino group and a carboxygroup is not specific and any amino group can conjugate to any carboxylgroup present in a particular system. Therefore, we needed to change the synthesis strategy of the peptide linker since our chosen amino acid sequence contains side chains carrying both carboxyl group (e.g., glutamic acid) and amino groups (e.g., lysine). The peptide sequence was synthesized according to the conventional protocol using the CTC resin; however, the cleavage off from the resin was performed using only 1% (v/v) TFA in DCM. This would allow the protective groups of the linker to remain intact during the conjugation reaction to chelocardin, which would then only attach to the free *C*-terminus. After successful coupling, the peptide would be incubated in 90% TFA in DCM (v/v) in order to detach the protecting groups (**Figure 52**).

To conjugate our linker-CHD system to a PEG carrier, the *N*-terminus of the peptide sequence was functionalized with an azido group provided by 2-azidoacetic acid. This compound provides an advantage in comparison to traditionally utilized azido-amino acids such as azidoalanine, since the azido group is not localized within a side chain but at the backbone of the peptide sequence.

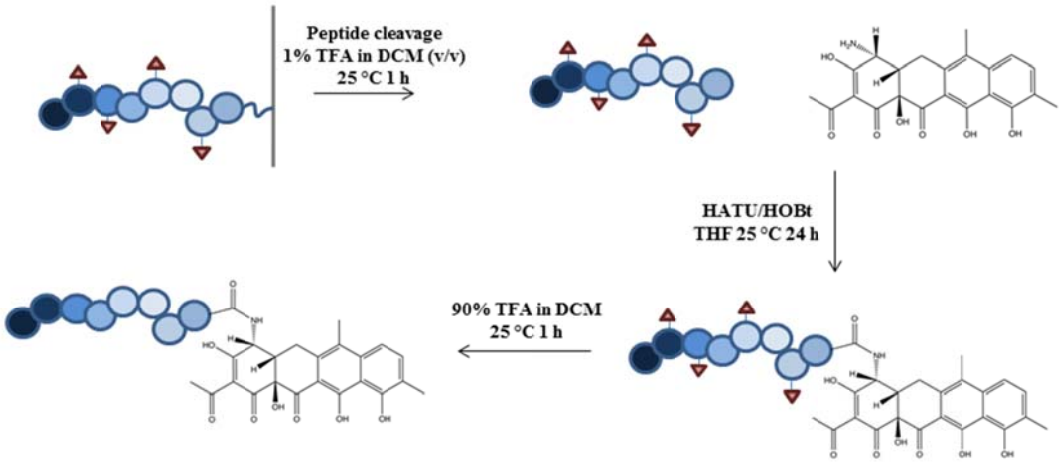

Figure 52 – Schematic depiction of linker synthesis strategy followed by conjugation to tetracycline via HATU/HOBt coupling. Peptide sequence is synthesized using acid labile resin CTC and cleaved using a mixture of only 1% TFA in DCM (v/v), which would leave protecting groups (depicted as red triangles) still attached to the amino acid side chains. After the conjugation with chelocardin, the linker-antibiotic system is incubated in 90% TFA in DCM (v/v) for one hour to detach those groups.

After the linker synthesis and its cleavage from the resin, the resulted product was poorly soluble in water and acetonitrile due to the presence of the respective side chain protecting groups, making its purification with the Äkta system unviable. However, at least dissolving partial amounts allowed to analyze the product by RP-HPLC (**Figure 53**) which confirmed an acceptable purity › 90% and therefore could be directly used for conjugation steps. Of note, the expected mass 1433.9 m/z was found (**Figure 54**).

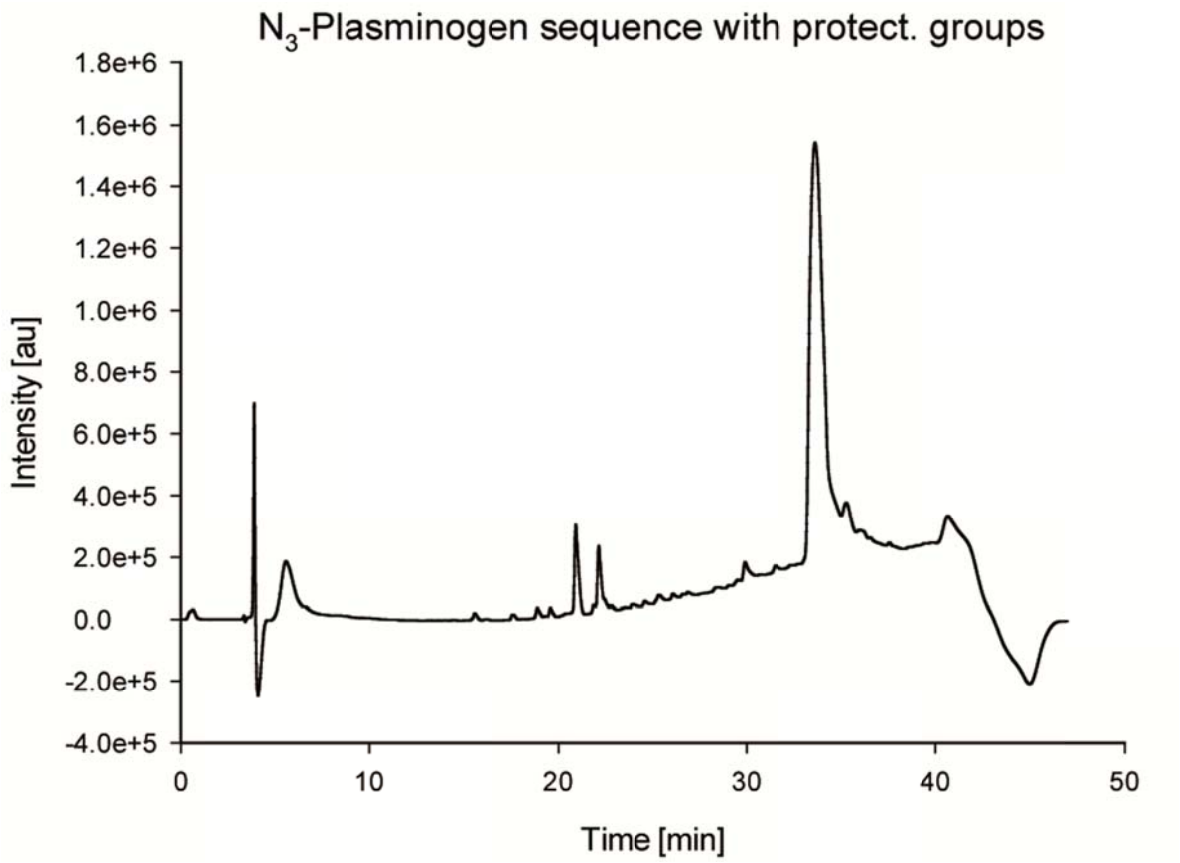

Figure 53 – Chromatogram of N_3-plasminogen peptide sequence with protecting groups (ID 3e).

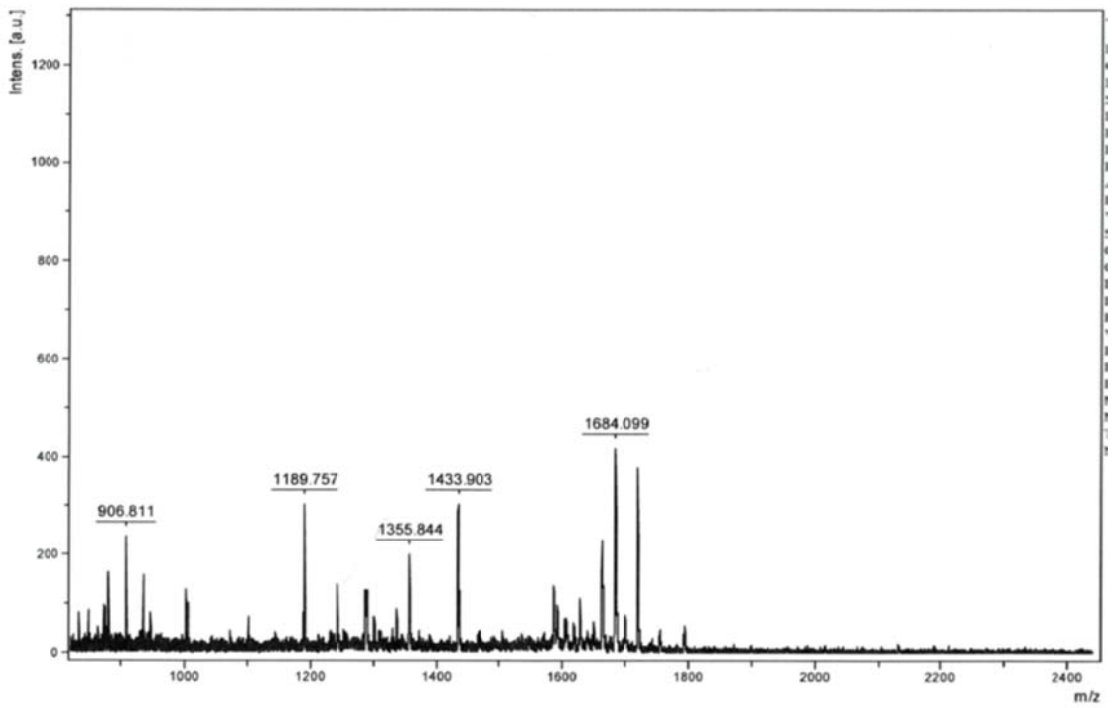

Figure 54 – Mass spectrum of N_3-plasminogen peptide sequence with protecting groups (ID 3e). Expected mass: 1434.53 m/z.

After finding the right mass, we coupled the protected linker to CHD (**Figures 55, 56**). It was chosen not to perform an EDC/NHS reaction due to the possible epimerization of the compound because the corresponding epimer does not have any antimicrobial activity. The reaction was performed after a protocol developed at HIPS in Saarbrücken by Dr. Antoine Abou Fayad using HATU and HOBt as coupling reagents along with DIPEA to provide a basic condition.

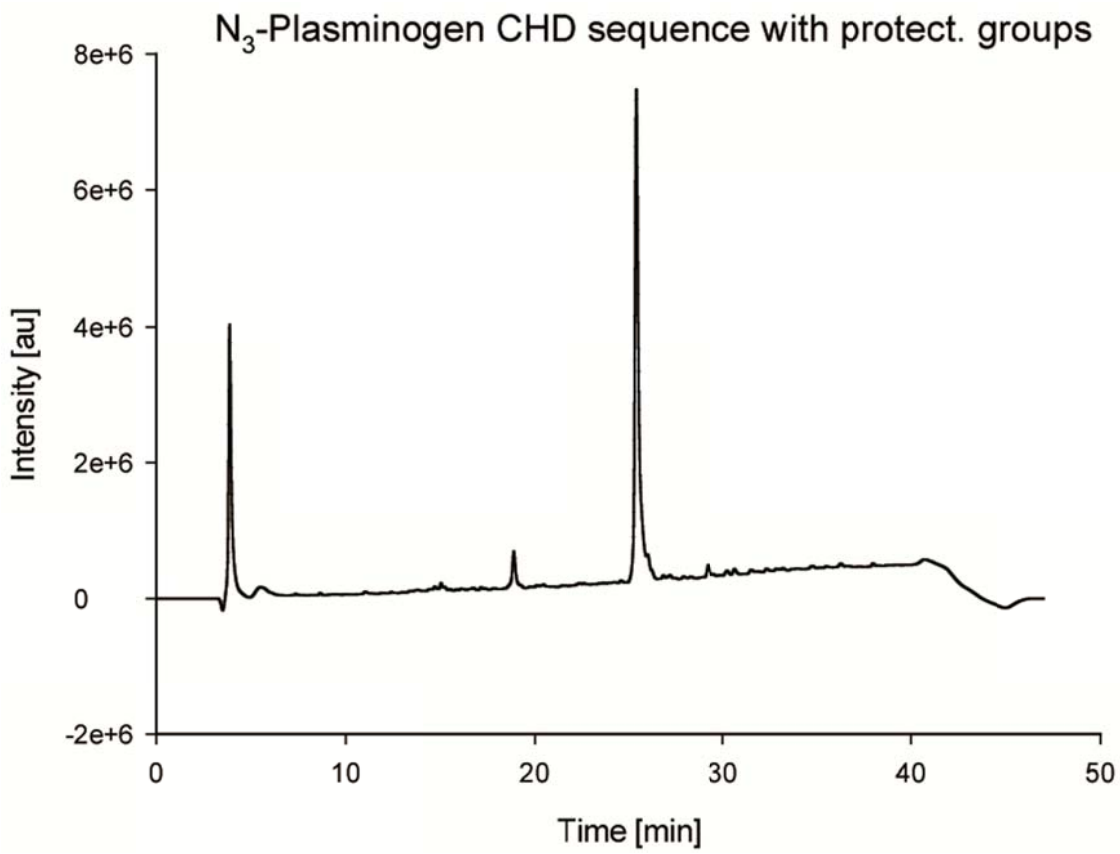

Figure 55 – Chromatogram of N_3-plasminogen peptide sequence with protecting groups after conjugation reaction with CHD.

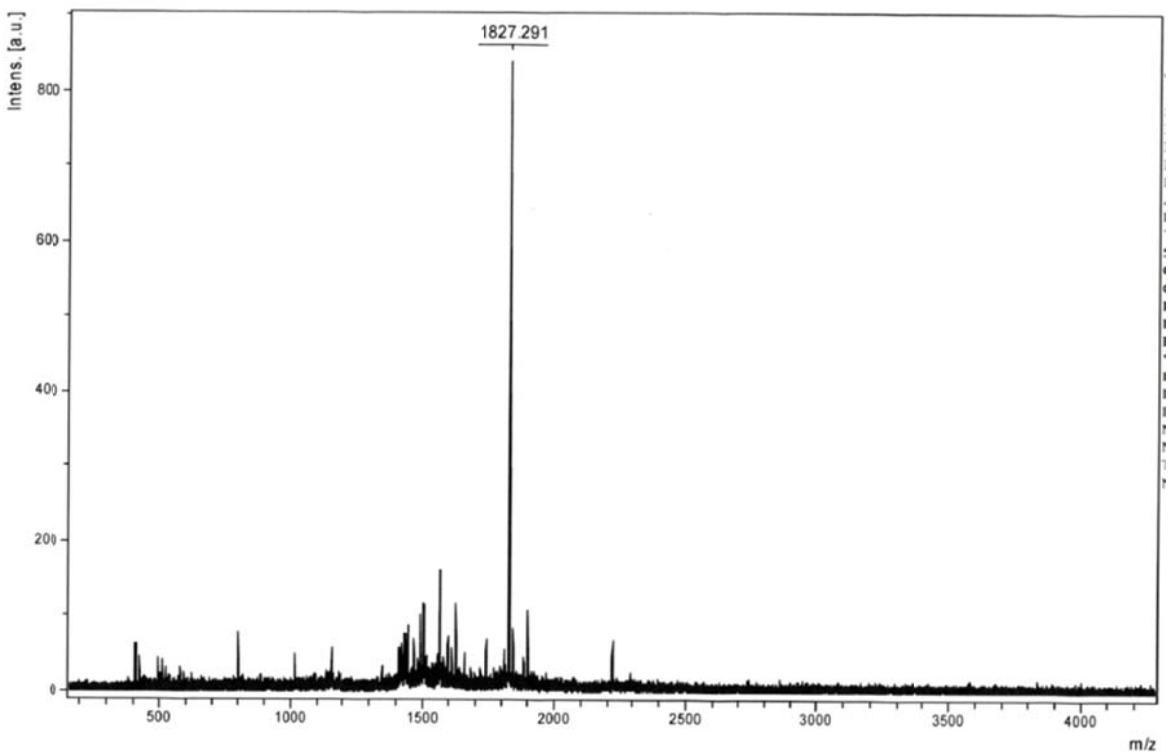

Figure 56 – Mass spectrum of N_3-plasminogen peptide sequence with protecting groups coupled to CHD. Expected mass: 1827.818 m/z.

After successfully conjugating CHD to the peptide sequence, it was incubated in 95% (v/v) TFA in DCM in order to deprotect the amino acid side chains. Protecting groups such as *tert*-butyloxycarbonyl (BOC) or *tert*-butyl substituents (t-Bu) are only cleaved when incubated in a strong acidic medium.

After the incubation in an acidic medium it is expected that the peptide linker becomes more hydrophilic and therefore, is more likely to be soluble in water. Indeed, the protected linker was only partially soluble in 100% ACN and the deprotected product could be completely dissolved in 35% (v/v) of ACN in water. The difference in polarity could be confirmed by RP-HPLC (**Figure 57**) and the identity of the unprotected sequence was verified by MALDI (**Figure 58**).

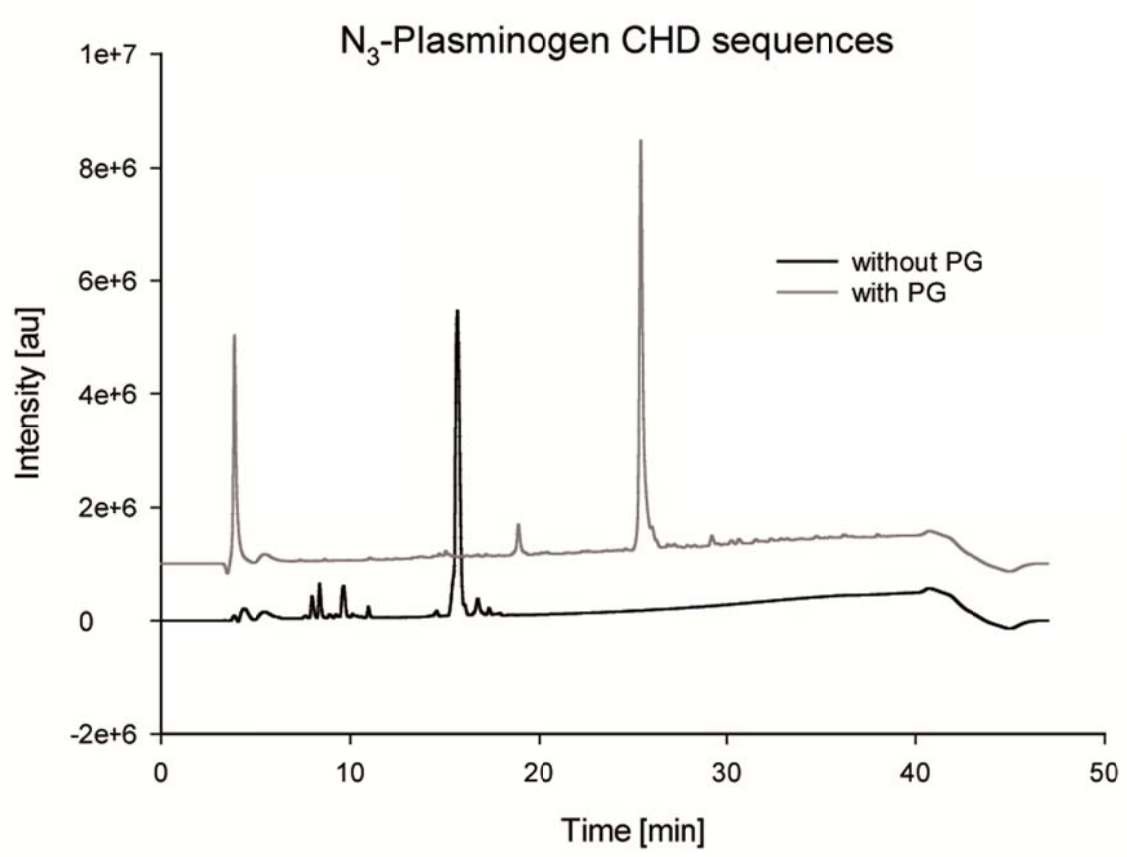

Figure 57 – Chromatogram of N3-plasminogen CHD peptide sequence with and without PG.

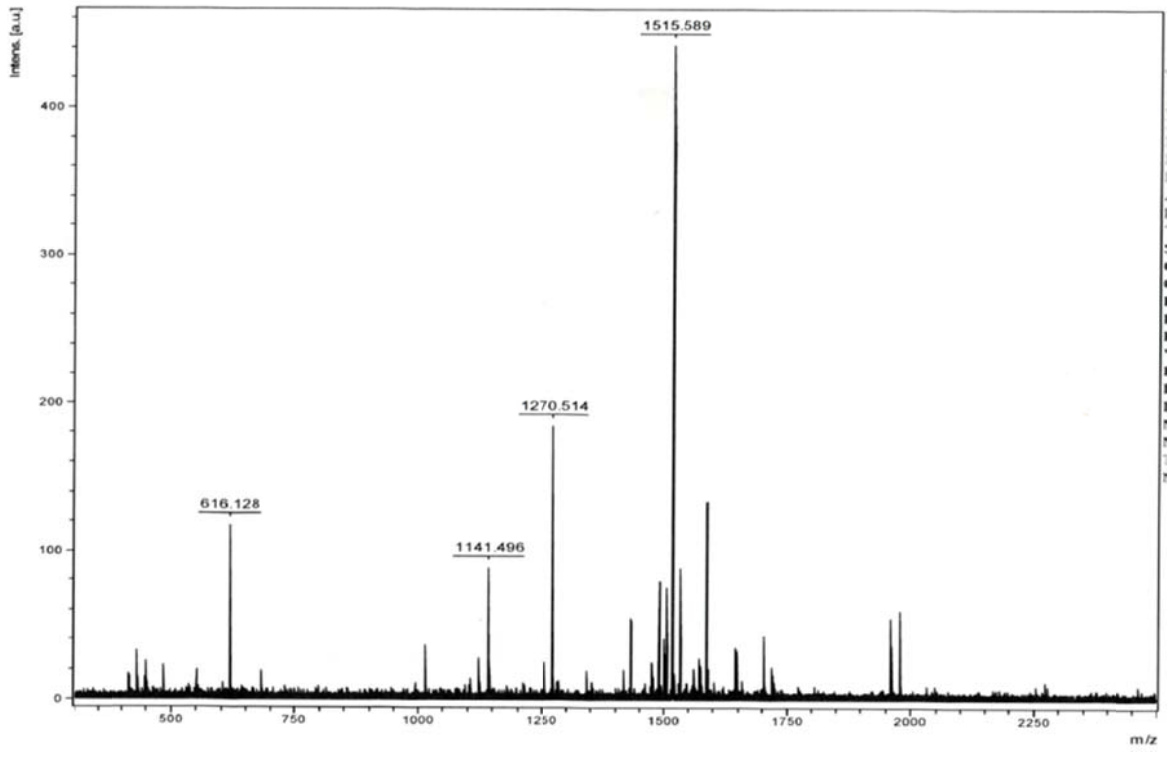

Figure 58 – Mass spectrum of N_3-plasminogen peptide sequence without protecting groups coupled to CHD. Expected mass: 1517.314 m/z.

4.5.2 Conjugation of CHD linker to PEG via copper-free click reaction

After the synthesis of a peptide linker conjugated to chelocardin, the next step was to click the construct to a linear PEG polymer. The PEG has the function of enhancing the pharmacokinetic profile of the system which would circulate through the body for a longer time period [153]. This conjugation was performed by copper free click chemistry, a bioorthogonal reaction which is a variant to the *Huigen* cycloaddition having the advantage of avoiding any cytotoxic copper catalysis [154].

In order to perform the cycloaddition, a 10 kDa PEG functionalized with a DBCO group was used. DBCO will click with the azido group already present at the *N*-terminus from the synthesized linker. The reaction was incubated for 48 hours in PBS, pH = 7.4 at 25 °C. Afterwards, the product was purified using Äkta Systems. To optimize purification and to allow a quicker identification of the construct, two different wavelengths were used, i.e. 214 nm and 307 nm. Usually, amide bounds can be determined at 214 nm, whereas the DBCO group exhibits an absoprtion maximum at 307 nm. Thus, peaks being detectable at those two wavelengths would probably indicate the presence of our construct (**Figure 59**).

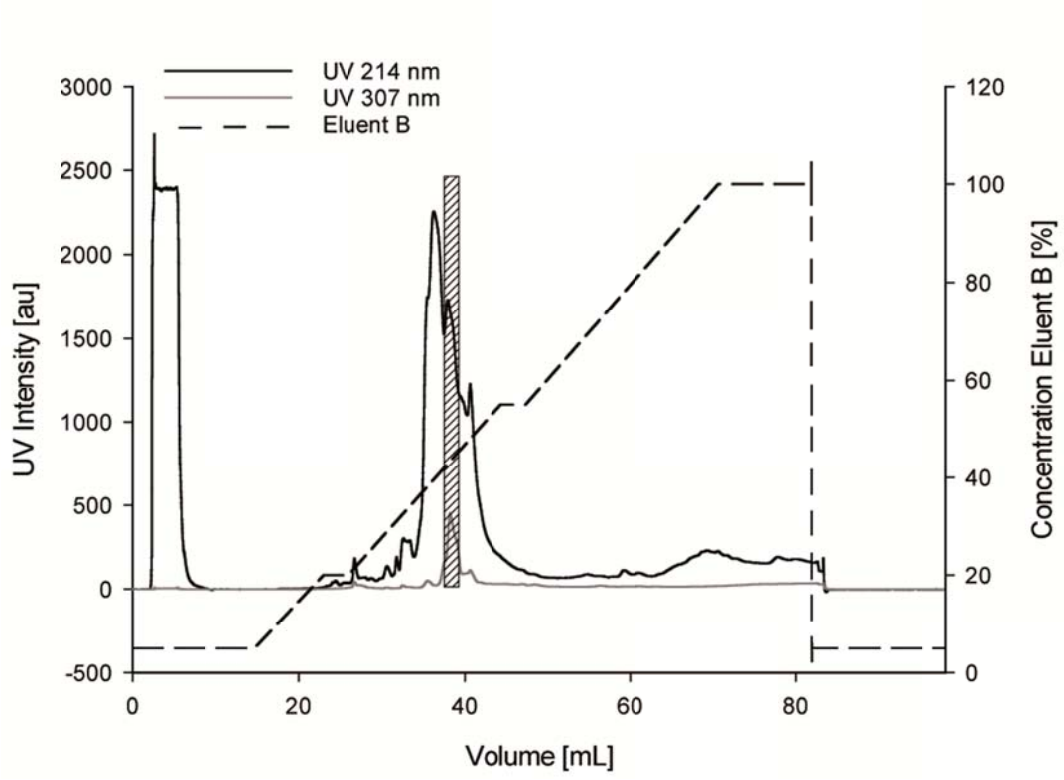

Figure 59 – ÄKTA chromatogram of PEG-linker-CHD construct purification.. The collected fraction is marked in the chromatogram.

Confirming the conjugation of our release system was performed by MALDI. The used DBCO-PEG has a molar mass of about 10 kDa. However, since the system is polydisperse, it is not possible to determine an exact mass rather than a mass distribution. Therefore, analysis was based on a peak shift observed at the respective spectrum. Indeed, the collected fraction presented a compound having a mass of about 11900 Da which would corroborate to a successful conjugation of the linker-CHD (molar mass: 1517 Da) with PEG-DBCO (**Figure 60**).

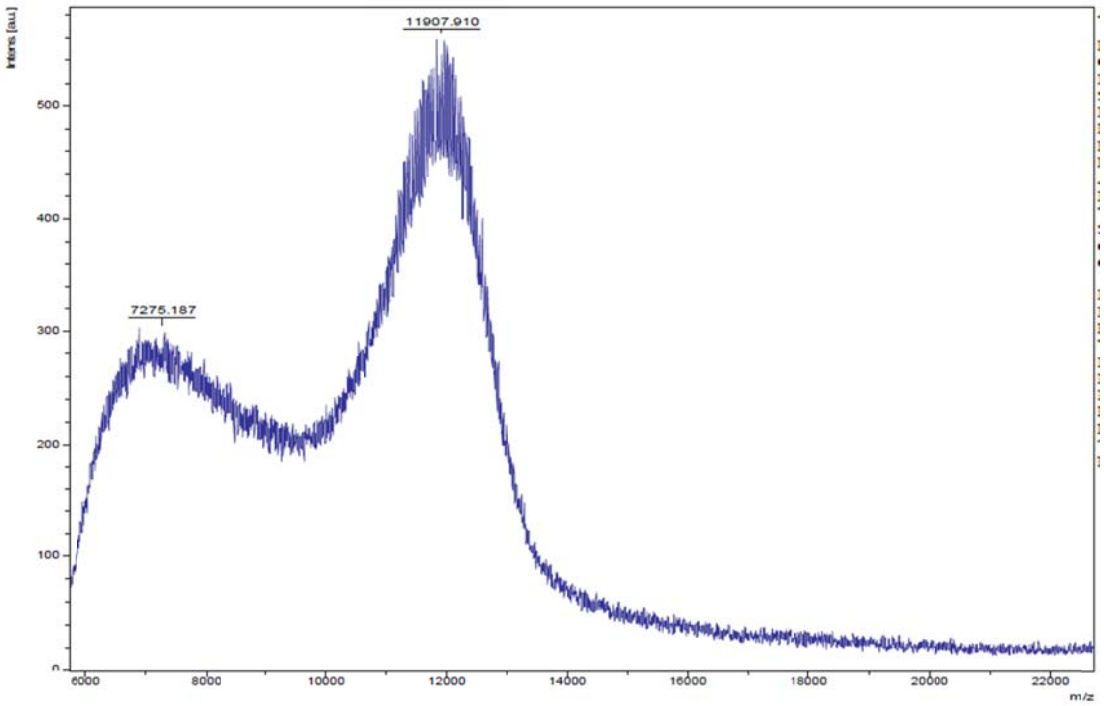

Figure 60 – Mass spectrum of PEG-Plasminogen-CHD construct. As the used DBCO-PEG is a polydisperse system, a mass distribution was obtained instead of an exact peak.

4.5.3 Antibiotic release by aureolysin cleavage

Having achieved the construction of the designed system, we wanted to investigate the release profile by aureolysin, i.e., if the conjugated polymer would interfere during the protease reaction. For this, the system was incubated with the bacterial enzyme under the same conditions established before. Since achieving a rapid response is very desirable, we wanted to investigate how much antibiotic would be released after two hours of incubation. Thus, the experiment was not performed any longer.

A peak having a retention time of 12.1 min appeared, corresponding to the released fragment after aureolysin cleavage. Another broader peak appears right after the construct. This corresponds to the PEG fragment after linker cleavage by aureolysin. Since the PEG polymer does not present an exact mass but a polydisperse distribution, HPLC analysis did not provide a sharp

peak but a broad distribution as well (**Figure 61**). Therefore, it was not possible to quantify the release profile based on the decrease of the uncleaved peak as done before. Instead, the area under the curve of the emerging peak corresponding to the released fragment was evaluated and normalized to a CHD standard curve (**Figure 62**).

The cleavage profile for the PEGylated construct is similar of those observed for the non-PEGylated linker. Within two hours, about 60% of the initial sequence was cleaved for both constructs.

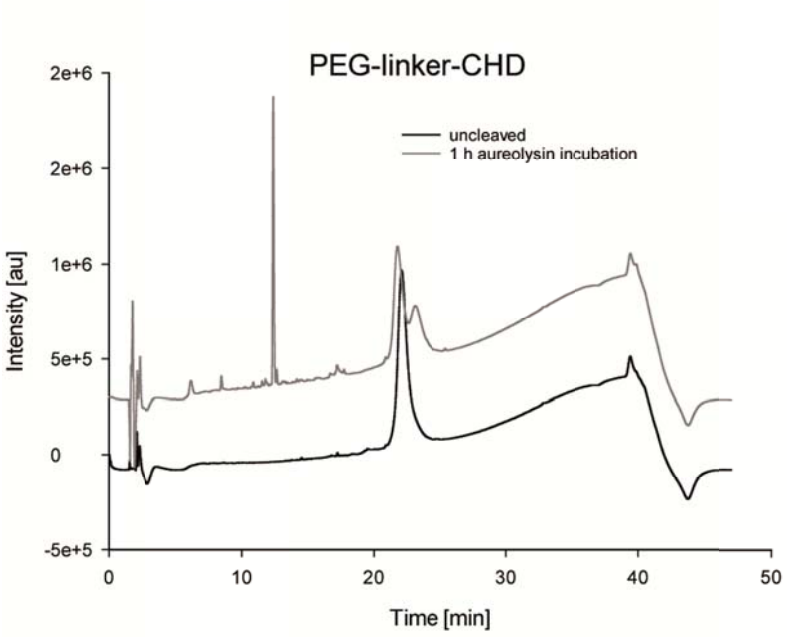

Figure 61 – Chromatograms of PEG-linker-CHD construct before and after incubation with aureolysin. After incubation, a sharp peak correspondent to the released peptide-CHD fragment appears, as well as a broader peak next to the uncleaved construct, which corresponds to the PEG polymer released after cleavage.

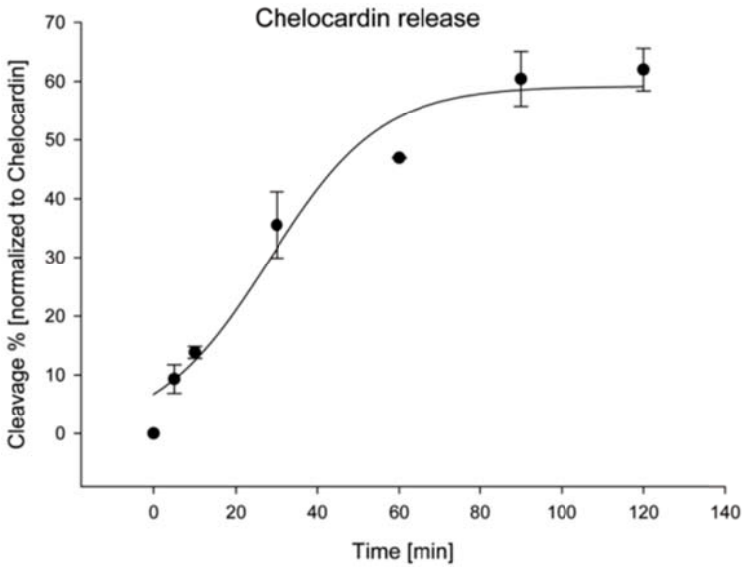

Figure 62 – Release profile of CHD from PEG-linker-CHD release system after incubation with aureolysin.

4.5.4 Loading optimization of CHD

The obtained PEGylated antibiotic release system presents a polymer:CHD ratio of 1:1. In order to increase the loading and therefore optimizing the system, we chose to prepare a conjugate using a 4-armed star PEG. Commercially available multi-armed PEGs are widely used in bioconjugation, hydrogel crosslinking, surface functionalization, and drug delivery. The use of a 4-armed PEG polymer as a carrier could increase the ratio to 3 – 4 CHD molecules per PEG, depending on the loading obtained.

Since there are no commercially available 4-armed PEG functionalized with DBCO at each terminus, our strategy consisted of functionalizing a 4-armed NH_2 PEG polymer (molecular weight: 10 kDa) with DBCO-PEG4-hydroxysuccinimidyl ester (**Figure 63**). After the conjugation of the primary amino groups with the NHS activated carboxylgroup, the linker-CHD would be clicked to DBCO as described previsouly.

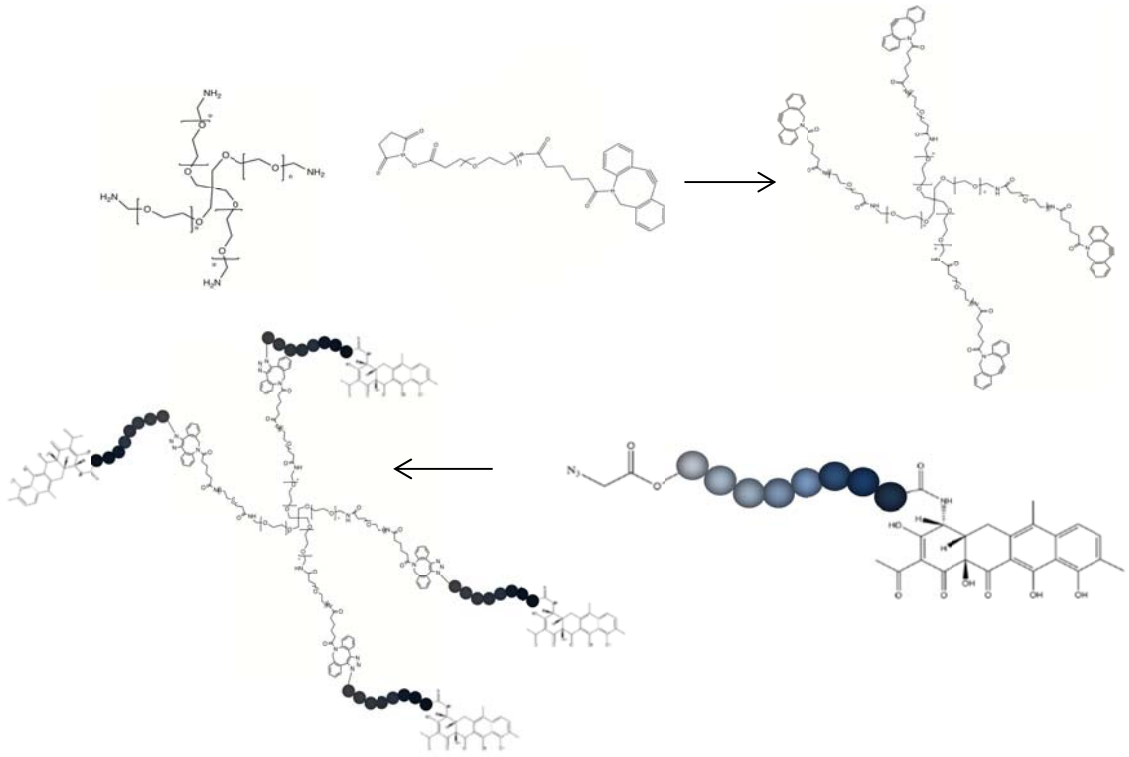

Figure 63 – Strategy of constructing a 4-armed CHD release system. Commercially available 4-armed NH_2 PEG polymers were conjugated with a NHS-PEG4-DBCO spacer. The designed peptide linker, already coupled to CHD, clicks to the DBCO via copper-free click chemistry.

To obtain the intermediate structure, an initial solution of NHS-PEG4-DBCO reagent in DMSO was prepared at a concentration of 10 mM. 10 mg of 4-armed PEG was diluted in PBS and the spacer was added in a 10 fold molar excess, since the NHS activated carboxygroups tend to hydrolyze very quickly when in aqueous solution, therefore needing an excess of the subtract to guarantee

an efficient loading of the spacer to the 4-armed PEG. A mass shift was observed by MALDI after the reaction and the mean mass difference was used to establish the mean loading for each PEG polymer (**Figure 64**).

A full loading, i.e., four spacers coupled to each star-PEG polymer, would yield an average mass distribution of 12651 m/z. The average mass shift obtained by MALDI-TOF for the 4-armed PEG-DBCO conjugate was about 12165 m/z. By calculating the expected mass difference for the fully loaded conjugate and comparing it to the measured value, it is possible concluding that the EDC/NHS reaction resulted in a loading of 85% of 4-armed PEG's full capacity. This corresponds to an average of 3.4 available DBCO groups per PEG polymer.

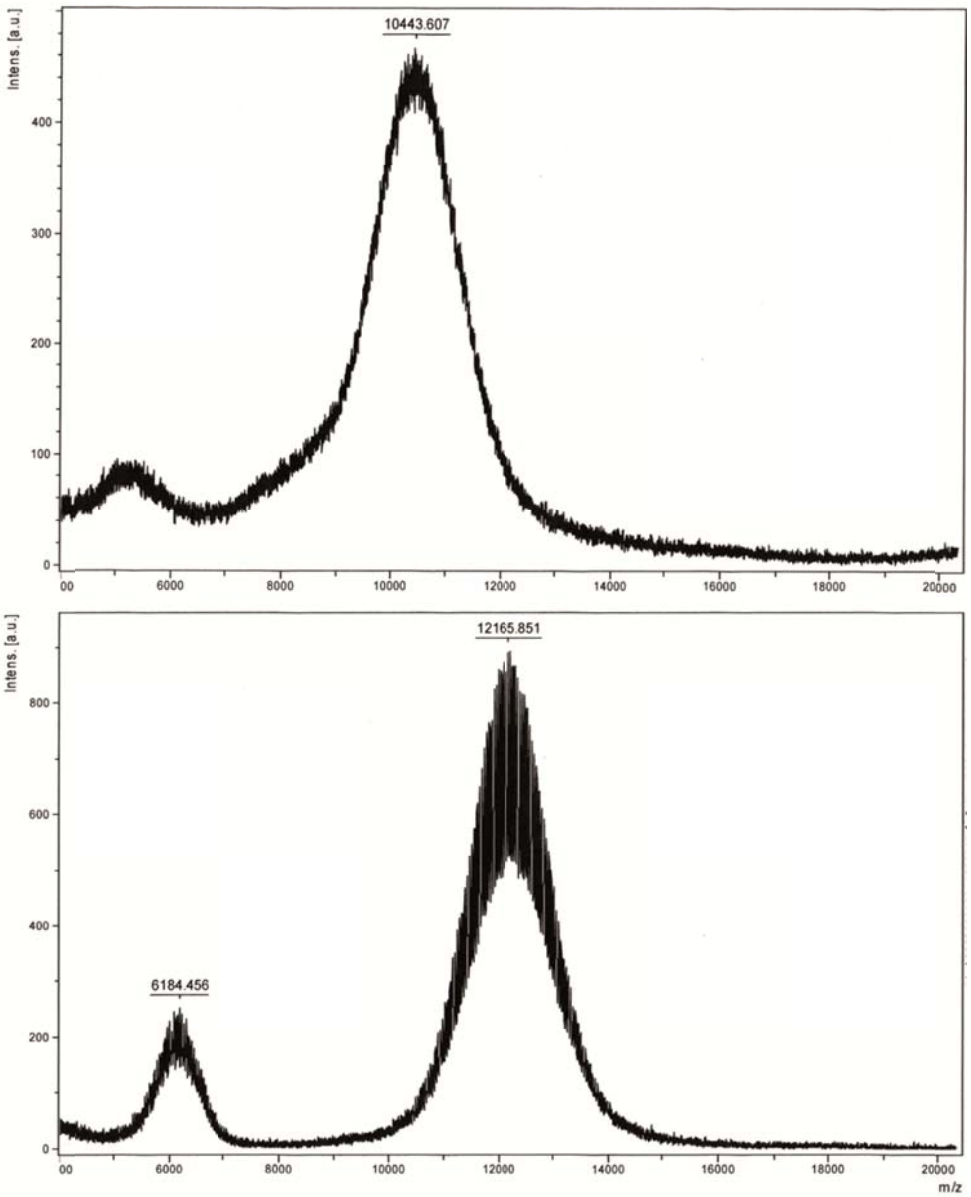

Figure 64 – Mass spectra of 4-armed PEG (average molecular weight: 10 kDa – above) and of 4-armed PEG-DBCO conjugate (below). The product shows a loading average of 3.4 DBCO groups per PEG polymer.

For the next step, we tried to click the linker-CHD to the intermediate PEG-DBCO construct under the same conditions applied for the former PEG-linker-CHD construct, i.e., the 4-armed PEG-DBCO, which was incubated with the linker-CHD in PBS pH = 7.4 for 48 hours.

Again, we checked the reaction product by MALDI. It was expected to find a mass distribution shift in which the peak would be at around 17000 m/z. However, the spectrum did not show this shift, but instead a mass distribution of around 12000 m/z was observed which indicates that the click reaction was not successful under these conditions (**Figure 65**).

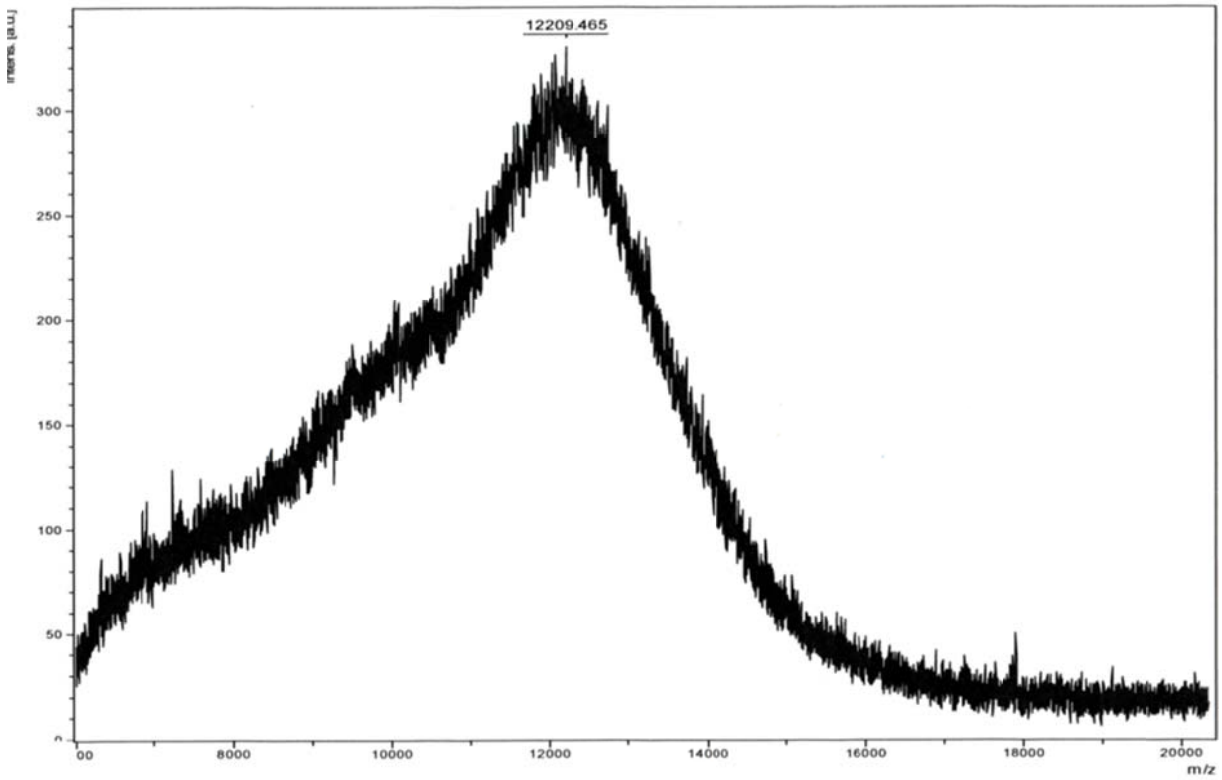

Figure 65 – Mass spectrum of first click attempt between 4-armed PEG-DBCO and linker-CHD. A mass shift to around 17000 m/z was expected, however it was not found, indicating a non-successful reaction.

It was hypothesized whether the 4-armed PEG-DBCO, due to the mobility and hydrophilicity of the long PEG chains and the hydrophobic nature of the DBCO groups, would form aggregates, and whether the reactive cyclooctine rings are not available for the click chemistry with azido groups of the peptide. Thus, a second coupling attempt was performed using a mixture of 70% (v/v) THF in PBS and incubated at 45 °C, since Liang *et al.* described a more efficient click reaction at higher temperatures [155]. The reaction was again incubated for 48 hours and once more the mass shift was analyzed by MALDI. This time, the predicted mass shift of about 16800 m/z corresponding to a loading of 3.4 linker-CHD per PEG polymer, was observed, indicating that the conjugation was successful when performed under the newly established conditions (**Figure 66**).

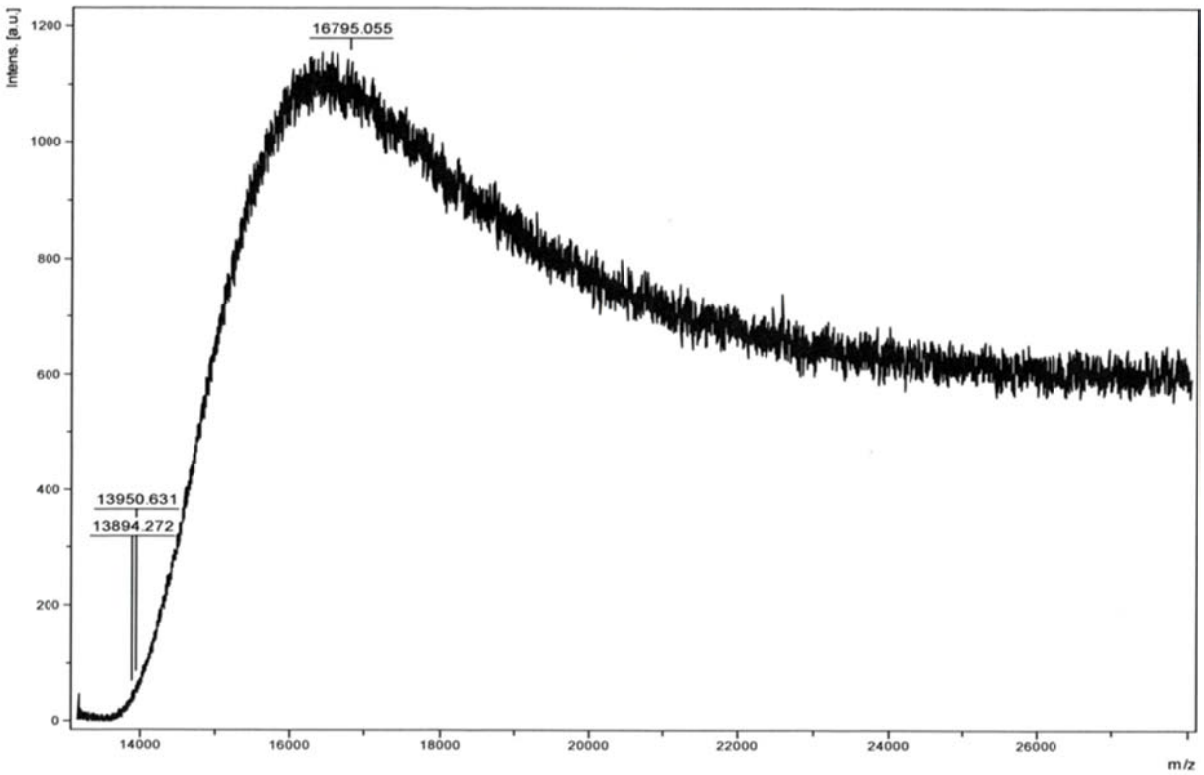

Figure 66 – Mass spectrum of second click attempt between 4-armed PEG-DBCO and linker-CHD. The expected mass shift to around 17000 m/z is observed. Loading: 3.4 linker-CHD/PEG polymer.

After its purification, the CHD-release system was incubated with aureolysin. Before running an assay to observe the effect of the bacterial protease over time, we first wanted to find out whether there would be a cleavage and a partial release of CHD-peptide fragment at all like it was observed for the first constructed PEG-linker-CHD system. A free linker-CHD was used as a positive control. Both CHD construct and free linker were incubated with two different concentrations of aureolysin (50 ng/mL and 1 µg/mL, respectively) for two different time periods (one and four hours). Since the PEGylated system also presented a broad initial peak due to its polydispersity in the respective chromatogram, the comparison for release was again based on the resulted peptide-CHD fragment and normalized to a CHD standard curve as described previously.

The PEGylated linker presented a much lower cleavage rate when compared to the free linker. Incubating it with the usual concentration of 50 ng/mL, less than 1% was cleaved after three hours of incubation, whereas the free linker-CHD presented a rate of over 75% (**Figure 67**). With a higher aureolysin concentration, the percentage of cleavage for the PEGylated system only reached 4.5% after three hours, while the free linker was almost fully cleaved after only one hour of incubation.

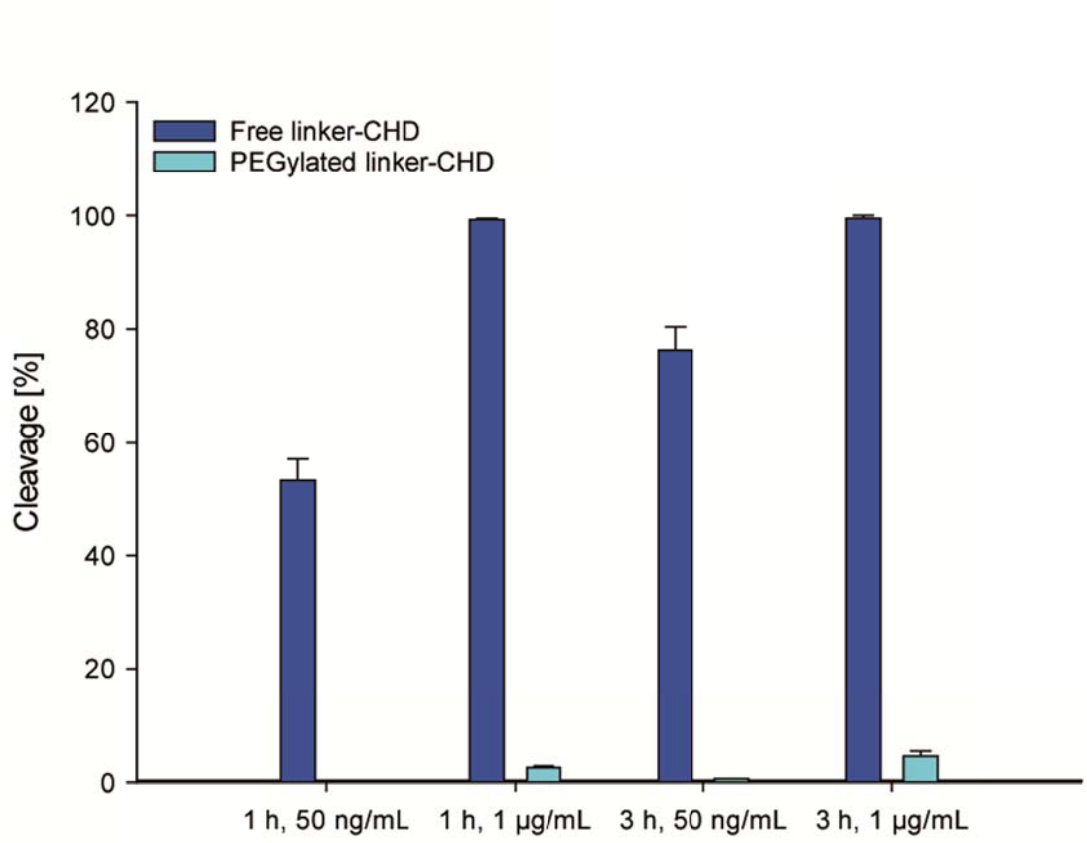

Figure 67 – Cleavage rates for free and PEGylated linker-CHD systems after incubation with 50 ng/mL and 1 µg/mL aureolysin for one and three hours.

4.5.5 Analysis of aggregates by DLS

The stability of PEGylated drug release systems can be characterized by analyzing the formation of aggregates. The presence of aggregates, which could be caused due improper formulation conditions, inactivates the system since the bacterial proteases could not attack the cleavable linker and thus triggering the release. For that purpose, we analyzed the particle size distribution of formed aggregates in the nanometer range by Dynamic Light Scattering (DLS) as well as their polydispersity indices. The linear PEGylated linker-CHD and the 4-armed PEG linker-CHD systems were incubated in aureolysin buffer and measurements took place at 37 °C (**Figure 68**).

The polydispersity index (PdI) characterizes the size distribution width of the particle collective. It is applied in a scale from 0 to 1, whereby a low PdI value such as 0.1 indicates a narrow size representation within the sample and higher PdIs indicate polydispersity [156]. The PdI obtained for the linear PEGylated system was below 0.2, therefore indicating a relative monodisperse distribution. A lack of aggregation could be assumed. However, the 4-armed PEGylated release system presented a high PdI which indicates the formation of aggregates under these conditions.

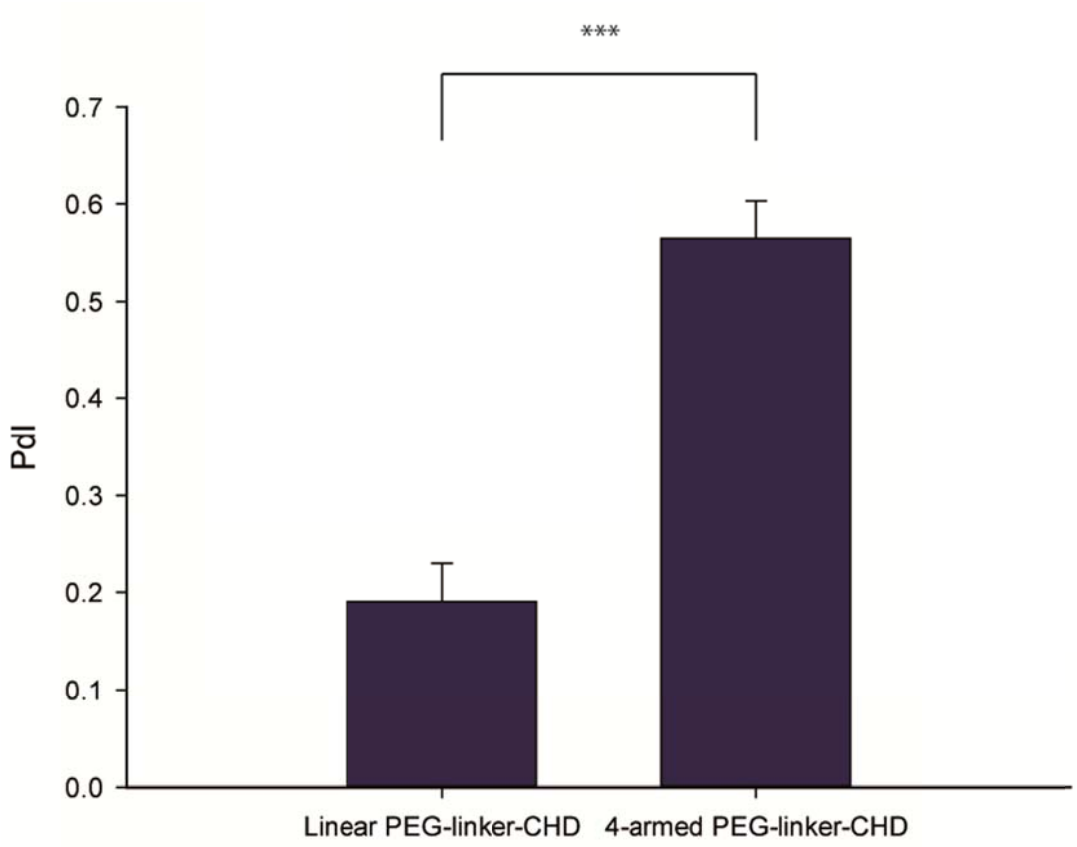

Figure 68 – Polydispersity index (PdI) of PEGylated CHD release systems after incubation in aureolysin buffer at 37 °C. The mean differences of both formulations are statistically extremely different ($p < 0.001$ – marked as ***).

Discussion and outlook

5. Discussion and outlook

We designed a bioresponsive antibiotic release system which is solely triggered by the presence of virulent proteases. The main focus of the developed strategy was upon the cleavable linker, a peptide being sensitive towards the target enzymes. For our purpose it was imperative that no other human protease could cleave the sequence, assuring that antibiotics would only be released in case of a bacterial infection and thus guaranteeing the specificity of the system. After searching for possible prototypes to be used as those linkers, we synthesized three different sequences obtained from natural substrates for aureolysin, i.e., C3 complement protein, insulin, and plasminogen [51, 146, 147]. We incubated each sequence not only with aureolysin, but also with various types of human metalloproteinases, mostly known as MMPs. MMPs are a vast family of more than 20 enzymes usually involved in tissue remodeling and wound healing [157]. For that reason, their expression rates usually increase significantly after surgical procedures in comparison to healthy individuals [148, 158-160]. The use of a bioresponsive antibiotic release system as a prophylactic in postoperative procedures, for example, could be highly influenced by the enhanced levels of MMPs.

By incubating the three linker prototypes with aureolysin, all sequences were cleaved as expected, since they were obtained from natural aureolysin substrates (**Figure 18**). Sequence 2a, obtained from the B chain of insulin, was almost completely cleaved after one hour of incubation with aureolysin, whereas the C3 complement sequence presented a cleavage by this enzyme of about 65% and the plasminogen originated sequence of only 35%. However, not all sequences were insensitive towards the tested human proteinases. MMP-8 and MMP-1, respectively, were able to cleave the insulin sequence, whereas the C3 complement was also cleaved by MMP-1. Rozanov *et al.* described the cleavage of C3b complement protein by MMP-1 during metastatic neoplasms [161, 162]. None of the linkers were cleaved by MMP-9 and MMP-13.

Further characterization of how efficiently aureolysin would cleave the designed linker was performed in order to better understand the behavior of this enzyme, since this is the main component of the developed release strategy. Azocasein digestion assays have been used for almost 70 years for the determination and characterization of proteolytic activity. The digestion of a suspension with those chromophores releases acid soluble peptides producing a reddish to orange color of the solution [163]. Trypsin was used for comparison since its activity towards azocasein is already well described in literature [164]. Aureolysin presented a better activity and longer duration when compared to trypsin. It is known that due to their role in infections, bacterial proteases serving as virulence factors tend to have a more aggressive activity in comparison to other proteases [165, 166]. While this is concerning regarding a staphylococcal

infection, we use this prolonged activity in our favor as the main trigger for the release of antibiotics.

One encountered challenge in this project was to establish and quantify the range of aureolysin amount expressed during a bacterial infection. Even though the transcription of the *aur* gene being responsible for aureolysin expression, is much higher in virulent *S. aureus* strains when compared to non-virulent ones [167, 168], the real concentration range is still unknown. The indirect ELISA method is known for a more specific and sensible detection of antigens in comparison to the traditional direct method [169]. In order to validate this method with regard to a specific detection of aureolysin and to establish the optimal concentration of the primary antibody known as α-aureolysin, we first performed this assay using purchased aureolysin as the antigen. By reading the plates at λ = 450 nm, we observed a good absorption showing that the use of ELISA is suitable for the detection and quantification of aureolysin in bacterial supernatants (**Figure 22**). The chosen staphylococcal strains, whose supernatants were used for the following ELISA assays, were mutant strains of ATCC strains 8325, MA12, and Newman in which their *spa* gene was deleted. This gene is responsible for another virulence factor of *Staphylococcus aureus* named protein A, interfering during ELISA by binding to the Fc region of most mammalian IgG used as the capturing antibodies in these assays [170, 171]. Bacterial cultures were sterile filtered once their growth reached the stationary phase, in which there is a maximal expression of aureolysin [167, 168].

However, by initially trying to detect the presence of aureolysin in *S. aureus* strains cultivated in LB medium, no absorption was obtained. It was hypothesized that since aureolysin is a virulence factor for *S. aureus*, it is only expressed when bacteria encounter a hostile environment and stressful situation, thus immunological methods for protein quantification are not able to detect it in a normal bacterial culture [172, 173]. For this reason, we repeated the assay using FBS as culture medium to mimic the usual environment and available nutrients during a systemic infection and again, no signal was observed. In order to obtain a real detection and subsequent quantification of aureolysin during infections, it would be necessary to obtain abscess and plasma samples from infected patients or animals. The mimicking of hostile conditions for the proliferation of microorganisms *in vitro* does not always provide a reliable model for simulating the mechanisms of the expression of their virulence factors.

Since we could not obtain a real aureolysin concentration range during staphylococcal infections, we performed a logarithmic screening of enzymatic concentration to determine the range of its activity. The results showed that aureolysin already presents a good proteolytic activity in lower concentration levels (**Figure 24**). The range in which aureolysin cleaves from 0 to 100% of the

substrate was defined as 10^1 to 10^3 ng/mL, respectively. A further assay within this measured concentration range on the cleavage of the synthesized linker provided some more specific information of the activity range (**Figure 25**). Aureolysin was able to cleave 100% of the present substrate within one hour at a concentration of 100 ng/mL and the lowest concentration tested in which aureolysin presented any activity was 10 ng/mL. The level of 50 ng/mL was chosen as the concentration to analyze the cleavage over time since in this concentration the enzyme was able to cleave about 50% from the original sequence in the first assay. After two hours of incubation, already 100% of the sequence was cleaved, indicating a rapid and efficient cleavage by the target protease. Since the presence of aureolysin indicates a virulent and aggressive infection by *S. aureus*, it is important that the antibiotic release is triggered very rapidly with the concentration threshold for the linker cleavage being as low as possible. Xiong *et al.* presented a vancomycin release nanogel system triggered by 0.5 and 1.0 mg/mL *Pseudomonas cepacia* lipase in which a maximum of 80% cumulative release was obtained after an incubation of 10 hours [136], whereas the peptide sequences introduced between block polymers for delivery of antineoplastic antibody was 90% degraded after 3 days incubation with lysosomal enzymecathepsin B [174]. Our designed system showed very good rates of cleavage in a few hours using low concentrations of aureolysin only.

For our first formulation attempt, we used a commercially available PVA hydrogel matrix functionalized with maleimide groups. The choice of using a PVA based polymer matrix for the hydrogel system is based on the fact that these are stable against enzymatic activity [175]. Together with thiol containing linear PEGs, we used the aureolysin sensitive peptide sequence as crosslinkers. Those linkers were synthesized with cysteine at each terminus in order to provide the thiol group necessary for the conjugation with maleimide group at the PVA matrix. An antimicrobial component would be physically incorporated into the hydrogel pores, and during an infection caused by *S. aureus* the expressed aureolysin would cleave those sequences, releasing the compound entrapped in the hydrogel (**Figure 29**). For that purpose we used three different fluorophores as prototypes for active substances: linear FITC-Dextran having a molecular weight of 20 and 40 kDa, respectively, as well as a glomerular GFP (molecular weight: 27.2 kDa).

The first requirement is to establish a suitable matrix concentration in which the fluorophore would not diffuse into the medium. For that purpose we formulated hydrogels with two different matrix concentrations of 5 and 10 mM and determined the diffusion of fluorophores over time. All formulations containing FITC-Dex were not able to entrap the fluorophore for a longer time, which was completely diffused within a few hours. This could be explained due to the elongated shape of those compounds, which would allow a better diffusion throughout the pores of the hydrogel. On the other hand, the glomerular shape of GFP helped to entrap them in the pores and only 40

and 20% diffused after three weeks for the 5 and 10 mM matrix concentration formulations, respectively (**Figure 32**). However, the next generation of formulations containing cleavable linkers presented similar patterns of fluorophore release when the samples (incubation with aureolysin; L-amino acid sequence) were compared to their respective negative controls (without aureolysin incubation and/or using the D-amino acid sequence). 80 to 100% of the fluorophore was diffused for each sample and their negative controls in the 5 mM hydrogel matrix formulations in two days, whereas the fractions of 10 mM hydrogels only reached a maximum of 10% during the same period of time (**Figure 38**). The only formulation whose release by incubation with aureolysin was faster when compared to the respective negative controls was 10GFP30. However, the release rate was still too low to be considered as an effective antibiotic release system. It was hypothesized that the 5 mM formulations were not stiff enough to prevent the fluorophore of passively diffusing through the pores to the medium, whereas the 10 mM samples were too densely crosslinked for a bacterial protease being capable of penetrating inside the hydrogel. We did not perform any further investigations to confirm this hypothesis.

Nevertheless, we wanted to check whether the covalent binding of a linker-antibiotic complex to the PVA matrix would be a valid alternative for the strategy of using hydrogels as our carrier polymer. As a proof of concept, we synthesized a linker carrying cysteine at the *C*-terminus, thus providing a thiol group necessary for the conjugation reaction with the maleimide groups present at the PVA backbone as well as carboxyfluorescein as an antibiotic model compound coupled to the *N*-terminus (**Figure 39**). The hydrogel was loosely formulated so that aureolysin could easily penetrate inside the system and reach the cleavable linkers attached to the PVA matrix. The proteolytic assays regarding the incubation of the free linker as well as the conjugates to the polymer showed a common peak at 18.4 min in the respective chromatograms indicating that the redesigned strategy of conjugating both linker and antibiotic to the polymer could be applied to a bioresponsive antibiotic delivery system. Tanihara *et al.* presented a similar strategy for antibiotic release during infections in which a peptide linker was attached to the insoluble PVA matrix by one terminus and gentamycin coupled to the other terminus, being released in the presence of thrombin [176]. This enzyme is increasingly expressed infected wounds by *Staphylococcus aureus* [177]; however, its presence is not exclusive under those situations, and therefore compromises the selectivity of the circumstances in which the antimicrobial drug is released. A system based on a responsiveness triggered by a particular bacterial virulence factor only guarantees an action with the presence of the targeted pathogens.

The conjugation of the antibiotic to the peptide linker has an obstacle which needs to be overcome: after the proteolytic cleavage by aureolysin, the antibiotic would still be bound covalently to some amino acid artefacts. This would most certainly influence the antimicrobial

activity of the compound. For example, antibiotics from the tetracycline family inhibiting protein synthesis by blocking the attachment of charged aminoacyl-tRNA to the A site on the ribosome by binding to the 30S subunit of microbial ribosomes [77, 178] need to pass several biomembranes: Thus, the presence of residual amino acids could prevent them from actually reaching the respective target at all [179].

Once again we apply a biological tool for the degradation of those residual amino acids and the subsequent release of our antibiotic. Aminopeptidase belongs to a class of proteases which cleaves amino acids from the *N*-terminus of peptides and proteins, respectively [139]. These enzymes, being widely distributed in plasma, would cleave the residual amino acids linked to the antibiotic until its complete release. Ritzer *et al.* used a similar strategy for the release of bitter substances in bioresponsive diagnostic systems of peri-implant diseases [135]. For that purpose we synthesized the residual amino acid sequence KVYL resulting after cleavage by aureolysin and coupled the *C*-terminus to the primary amino group of aminofluorescein, again serving as a model for any antibiotic compound. This reaction was performed by EDC/NHS in which the carboxyl group is activated by carbodiimide and subsequently bound to the free amine [180].

Estimating the concentration range in which aminopeptidases are present in plasma is important to determine whether the release would take place under those conditions. Tanihara described that aminopeptidase activity in infected plasma was 1.4 times higher when compared to non-infected samples; however, no distinct concentration for neither of both samples was determined [176]. We measured the aminopeptidase plasmatic concentrations from healthy plasma samples to simulate a "worst case scenario" in which the levels would not be yet increased by the emergence of an infection. With the obtained range from 0.72 to 3.6 µg/mL (**Figure 48**), we investigated the effect of aminopeptidase concentration starting from the highest concentration and going even below the lowest measured point. The degradation of residual amino acids showed to be the very efficient. Already the concentration of 0.72 µg/mL of aminopeptidase was able to completely release 50% of the fluorophore. With this value we performed a release assay over time and after two hours, all residual amino acids were degraded (**Figure 49**). For the average concentration of 1.7 µg/mL, all fluorophores were released after only 30 minutes of incubation (**Figure 50**).

The proteolytic cleavage of the peptide linker by aureolysin indicates the presence of virulent *Staphylococcus aureus.* Therefore, it is essential that the subsequent degradation of residual amino acids and the release of the antimicrobial agent is accomplished as quickly as possible to fight the infection. The obtained results present an efficient activity for aminopeptidase, even when working with the presumption of the lowest plasmatic levels.

The final phase of this work was the construction of a PEG-linker-antibiotic system. The choice of using a linear PEG polymer as the carrier instead of continuing with the PVA hydrogel matrix was based on the fact that since the previous hydrogel formulation was primary developed for 3D imaging of cell cultures, it was not suitable for an intravenous application and therefore could not be used for systemic drug delivery. A systemic distribution is essential when aiming to fight possible post-operative infections.

For already planned *in vitro* and *in vivo* assays for release testing, we designed this system by not incorporating fluorophores anymore, but an antimicrobial substance instead. For this purpose, we chose the tetracycline like antibiotic chelocardin (**Figure 3**) which was synthesized at the Helmholtz Institute for Pharmaceutical Research in Saarbrücken, Germany. CHD presents a MIC value of 4 µg/mL against MRSA and is known for its dual mechanism of action [82]. The primary amino group located at C4 is strategic for being coupled with the *C*-terminus of the linker. However, the use of EDC and NHS as amide coupling reagents often leads to a racemization of the amine bond [181-183]. EpiCHD does not present antimicrobial activity and besides, some epimers of tetracycline present some level of hepatotoxicity [184, 185]. Even though there is no data available for EpiCHD hepatotoxicity, its formation should be avoided. Thus, a solution was to perform a conjugation using HATU as the coupling agent and HOBt as additive which significantly slows down racemization [186]. In addition, another obstacle is the unspecific nature of such reactions. An amide can be formed deliberately by coupling any primary amino- and carboxyl group. Thus, since the peptide linker contained both groups in its amino acid side chains, the coupling was performed with the sequence still having their protecting groups attached. This is also true for antibiotics containing more than one primary amino groups or other reactive moieties. The resulted coupling product was poorly water soluble which was expected since all protecting groups are hydrophobic. However, after the incubation with TFA, the acid labile groups were detached and the linker solubility could be increased (**Figure 57**).

Another change of strategy was regarding the coupling of the linker-CHD to the chosen polymer. Even though thiol-maleimide is considered to trigger a specific reaction, maleimide groups can favor a reaction with primary amines like lysine side chains over thiol [187]. Since we had lysine integrated in our linker, we decided to perform a copper free click reaction instead. For that reason, the *N*-terminus of the linker was functionalized with azidoacetic acid. This provides an azido group for the click reaction which is integrated to the peptide backbone. The very specific bioorthogonal reaction between the azido group and cyclooctine has the advantage of not needing copper as a catalyst and therefore eliminating a relevant cytotoxicity factor [154]. For that purpose, we used a linear 10 kDa PEG polymer modified with a DBCO group. Since the chosen polymer does not present a specific mass but instead possesses a polydisperse distribution

pattern [188], the mass shift to around 11500 m/z observed by MALDI was the indicative for the successful conjugation (**Figure 60**). Besides, during the purification using ÄKTA system, different wavelengths were used and the collected fractions projected peaks obtained at 214 and 307 nm, corresponding to the peptide linker and DBCO groups, respectively.

By performing the established cleavage assay with the PEGylated linker, we observe a similar cleavage rate when compared to the free linker. 60% of the initial sequence was cleaved after two hours of incubation. This indicates that the PEGylation does not have any influence over aureolysin activity. The PEGylation of peptide substrates was already shown to have a positive effect on enzymatic proteolytic activity since it improves their solubility and thus increases their susceptibility [189-191].

However, since the chosen PEG polymer only possesses one DBCO group, it provides a very low loading capacity of only one linker per polymer. In order to optimize the antibiotic loading, we applied a 4-armed PEG with a similar molecular weight of 10 kDa. Since there are no commercially available multi-armed PEG polymers functionalized with DBCO, we constructed an intermediate polymer by conjugating a DBCO containing spacer to the multi-armed PEG. This four-armed PEG system contained a free primary amino group at each side chain and was linked to a spacer constituted of one NHS activated carboxyl group at one terminus, followed by four units of PEG and finished with a DBCO group at the other terminus. After the expected mass shift for the polydisperse system to around 12000 m/z (observed by MALDI-MS), we once again tried to click the linker-CHD to the new polymer construct after the already successfully performed protocol. However, it was not possible to click the linker-CHD system to the new construct using conventional protocols. This could be due to the amphiphilic nature of the intermediate polymer; since the PEG moiety is highly hydrophilic while the DBCO has a strong hydrophobicity. The construct could form micellar structures in aqueous solutions; hence, the DBCO groups would not be available to perform a click reaction with the azido group from the linker.

A second click attempt was performed in a mixture of 70% (v/v) THF in PBS at 45 °C. This time, a shift to around 16800 m/z was observed, indicating an average loading of 3.4 linkers per PEG molecule (**Figure 66**). However, aureolysin was not able to cleave the linker and provide the antibiotic release, even with longer incubation times and higher protease concentration (**Figure 67**). Once again it was hypothesized that the system would form aggregates with the linker remaining entrapped in the core and not available for proteolytic cleavage by the bacterial enzyme. To investigate this theory, we analyzed the size distribution and polydispersity of multi armed and linear PEGylated systems in buffer by DLS (**Figure 68**). The PdI is a parameter to characterize the size distribution width of a particle collective. In a scale from 0 to 1, low PdI values such as 0.1 represent narrow size distribution whereas higher values indicate

polydispersity and particle aggregation [192]. Both PEG systems are polydisperse systems, thus it was expected that none of the samples would present a very low PdI. However, the linear PEGylated construct was still able to present a PdI below 0.2, thus not indicating the presence of aggregates in solution. The PdI value for the multi-armed PEG was above 0.6 and the formation of aggregates could be assumed. The aggregation of the PEGylated release systems explains the low release profile observed after aureolysin incubation. The strategic approach of increasing the antibiotic release per polymer should be followed by a formulation study to prevent such aggregation in physiological conditions.

In this work, we were able to successfully develop the concept of a bioresponsive antibiotic release system triggered by aureolysin. This bacterial protease is a potent virulence factor only expressed when *S. aureus* reaches a pathogenic state. The novelty of this profile guarantees maximum specificity in which the antibiotic would only be released during an infection and not caused by any cross signaling coming from human or symbiotic bacterial biomolecules. It is of extreme importance that antibiotic therapy is applied only when necessary to avoid the emergence of new resistant strains and the appearance of side effects. Our release system goes one step beyond and releases the antibiotic only when it is really necessary. This would be extremely useful as a prophylactic in postoperative procedures, in which there is a high risk of occurrence of an opportunistic infection. The linker was proven to be sensitive towards very low enzymatic concentrations in comparison to similar developed systems, exhibiting a very fast release rate. The same is true for the second release component, the human protease class of aminopeptidases. By incubating the enzyme within the measured concentrations, the full release of antibiotic was achieved after only a few minutes. These features are positive since we expect a rapid response in case of an infection. Smart, specific, and sensitive bioresponsive delivery systems are the next generation in drug release. It is however necessary to further investigate the antibacterial effect of the release system in bacterial culture as well as in infected animal models. The loading is also an asset to be considered, since the stable formulation only presents a ratio of one antibiotic per polymer. Nevertheless, the applications of the concept could be extrapolated to other infections, only by adapting and tailoring the cleavable linker to the specific need.

Summary

6. Summary

A major problem regarding public health is the emergence of antibiotic resistant bacterial strains, especially methicillin resistant *Staphylococcus aureus* (MRSA). This is mainly attributed to the unnecessary overuse of antimicrobial drugs by patients; however, one aspect that is often neglected is their untargeted mechanism of action, affecting not only the infection itself but also commensal bacteria which are often opportunistic pathogens causing many diseases as well. Therefore, our goal was to develop a bioresponsive antibiotic delivery system triggered by virulence factors. The designed system is comprised of a polymer to enhance its pharmacokinetic profile, a peptide cleavable linker, and the antibiotic agent itself. The bacterial protease aureolysin which is expressed by *S. aureus* during infections would cleave the linker and partially release the antibiotic which would be still attached to a remaining tetrapeptide. These would be cleaved by a group of proteases naturally present in plasma called aminopeptidases, finally releasing the compound.

In the first part of this project, we searched for a suitable sequence to serve as a cleavable linker. It should be sensitive towards the target bacterial protease but not be cleaved by any human enzymes to guarantee the specificity of the system. Therefore, we synthesized three peptide sequences via Solid Phase Peptide Synthesis and incubated them with aureolysin as well as with many human matrix Metalloproteases. The analysis and quantification of enzymatic activity was monitored chromatographically (RP-HPLC). The plasminogen originated sequence was chosen since it was not sensitive towards MMPs, but cleaved by aureolysin.

In the second part, we tried to incorporate the chosen peptide sequences as crosslinkers in hydrogel formulations. The purpose was to physically incorporate the antibiotic within the hydrogel, which would be released by the cleavage of those sequences and the consequent loosening the hydrogel net. For that purpose we used a commercially available hydrogel kit with a PVA matrix modified with maleimide, which allows a conjugation reaction with thiol functionalized crosslinkers. Three fluorophores were chosen to serve as antibiotic models and a diffusion assay was performed. Only the glomerular structured Green Fluorescent Protein (GFP) presented a low diffusion rate, thus the aureolysin release assays were performed only using this prototype. Assays showed that with a low hydrogel polymer concentration, the fluorophore either quickly diffused into the medium or was not released at all. The physical incorporation of the antibiotic within the hydrogel pores was therefore abolished as a suitable release approach. For a second attempt, we covalently bound a fluorophore to the linker, which was conjugated to the hydrogel matrix. The incubation with aureolysin and subsequent RP-HPLC analysis showed a peak with the same retention time correspondent to the fragment product after cleavage of the

free linker. This is a proof that the concept of linking the peptide sequence to the antibiotic is a promising strategy for its bioresponsive release.

Within the third part of this study, we analyzed the degradation of the resulted fragment after aureolysin activity and subsequent full release of the antibiotic by human aminopeptidases. We determined the concentration of those enzymes in human plasma and synthesized the fragment by conjugating the tetrapeptide sequence to aminofluorescein via EDC/NHS reaction. By incubating the construct with the lowest aminopeptidase concentration measured in plasma, the fluorophore was completely released within two hours, showing the efficacy of these enzymes as bioresponsive agents.

The last part was the construction of the PEGylated linker-antibiotic. For this purpose we chose the tetracycline like antibiotic chelocardin (CHD) as our prototype. The conjugation of the linker-CHD to the polymer was performed by copper free click chemistry. The cleavage rate of the linker by aureolysin was very similar to the one obtained for the free peptide, indicating that the PEGylation does not interfere on the enzymatic activity. However, by trying to increase the loading ratio of chelocardin onto the polymer, we observed a very low cleavage rate for the system, indicating the formation of aggregates by those constructs.

The designed system has proved to be a smart strategy for the delivery on demand of antibiotics in which the drug is only released by the presence of *S. aureus* during their virulent state.

Zusammenfassung

7. Zusammenfassung

Ein weltweites Problem des Gesundheitswesens ist die Entstehung von antibiotikaresistenten Bakterienstämmen, besonders Methicillin-resistenter *Staphylococcus aureus* (MRSA). Eine wichtige Ursache für Resistenzentwicklungen ist die unüberlegte Verschreibung von Antibiotika; allerdings das breite Wirkspektrum der meisten Substanzen ist ein stets vernachlässigter Aspekt. Dies betrifft nicht nur die Pathogene selbst, sondern auch die bakterielle Mikroflora des Patienten, die opportunistische Pathogene darstellen und in machen Fallen ebenfalls verschiedene Erkrankungen hervorrufen können. Unser Ziel ist die Entwicklung eines bioresponsiven Freisetzungssystems für Antibiotika. Das System besteht aus einem Polymer zur Optimierung der Pharmakokinetik, einem Peptidlinker sowie dem eigentlichen Antibiotikum. Die bakterielle Protease Aureolysin wird von *S. aureus* exprimiert, sobald sich das Bakterium in seinem virulenten Zustand befindet. Das Enzym schneidet den Linker, wodurch das Antibiotikum zum Teil freigesetzt wird. Da es noch an Aminosäureartefakte gebunden ist, muss es im Anschluss durch eine Aminopeptidase, einer Gruppe von Exoproteasen des humanen Plasmas, abgespalten werden.

Die erste Phase des Projektes war die Suche nach einer passenden Peptidsequenz, die als Linker geeignet ist. Diese soll nur durch die Zielprotease und nicht durch andere humane Proteasen geschnitten werden, um die Spezifizität des Systems zu gewährleisten. Es wurden drei Sequenzen ausgewählt und mittels Festphasen-Peptidsynthese hergestellt. Diese wurden mit Aureolysin sowie humanen Matrix-Metalloproteasen (MMP) inkubiert; die Produkte wurden chromatographisch (RP-HPLC) charakterisiert und die enzymatische Aktivität bestimmt. Die von Plasminogen abgeleitete Sequenz wurde von keiner der Matrix-Metalloproteasen geschnitten, wohl aber von Aureolysin. Eine ausführliche Analyse des Aureolysin-Verdaus zeigte, dass der Linker innerhalb weniger Stunden komplett geschnitten wird.

In der zweiten Phase wurde die Peptidsequenz als *Crosslinker* in verschiedene Hydrogelmatrices inkorporiert. Die Strategie war der physikalische Einschluss des Antibiotikums in das Hydrogel und die anschließende Freisetzung durch Spaltung dieser Sequenzen und Lockerung des Hydrogelnetzes auf molekularer Ebene. Hierfür wurde ein kommerzielles Hydrogelkit mit Maleinsäureamid-modifizierter PVA Matrix verwendet, die mit Thiol-funktionalisierten Linkern konjugiert werden können. Drei verschiedene Fluorophore wurden als Modelle für die Diffusionsversuche verwendet. Nur das glomeruläre *green fluorescent protein* (GFP) besaß eine ausreichend niedrige Diffusionskonstante und wurde deshalb als Prototyp für die weiteren Schneidversuche verwendet. Die Ergebnisse zeigen, dass der Fluorophor bei niedrigen Matrixkonzentrationen schnell aus den Poren in das umgebende Medium diffundiert, während er

bei höheren Konzentrationen nicht freigesetzt wird. Die physikalische Inkorporierung des Antibiotikums wurde aus diesen Gründen verworfen und nicht durchgeführt. Als zweiter Versuch wurde der Fluorophor kovalent an den Linker gekoppelt, welcher im Anschluß an die Matrix konjugiert wurde. Die Inkubation mit Aureolysin und die nachfolgende RP-HPLC-Analyse zeigte einen Peak bei der Retentionszeit entsprechend dem Fragmentprodukt, das durch Inkubation des freien Linkers entsteht. Die kovalente Bindung zwischen der antimikrobiellen Substanz und dem Linker ist eine vielversprechende Strategie für eine bio-responsive Freisetzung.

In der dritten Phase des Projektes wurde die Zersetzung des resultierenden Fragments nach Aureolysin-Verdau und die anschließende vollständige Freisetzung des Antibiotikums durch humane Aminopeptidasen untersucht. Die Konzentration an Aminopeptidasen im humanen Plasma wurde bestimmt und die durch Aureolysin entstehende Peptidsequenz an Aminofluorescein mittels EDC/NHS-Reaktion gekoppelt. Die Inkubation des Konstruktes mit der niedrigsten Aminopeptidase-Konzentration, die im Plasma bestimmt werden konnte zeigte, dass der Fluorophor in zwei Stunden vollständig freigesetzt wurde.

Die letzte Phase hat sich mit der PEGylierung des Linker-Antibiotikum-Komplexes beschäftigt. Das Tetracyclin-analoge Antibiotikum Chelocardin wurde als Prototyp ausgewählt und am Helmholtz-Institut für Pharmazeutische Forschung des Saarlandes synthetisiert. Die Konjugation des Linker-CHD-Konstruktes an das Polymer wurde mittels kupferfreier Click-Chemie durchgeführt. Der PEGylierte Linker wurde in einer ähnlichen Rate durch Aureolysin geschnitten wie der freie Linker, was beweist, dass das Polymer keinen Einfluss auf die enzymatische Aktivität hat. Allerdings wurde während der Optimierung der Beladung von CHD je Polymermolekül eine sehr niedrige Freisetzung des Antibiotikums beobachtet, was durch Aggregatbildung der Konstrukte erklärt werden kann.

Das entwickelte System ist eine interessante *Delivery*-Strategie für Antibiotika, welche hierdurch nur durch virulente *S. aureus*-Erreger freigesetzt werden.

References

8. References

1. Piddock, L.J., *The crisis of no new antibiotics--what is the way forward?* Lancet Infect Dis, 2012. **12**(3): p. 249-53.
2. Ventola, C.L., *The antibiotic resistance crisis: part 1: causes and threats.* Pharmacy and Therapeutics, 2015. **40**(4): p. 277.
3. Podolsky, S.H., *Pneumonia before antibiotics: therapeutic evolution and evaluation in twentieth-century America*. 2006: JHU Press.
4. Laxminarayan, R., P. Matsoso, S. Pant, C. Brower, J.A. Rottingen, K. Klugman, and S. Davies, *Access to effective antimicrobials: a worldwide challenge.* Lancet, 2016. **387**(10014): p. 168-75.
5. Tilghman, R.C. and M. Finland, *Clinical significance of bacteremia in pneumococcic pneumonia.* Archives of internal medicine, 1937. **59**(4): p. 602-619.
6. Kanof, A., B. Kramer, and M. Carnes, *Staphylococcus pneumonia: A clinical, pathologic, and bacteriologic study.* The Journal of Pediatrics, 1939. **14**(6): p. 712-724.
7. Fine, M.J., M.A. Smith, C.A. Carson, S.S. Mutha, S.S. Sankey, L.A. Weissfeld, and W.N. Kapoor, *Prognosis and outcomes of patients with community-acquired pneumonia: a meta-analysis.* Jama, 1996. **275**(2): p. 134-141.
8. Rossolini, G.M., F. Arena, P. Pecile, and S. Pollini, *Update on the antibiotic resistance crisis.* Curr Opin Pharmacol, 2014. **18**: p. 56-60.
9. Hedrick, T.L., P.W. Smith, L.M. Gazoni, and R.G. Sawyer, *The appropriate use of antibiotics in surgery: a review of surgical infections.* Current problems in surgery, 2007. **44**(10): p. 635-675.
10. Hamouda, K., M. Oezkur, B. Sinha, J. Hain, H. Menkel, M. Leistner, R. Leyh, and C. Schimmer, *Different duration strategies of perioperative antibiotic prophylaxis in adult patients undergoing cardiac surgery: an observational study.* J Cardiothorac Surg, 2015. **10**: p. 25.
11. Zitvogel, L., M. Ayyoub, B. Routy, and G. Kroemer, *Microbiome and anticancer immunosurveillance.* Cell, 2016. **165**(2): p. 276-287.
12. Zitvogel, L., R. Daillère, M.P. Roberti, B. Routy, and G. Kroemer, *Anticancer effects of the microbiome and its products.* Nature Reviews Microbiology, 2017.
13. Spellberg, B. and D.N. Gilbert, *The future of antibiotics and resistance: a tribute to a career of leadership by John Bartlett.* Clin Infect Dis, 2014. **59 Suppl 2**: p. S71-5.

14. Enright, M.C., D.A. Robinson, G. Randle, E.J. Feil, H. Grundmann, and B.G. Spratt, *The evolutionary history of methicillin-resistant Staphylococcus aureus (MRSA).* Proceedings of the National Academy of Sciences, 2002. **99**(11): p. 7687-7692.
15. Sengupta, S., M.K. Chattopadhyay, and H.P. Grossart, *The multifaceted roles of antibiotics and antibiotic resistance in nature.* Front Microbiol, 2013. **4**: p. 47.
16. Organization, W.H., *Antimicrobial resistance: global report on surveillance*. 2014: World Health Organization.
17. Reardon, S., *Antibiotic resistance sweeping developing world: bacteria are increasingly dodging extermination as drug availability outpaces regulation.* Nature, 2014. **509**(7499): p. 141-143.
18. Kesah, C., S. Ben Redjeb, T. Odugbemi, C.B. Boye, M. Dosso, J. Ndinya Achola, S. Koulla-Shiro, M. Benbachir, K. Rahal, and M. Borg, *Prevalence of methicillin-resistant Staphylococcus aureus in eight African hospitals and Malta.* Clinical Microbiology and Infection, 2003. **9**(2): p. 153-156.
19. *When The Drugs Don't Work*, in *The Economist* 2016. p. 19-21.
20. Levy, S.B., *Balancing the drug-resistance equation.* Trends Microbiol, 1994. **2**(10): p. 341-2.
21. Levy, S.B., *The 2000 Garrod lecture. Factors impacting on the problem of antibiotic resistance.* J Antimicrob Chemother, 2002. **49**(1): p. 25-30.
22. Levy, S.B. and B. Marshall, *Antibacterial resistance worldwide: causes, challenges and responses.* Nature medicine, 2004. **10**: p. S122-S129.
23. Marshall, B.M. and S.B. Levy, *Food animals and antimicrobials: impacts on human health.* Clinical microbiology reviews, 2011. **24**(4): p. 718-733.
24. Venglovsky, J., N. Sasakova, and I. Placha, *Pathogens and antibiotic residues in animal manures and hygienic and ecological risks related to subsequent land application.* Bioresource technology, 2009. **100**(22): p. 5386-5391.
25. Gorbach, S.L., *The Need to Improve Antimicrobial Use in Agriculture.*
26. Hossein, K., C. Dahlin, and A. Bengt, *Influence of different prophylactic antibiotic regimens on implant survival rate: a retrospective clinical study.* Clinical implant dentistry and related research, 2005. **7**(1): p. 32-35.
27. Stone, S., R. Gonzales, J. Maselli, and S.R. Lowenstein, *Antibiotic prescribing for patients with colds, upper respiratory tract infections, and bronchitis: a national study of hospital-based emergency departments.* Annals of emergency medicine, 2000. **36**(4): p. 320-327.
28. Hickner, J.M., J.G. Bartlett, R.E. Besser, R. Gonzales, J.R. Hoffman, and M.A. Sande, *Principles of appropriate antibiotic use for acute rhinosinusitis in adults: background.* Annals of Internal Medicine, 2001. **134**(6): p. 498-505.

29. Simpson, S.A., F. Wood, and C.C. Butler, *General practitioners' perceptions of antimicrobial resistance: a qualitative study.* Journal of Antimicrobial Chemotherapy, 2006. **59**(2): p. 292-296.

30. Goossens, H., M. Ferech, R. Vander Stichele, M. Elseviers, and E.P. Group, *Outpatient antibiotic use in Europe and association with resistance: a cross-national database study.* The Lancet, 2005. **365**(9459): p. 579-587.

31. Macfarlane, J., C. van Weel, W. Holmes, P. Gard, D. Thornhill, R. Macfarlane, and R. Hubbard, *Reducing antibiotic use for acute bronchitis in primary care: blinded, randomised controlled trial of patient information leafletCommentary: More self reliance in patients and fewer antibiotics: still room for improvement.* Bmj, 2002. **324**(7329): p. 91-94.

32. Fridkin, S., J. Baggs, R. Fagan, S. Magill, L.A. Pollack, P. Malpiedi, R. Slayton, K. Khader, M.A. Rubin, and M. Jones, *Vital signs: improving antibiotic use among hospitalized patients.* MMWR. Morbidity and mortality weekly report, 2014. **63**(9): p. 194-200.

33. Willing, B.P., S.L. Russell, and B.B. Finlay, *Shifting the balance: antibiotic effects on host–microbiota mutualism.* Nature Reviews Microbiology, 2011. **9**(4): p. 233-243.

34. Lozupone, C.A., J.I. Stombaugh, J.I. Gordon, J.K. Jansson, and R. Knight, *Diversity, stability and resilience of the human gut microbiota.* Nature, 2012. **489**(7415): p. 220-230.

35. Jernberg, C., S. Löfmark, C. Edlund, and J.K. Jansson, *Long-term impacts of antibiotic exposure on the human intestinal microbiota.* Microbiology, 2010. **156**(11): p. 3216-3223.

36. Ivanov, I.I., R. de Llanos Frutos, N. Manel, K. Yoshinaga, D.B. Rifkin, R.B. Sartor, B.B. Finlay, and D.R. Littman, *Specific microbiota direct the differentiation of IL-17-producing T-helper cells in the mucosa of the small intestine.* Cell host & microbe, 2008. **4**(4): p. 337-349.

37. Brandl, K., G. Plitas, C.N. Mihu, C. Ubeda, T. Jia, M. Fleisher, B. Schnabl, R.P. DeMatteo, and E.G. Pamer, *Vancomycin-resistant enterococci exploit antibiotic-induced innate immune deficits.* Nature, 2008. **455**(7214): p. 804-807.

38. Ivanov, I.I., K. Atarashi, N. Manel, E.L. Brodie, T. Shima, U. Karaoz, D. Wei, K.C. Goldfarb, C.A. Santee, and S.V. Lynch, *Induction of intestinal Th17 cells by segmented filamentous bacteria.* Cell, 2009. **139**(3): p. 485-498.

39. van der Waaij, D.a., J. Berghuis, and J. Lekkerkerk, *Colonization resistance of the digestive tract of mice during systemic antibiotic treatment.* Epidemiology & Infection, 1972. **70**(4): p. 605-610.

40. Aly, R., H.I. Maibach, W.G. Strauss, and H.R. Shinefield, *Effects of a systemic antibiotic on nasal bacterial ecology in man.* Applied microbiology, 1970. **20**(2): p. 240-244.

41. Slots, J. and M. Ting, *Systemic antibiotics in the treatment of periodontal disease.* Periodontology 2000, 2002. **28**(1): p. 106-176.

42. Feres, M., L.C. Figueiredo, G.M.S. Soares, and M. Faveri, *Systemic antibiotics in the treatment of periodontitis.* Periodontology 2000, 2015. **67**(1): p. 131-186.

43. Schenck, L.P., M.G. Surette, and D.M. Bowdish, *Composition and immunological significance of the upper respiratory tract microbiota.* FEBS letters, 2016. **590**(21): p. 3705-3720.

44. Hauser, C., B. Wuethrich, L. Matter, J. Wilhelm, W. Sonnabend, and K. Schopfer, *Staphylococcus aureus skin colonization in atopic dermatitis patients.* Dermatology, 1985. **170**(1): p. 35-39.

45. Round, J.L. and S.K. Mazmanian, *The gut microbiota shapes intestinal immune responses during health and disease.* Nature Reviews Immunology, 2009. **9**(5): p. 313-323.

46. Tong, S.Y., J.S. Davis, E. Eichenberger, T.L. Holland, and V.G. Fowler, Jr., *Staphylococcus aureus infections: epidemiology, pathophysiology, clinical manifestations, and management.* Clin Microbiol Rev, 2015. **28**(3): p. 603-61.

47. Kobayashi, S.D., N. Malachowa, and F.R. DeLeo, *Pathogenesis of Staphylococcus aureus abscesses.* The American journal of pathology, 2015. **185**(6): p. 1518-1527.

48. Otto, M., *MRSA virulence and spread.* Cellular microbiology, 2012. **14**(10): p. 1513-1521.

49. Cheung, A.L., A.S. Bayer, G. Zhang, H. Gresham, and Y.-Q. Xiong, *Regulation of virulence determinants in vitro and in vivo in Staphylococcus aureus.* FEMS Immunology & Medical Microbiology, 2004. **40**(1): p. 1-9.

50. Banbula, A., J. Potempa, J. Travis, C. Fernandez-Catalén, K. Mann, R. Huber, W. Bode, and F. Medrano, *Amino-acid sequence and three-dimensional structure of the Staphylococcus aureus metalloproteinase at 1.72 Å resolution.* Structure, 1998. **6**(9): p. 1185-1193.

51. Laarman, A.J., M. Ruyken, C.L. Malone, J.A. van Strijp, A.R. Horswill, and S.H. Rooijakkers, *Staphylococcus aureus metalloprotease aureolysin cleaves complement C3 to mediate immune evasion.* The Journal of Immunology, 2011. **186**(11): p. 6445-6453.

52. Xu, Y., S.V. Narayana, and J.E. Volanakis, *Structural biology of the alternative pathway convertase.* Immunological reviews, 2001. **180**(1): p. 123-135.

53. Sieprawska-Lupa, M., P. Mydel, K. Krawczyk, K. Wójcik, M. Puklo, B. Lupa, P. Suder, J. Silberring, M. Reed, and J. Pohl, *Degradation of human antimicrobial peptide LL-37 by Staphylococcus aureus-derived proteinases.* Antimicrobial agents and chemotherapy, 2004. **48**(12): p. 4673-4679.

54. Morgenstern, M., C. Erichsen, S. Hackl, J. Mily, M. Militz, J. Friederichs, S. Hungerer, V. Bühren, T.F. Moriarty, and V. Post, *Antibiotic resistance of commensal Staphylococcus*

aureus and coagulase-negative staphylococci in an international cohort of surgeons: a prospective point-prevalence study. PloS one, 2016. **11**(2): p. e0148437.

55. Skinner, D. and C.S. Keefer, *Significance of bacteremia caused by Staphylococcus aureus: a study of one hundred and twenty-two cases and a review of the literature concerned with experimental infection in animals.* Archives of Internal Medicine, 1941. **68**(5): p. 851-875.
56. Spink, W.W. and W.H. Hall, *Penicillin therapy at the University of Minnesota hospitals: 1942-1944.* Annals of Internal Medicine, 1945. **22**(4): p. 510-525.
57. Van Hal, S.J., S.O. Jensen, V.L. Vaska, B.A. Espedido, D.L. Paterson, and I.B. Gosbell, *Predictors of mortality in Staphylococcus aureus bacteremia.* Clinical microbiology reviews, 2012. **25**(2): p. 362-386.
58. Frimodt-Moller, N., F. Espersen, P. Skinhoj, and V.T. Rosdahl, *Epidemiology of Staphylococcus aureus bacteremia in Denmark from 1957 to 1990.* Clin Microbiol Infect, 1997. **3**(3): p. 297-305.
59. Klevens, R.M., M.A. Morrison, J. Nadle, S. Petit, K. Gershman, S. Ray, L.H. Harrison, R. Lynfield, G. Dumyati, and J.M. Townes, *Invasive methicillin-resistant Staphylococcus aureus infections in the United States.* Jama, 2007. **298**(15): p. 1763-1771.
60. Gerber, J.S., S.E. Coffin, S.A. Smathers, and T.E. Zaoutis, *Trends in the incidence of methicillin-resistant Staphylococcus aureus infection in children's hospitals in the United States.* Clinical infectious diseases, 2009. **49**(1): p. 65-71.
61. Holmberg, S.D., S.L. Solomon, and P.A. Blake, *Health and economic impacts of antimicrobial resistance.* Rev Infect Dis, 1987. **9**(6): p. 1065-78.
62. Rubin, R.J., C.A. Harrington, A. Poon, K. Dietrich, J.A. Greene, and A. Moiduddin, *The economic impact of Staphylococcus aureus infection in New York City hospitals.* Emerg Infect Dis, 1999. **5**(1): p. 9-17.
63. Phelps, C.E., *Bug/drug resistance. Sometimes less is more.* Med Care, 1989. **27**(2): p. 194-203.
64. Hiramatsu, K., *Vancomycin-resistant Staphylococcus aureus: a new model of antibiotic resistance.* The Lancet infectious diseases, 2001. **1**(3): p. 147-155.
65. Gladwin, M. and B. Trattler, *Clinical microbiology made ridiculously simple*. 2001: MedMaster.
66. Drawz, S.M. and R.A. Bonomo, *Three decades of beta-lactamase inhibitors.* Clin Microbiol Rev, 2010. **23**(1): p. 160-201.
67. Leonard, D.A., R.A. Bonomo, and R.A. Powers, *Class D beta-lactamases: a reappraisal after five decades.* Acc Chem Res, 2013. **46**(11): p. 2407-15.

68. Olowe, O., K. Eniola, R. Olowe, and A. Olayemi, *Antimicrobial Susceptibility and Beta-lactamase detection of MRSA in Osogbo. SW Nigeria.* SKIN, 2007. **12**(6): p. 9.0.

69. Hackbarth, C.J. and H.F. Chambers, *blaI and blaR1 regulate beta-lactamase and PBP 2a production in methicillin-resistant Staphylococcus aureus.* Antimicrobial agents and chemotherapy, 1993. **37**(5): p. 1144-1149.

70. Chambers, H.F., *Methicillin resistance in staphylococci: molecular and biochemical basis and clinical implications.* Clinical microbiology reviews, 1997. **10**(4): p. 781-791.

71. Lowy, F.D., *Antimicrobial resistance: the example of Staphylococcus aureus.* J Clin Invest, 2003. **111**(9): p. 1265-73.

72. Hartman, B.J. and A. Tomasz, *Low-affinity penicillin-binding protein associated with beta-lactam resistance in Staphylococcus aureus.* J Bacteriol, 1984. **158**(2): p. 513-6.

73. Hooper, D.C., *Fluoroquinolone resistance among Gram-positive cocci.* The Lancet infectious diseases, 2002. **2**(9): p. 530-538.

74. Ng, E.Y., M. Trucksis, and D.C. Hooper, *Quinolone resistance mutations in topoisomerase IV: relationship to the flqA locus and genetic evidence that topoisomerase IV is the primary target and DNA gyrase is the secondary target of fluoroquinolones in Staphylococcus aureus.* Antimicrob Agents Chemother, 1996. **40**(8): p. 1881-8.

75. Walsh, T.R. and R.A. Howe, *The prevalence and mechanisms of vancomycin resistance in Staphylococcus aureus.* Annu Rev Microbiol, 2002. **56**: p. 657-75.

76. Mitscher, L.A., J.V. Juvarkar, W. Rosenbrook Jr, W.W. Andres, J.R. Schenck, and R.S. Egan, *Structure of chelocardin, a novel tetracycline antibiotic.* Journal of the American Chemical Society, 1970. **92**(20): p. 6070-6071.

77. Connell, S.R., D.M. Tracz, K.H. Nierhaus, and D.E. Taylor, *Ribosomal protection proteins and their mechanism of tetracycline resistance.* Antimicrobial agents and chemotherapy, 2003. **47**(12): p. 3675-3681.

78. Roberts, M., *Tetracycline resistance determinants: mechanisms of action, regulation of expression, genetic mobility, and distribution.* FEMS microbiology reviews, 1996. **19**(1): p. 1-24.

79. Chabbert, Y.A. and M.R. Scavizzi, *Chelocardin-inducible resistance in Escherichia coli bearing R plasmids.* Antimicrobial agents and chemotherapy, 1976. **9**(1): p. 36-41.

80. Burdett, V., J. Inamine, and S. Rajagopalan, *Heterogeneity of tetracycline resistance determinants in Streptococcus.* Journal of bacteriology, 1982. **149**(3): p. 995-1004.

81. Chopra, I., *Tetracycline analogs whose primary target is not the bacterial ribosome.* Antimicrobial agents and chemotherapy, 1994. **38**(4): p. 637.

82. Stepanek, J.J., T. Lukežič, I. Teichert, H. Petković, and J.E. Bandow, *Dual mechanism of action of the atypical tetracycline chelocardin.* Biochimica et Biophysica Acta (BBA)-Proteins and Proteomics, 2016. **1864**(6): p. 645-654.

83. Mao, J.C.-H. and E.E. Robishaw, *Mode of action of β-chelocardin.* Biochimica et Biophysica Acta (BBA)-Nucleic Acids and Protein Synthesis, 1971. **238**(1): p. 157-160.

84. Allen, T.M. and P.R. Cullis, *Drug delivery systems: entering the mainstream.* Science, 2004. **303**(5665): p. 1818-1822.

85. Allen, T.M., *Ligand-targeted therapeutics in anticancer therapy.* Nat Rev Cancer, 2002. **2**(10): p. 750-63.

86. Freeman, A.I. and E. Mayhew, *Targeted drug delivery.* Cancer, 1986. **58**(S2): p. 573-583.

87. Ulbrich, W. and A. Lamprecht, *Targeted drug-delivery approaches by nanoparticulate carriers in the therapy of inflammatory diseases.* Journal of The Royal Society Interface, 2009: p. rsif20090285.

88. Penningroth, S., *Essentials of toxic chemical risk: Science and society*. 2016: CRC Press.

89. Pinto-Alphandary, H., A. Andremont, and P. Couvreur, *Targeted delivery of antibiotics using liposomes and nanoparticles: research and applications.* International journal of antimicrobial agents, 2000. **13**(3): p. 155-168.

90. van den Broek, P.J., *Antimicrobial drugs, microorganisms, and phagocytes.* Reviews of infectious diseases, 1989. **11**(2): p. 213-245.

91. Silverstein, S. and C. Kabbash, *Penetration, retention, intracellular localization, and antimicrobial activity of antibiotics within phagocytes.* Current opinion in hematology, 1994. **1**(1): p. 85-91.

92. Gilbert, P., P.J. Collier, and M. Brown, *Influence of growth rate on susceptibility to antimicrobial agents: biofilms, cell cycle, dormancy, and stringent response.* Antimicrobial agents and chemotherapy, 1990. **34**(10): p. 1865.

93. Costerton, J.W., P.S. Stewart, and E.P. Greenberg, *Bacterial biofilms: a common cause of persistent infections.* Science, 1999. **284**(5418): p. 1318-1322.

94. Smith, A.W., *Biofilms and antibiotic therapy: is there a role for combating bacterial resistance by the use of novel drug delivery systems?* Advanced drug delivery reviews, 2005. **57**(10): p. 1539-1550.

95. Lewis, K., *Riddle of biofilm resistance.* Antimicrobial agents and chemotherapy, 2001. **45**(4): p. 999-1007.

96. Mah, T.-F.C. and G.A. O'Toole, *Mechanisms of biofilm resistance to antimicrobial agents.* Trends in microbiology, 2001. **9**(1): p. 34-39.

97. Brooun, A., S. Liu, and K. Lewis, *A dose-response study of antibiotic resistance inPseudomonas aeruginosa biofilms.* Antimicrobial agents and chemotherapy, 2000. **44**(3): p. 640-646.

98. Keren, I., N. Kaldalu, A. Spoering, Y. Wang, and K. Lewis, *Persister cells and tolerance to antimicrobials.* FEMS microbiology letters, 2004. **230**(1): p. 13-18.

99. Keren, I., D. Shah, A. Spoering, N. Kaldalu, and K. Lewis, *Specialized persister cells and the mechanism of multidrug tolerance in Escherichia coli.* Journal of bacteriology, 2004. **186**(24): p. 8172-8180.

100. Lew, D.P. and F.A. Waldvogel, *Osteomyelitis.* The Lancet, 2004. **364**(9431): p. 369-379.

101. Feigin, R.D., L.K. Pickering, D. Anderson, R.E. Keeney, and P.G. Shackleford, *Clindamycin treatment of osteomyelitis and septic arthritis in children.* Pediatrics, 1975. **55**(2): p. 213-223.

102. Tetzlaff, T.R., J.B. Howard, G.H. McCracken, E. Calderon, and J. Larrondo, *Antibiotic concentrations in pus and bone of children with osteomyelitis.* The Journal of pediatrics, 1978. **92**(1): p. 135-140.

103. Peltola, H. and M. Pääkkönen, *Acute osteomyelitis in children.* New England Journal of Medicine, 2014. **370**(4): p. 352-360.

104. Drulis-Kawa, Z. and A. Dorotkiewicz-Jach, *Liposomes as delivery systems for antibiotics.* International journal of pharmaceutics, 2010. **387**(1): p. 187-198.

105. Price, C.I., J.W. Horton, and C.R. Baxter, *Liposome encapsulation: a method for enhancing the effectiveness of local antibiotics.* Surgery, 1994. **115**(4): p. 480-487.

106. Antos, M., E.A. Trafny, and J. Grzybowski, *Antibacterial activity of liposomal amikacin against Pseudomonas aeruginosa in vitro.* Pharmacological research, 1995. **32**(1-2): p. 85-87.

107. Oh, Y.-K., D.E. Nix, and R.M. Straubinger, *Formulation and efficacy of liposome-encapsulated antibiotics for therapy of intracellular Mycobacterium avium infection.* Antimicrobial agents and chemotherapy, 1995. **39**(9): p. 2104-2111.

108. Lasic, D.D., *Novel applications of liposomes.* Trends in biotechnology, 1998. **16**(7): p. 307-321.

109. Voinea, M. and M. Simionescu, *Designing of 'intelligent'liposomes for efficient delivery of drugs.* Journal of cellular and molecular medicine, 2002. **6**(4): p. 465-474.

110. Alhariri, M., A. Azghani, and A. Omri, *Liposomal antibiotics for the treatment of infectious diseases.* Expert opinion on drug delivery, 2013. **10**(11): p. 1515-1532.

111. Huh, A.J. and Y.J. Kwon, *"Nanoantibiotics": a new paradigm for treating infectious diseases using nanomaterials in the antibiotics resistant era.* Journal of Controlled Release, 2011. **156**(2): p. 128-145.

112. Zhang, L., D. Pornpattananangkul, C.-M. Hu, and C.-M. Huang, *Development of nanoparticles for antimicrobial drug delivery.* Current medicinal chemistry, 2010. **17**(6): p. 585-594.

113. Zhang, L., F. Gu, J. Chan, A. Wang, R. Langer, and O. Farokhzad, *Nanoparticles in medicine: therapeutic applications and developments.* Clinical pharmacology & therapeutics, 2008. **83**(5): p. 761-769.

114. Abeylath, S.C. and E. Turos, *Drug delivery approaches to overcome bacterial resistance to β-lactam antibiotics.* Expert opinion on drug delivery, 2008. **5**(9): p. 931-949.

115. Torrent Burgués, J., *Review on bibliography related to antimicrobials.* 2017.

116. Abed, N. and P. Couvreur, *Nanocarriers for antibiotics: A promising solution to treat intracellular bacterial infections.* International journal of antimicrobial agents, 2014. **43**(6): p. 485-496.

117. Cho, H., T.C. Lai, K. Tomoda, and G.S. Kwon, *Polymeric micelles for multi-drug delivery in cancer.* AAPS PharmSciTech, 2015. **16**(1): p. 10-20.

118. Abdelghany, S.M., D.J. Quinn, R.J. Ingram, B.F. Gilmore, R.F. Donnelly, C.C. Taggart, and C.J. Scott, *Gentamicin-loaded nanoparticles show improved antimicrobial effects towards Pseudomonas aeruginosa infection.* International journal of nanomedicine, 2012. **7**: p. 4053.

119. Cheow, W.S., M.W. Chang, and K. Hadinoto, *Antibacterial efficacy of inhalable antibiotic-encapsulated biodegradable polymeric nanoparticles against E. coli biofilm cells.* Journal of biomedical nanotechnology, 2010. **6**(4): p. 391-403.

120. Forier, K., K. Raemdonck, S.C. De Smedt, J. Demeester, T. Coenye, and K. Braeckmans, *Lipid and polymer nanoparticles for drug delivery to bacterial biofilms.* Journal of Controlled Release, 2014. **190**: p. 607-623.

121. Chakraborty, S.P., S.K. Sahu, P. Pramanik, and S. Roy, *In vitro antimicrobial activity of nanoconjugated vancomycin against drug resistant Staphylococcus aureus.* International journal of pharmaceutics, 2012. **436**(1): p. 659-676.

122. Fontana, G., G. Pitarresi, V. Tomarchio, B. Carlisi, and P.L. San Biagio, *Preparation, characterization and in vitro antimicrobial activity of ampicillin-loaded polyethylcyanoacrylate nanoparticles.* Biomaterials, 1998. **19**(11-12): p. 1009-1017.

123. Fontana, G., M. Licciardi, S. Mansueto, D. Schillaci, and G. Giammona, *Amoxicillin-loaded polyethylcyanoacrylate nanoparticles: influence of PEG coating on the particle size, drug release rate and phagocytic uptake.* Biomaterials, 2001. **22**(21): p. 2857-2865.

124. Chung, Y.-Y.H., T-W, *Microencapsulation of gentamicin in biodegradable PLA and/or PLA/PEG copolymer.* Journal of microencapsulation, 2001. **18**(4): p. 457-465.

125. Nandi, S.K., P. Mukherjee, S. Roy, B. Kundu, D.K. De, and D. Basu, *Local antibiotic delivery systems for the treatment of osteomyelitis–A review.* Materials Science and Engineering: C, 2009. **29**(8): p. 2478-2485.

126. You, J.-O., D. Almeda, J. George, and D.T. Auguste, *Bioresponsive matrices in drug delivery.* Journal of biological engineering, 2010. **4**(1): p. 15.

127. Dufresne, M.-H., D. Le Garrec, V. Sant, J.-C. Leroux, and M. Ranger, *Preparation and characterization of water-soluble pH-sensitive nanocarriers for drug delivery.* International journal of pharmaceutics, 2004. **277**(1): p. 81-90.

128. Sandhiya, S., S.A. Dkhar, and A. Surendiran, *Emerging trends of nanomedicine–an overview.* Fundamental & clinical pharmacology, 2009. **23**(3): p. 263-269.

129. Mura, S., J. Nicolas, and P. Couvreur, *Stimuli-responsive nanocarriers for drug delivery.* Nature materials, 2013. **12**(11): p. 991-1003.

130. Gemeinhart, R.A., J. Chen, H. Park, and K. Park, *pH-sensitivity of fast responsive superporous hydrogels.* J Biomater Sci Polym Ed, 2000. **11**(12): p. 1371-80.

131. You, J.O. and D.T. Auguste, *Feedback-regulated paclitaxel delivery based on poly(N,N-dimethylaminoethyl methacrylate-co-2-hydroxyethyl methacrylate) nanoparticles.* Biomaterials, 2008. **29**(12): p. 1950-7.

132. Zhu, L., P. Kate, and V.P. Torchilin, *Matrix metalloprotease 2-responsive multifunctional liposomal nanocarrier for enhanced tumor targeting.* ACS Nano, 2012. **6**(4): p. 3491-8.

133. Harris, T.J., G. von Maltzahn, M.E. Lord, J.H. Park, A. Agrawal, D.H. Min, M.J. Sailor, and S.N. Bhatia, *Protease-triggered unveiling of bioactive nanoparticles.* Small, 2008. **4**(9): p. 1307-12.

134. Braun, A.C., M. Gutmann, R. Ebert, F. Jakob, H. Gieseler, T. Lühmann, and L. Meinel, *Matrix metalloproteinase responsive delivery of myostatin inhibitors.* Pharmaceutical research, 2017. **34**(1): p. 58-72.

135. Ritzer, J., T. Lühmann, C. Rode, M. Pein-Hackelbusch, I. Immohr, U. Schedler, T. Thiele, S. Stübinger, B.v. Rechenberg, and J. Waser-Althaus, *Diagnosing peri-implant disease using the tongue as a 24/7 detector.* Nature Communications, 2017. **8**(1): p. 264.

136. Xiong, M.H., Y. Bao, X.Z. Yang, Y.C. Wang, B. Sun, and J. Wang, *Lipase-sensitive polymeric triple-layered nanogel for "on-demand" drug delivery.* J Am Chem Soc, 2012. **134**(9): p. 4355-62.

137. Arpigny, J.L. and K.E. Jaeger, *Bacterial lipolytic enzymes: classification and properties.* Biochem J, 1999. **343 Pt 1**: p. 177-83.

138. Jaeger, K.E., S. Ransac, B.W. Dijkstra, C. Colson, M. van Heuvel, and O. Misset, *Bacterial lipases.* FEMS Microbiol Rev, 1994. **15**(1): p. 29-63.

139. Taylor, A., *Aminopeptidases: structure and function.* The FASEB Journal, 1993. **7**(2): p. 290-298.

140. Chavira, R., T.J. Burnett, and J.H. Hageman, *Assaying proteinases with azocoll.* Analytical biochemistry, 1984. **136**(2): p. 446-450.

141. Stricklin, G.P., J.J. Jeffrey, W.T. Roswit, and A.Z. Eisen, *Human skin fibroblast procollagenase: mechanisms of activation by organomercurials and trypsin.* Biochemistry, 1983. **22**(1): p. 61-8.

142. Pfleiderer, G., *Methods in Enzymology*. 1970. p. 514-521.

143. Vigen, M., J. Ceccarelli, and A.J. Putnam, *Protease-Sensitive PEG Hydrogels Regulate Vascularization In Vitro and In Vivo.* Macromolecular bioscience, 2014. **14**(10): p. 1368-1379.

144. Sakurai, K., T.M. Snyder, and D.R. Liu, *DNA-templated functional group transformations enable sequence-programmed synthesis using small-molecule reagents.* Journal of the American Chemical Society, 2005. **127**(6): p. 1660-1661.

145. Rawlings, N.D., A.J. Barrett, and A. Bateman, *MEROPS: the peptidase database.* Nucleic Acids Res, 2010. **38**(Database issue): p. D227-33.

146. Potempa, J.T., J. , *Aureolysin*, in *Handbook of proteolytic enzymes*, A.J. Barrett, Rawlings,N.D. & Woessner,J.F, Editor. 2004, Elsevier, London. p. 389-393.

147. Beaufort, N., P. Wojciechowski, C.P. Sommerhoff, G. Szmyd, G. Dubin, S. Eick, J. Kellermann, M. Schmitt, J. Potempa, and V. Magdolen, *The human fibrinolytic system is a target for the staphylococcal metalloprotease aureolysin.* Biochem J, 2008. **410**(1): p. 157-65.

148. Huang, S.F., Y.H. Li, Y.J. Ren, Z.G. Cao, and X. Long, *The effect of a single nucleotide polymorphism in the matrix metalloproteinase-1 (MMP-1) promoter on force-induced MMP-1 expression in human periodontal ligament cells.* Eur J Oral Sci, 2008. **116**(4): p. 319-23.

149. Hasty, K.A., T.F. Pourmotabbed, G.I. Goldberg, J.P. Thompson, D.G. Spinella, R.M. Stevens, and C.L. Mainardi, *Human neutrophil collagenase. A distinct gene product with homology to other matrix metalloproteinases.* J Biol Chem, 1990. **265**(20): p. 11421-4.

150. Nagase, H. and J.F. Woessner, Jr., *Matrix metalloproteinases.* J Biol Chem, 1999. **274**(31): p. 21491-4.

151. Freije, J.M., I. Diez-Itza, M. Balbin, L.M. Sanchez, R. Blasco, J. Tolivia, and C. Lopez-Otin, *Molecular cloning and expression of collagenase-3, a novel human matrix metalloproteinase produced by breast carcinomas.* J Biol Chem, 1994. **269**(24): p. 16766-73.

152. Votintseva, A.A., R. Fung, R.R. Miller, K. Knox, H. Godwin, D.H. Wyllie, R. Bowden, D.W. Crook, and A.S. Walker, *Prevalence of Staphylococcus aureus protein A (spa) mutants in the community and hospitals in Oxfordshire.* BMC microbiology, 2014. **14**(1): p. 63.

153. Baumann, A., D. Tuerck, S. Prabhu, L. Dickmann, and J. Sims, *Pharmacokinetics, metabolism and distribution of PEGs and PEGylated proteins: quo vadis?* Drug discovery today, 2014. **19**(10): p. 1623-1631.

154. Baskin, J.M., J.A. Prescher, S.T. Laughlin, N.J. Agard, P.V. Chang, I.A. Miller, A. Lo, J.A. Codelli, and C.R. Bertozzi, *Copper-free click chemistry for dynamic in vivo imaging.* Proceedings of the National Academy of Sciences, 2007. **104**(43): p. 16793-16797.

155. Liang, B., M. Dai, J. Chen, and Z. Yang, *Copper-free Sonogashira coupling reaction with PdCl2 in water under aerobic conditions.* The Journal of organic chemistry, 2005. **70**(1): p. 391-393.

156. Gaumet, M., A. Vargas, R. Gurny, and F. Delie, *Nanoparticles for drug delivery: the need for precision in reporting particle size parameters.* European journal of pharmaceutics and biopharmaceutics, 2008. **69**(1): p. 1-9.

157. Kontogiorgis, C.A., P. Papaioannou, and D.J. Hadjipavlou-Litina, *Matrix metalloproteinase inhibitors: a review on pharmacophore mapping and (Q) SARs results.* Current medicinal chemistry, 2005. **12**(3): p. 339-355.

158. Ågren, M., I. Jorgensen, M. Andersen, J. Viljanto, and P. Gottrup, *Matrix metalloproteinase 9 level predicts optimal collagen deposition during early wound repair in humans.* British journal of surgery, 1998. **85**(1): p. 68-71.

159. Marín, F., D.A. Pascual, V. Roldán, J.M. Arribas, M. Ahumada, P.L. Tornel, C. Oliver, J. Gómez-Plana, G.Y. Lip, and M. Valdés, *Statins and postoperative risk of atrial fibrillation following coronary artery bypass grafting.* The American journal of cardiology, 2006. **97**(1): p. 55-60.

160. Kobayashi, H., Z.-X. Li, A. Yamataka, G.J. Lane, and T. Miyano, *Clinical evaluation of serum levels of matrix metalloproteinases and tissue inhibitors of metalloproteinases as predictors of progressive fibrosis in postoperative biliary atresia patients.* Journal of pediatric surgery, 2002. **37**(7): p. 1030-1033.

161. Rozanov, D.V., A.Y. Savinov, V.S. Golubkov, T.I. Postnova, A. Remacle, S. Tomlinson, and A.Y. Strongin, *Cellular membrane type-1 matrix metalloproteinase (MT1-MMP) cleaves C3b, an essential component of the complement system.* Journal of Biological Chemistry, 2004. **279**(45): p. 46551-46557.

162. Rozanov, D.V., A.Y. Savinov, V.S. Golubkov, S. Tomlinson, and A.Y. Strongin, *Interference with the complement system by tumor cell membrane type-1 matrix metalloproteinase*

plays a significant role in promoting metastasis in mice. Cancer research, 2006. **66**(12): p. 6258-6263.

163. Coêlho, D.F., T.P. Saturnino, F.F. Fernandes, P.G. Mazzola, E. Silveira, and E.B. Tambourgi, *Azocasein substrate for determination of proteolytic activity: Reexamining a traditional method using bromelain samples.* BioMed research international, 2016. **2016**.
164. Tomarelli, R., *The use of azocasein as a substrate in the colorimetric determination of peptic and tryptic activity.* J. Lab. Clin. Med., 1949. **34**: p. 428-433.
165. Marokházi, J., K. Lengyel, S. Pekár, G. Felföldi, A. Patthy, L. Gráf, A. Fodor, and I. Venekei, *Comparison of proteolytic activities produced by entomopathogenic Photorhabdus bacteria: strain-and phase-dependent heterogeneity in composition and activity of four enzymes.* Applied and environmental microbiology, 2004. **70**(12): p. 7311-7320.
166. Ha, M., A.E.D. Bekhit, A. Carne, and D.L. Hopkins, *Comparison of the proteolytic activities of new commercially available bacterial and fungal proteases toward meat proteins.* Journal of food science, 2013. **78**(2): p. C170-C177.
167. Gustafsson, E. and J. Oscarsson, *Maximal transcription of aur (aureolysin) and sspA (serine protease) in Staphylococcus aureus requires staphylococcal accessory regulator R (sarR) activity.* FEMS microbiology letters, 2008. **284**(2): p. 158-164.
168. Oscarsson, J., K. Tegmark-Wisell, and S. Arvidson, *Coordinated and differential control of aureolysin (aur) and serine protease (sspA) transcription in Staphylococcus aureus by sarA, rot and agr (RNAIII).* International journal of medical microbiology, 2006. **296**(6): p. 365-380.
169. Clark, M.F., R.M. Lister, and M. Bar-Joseph, *ELISA techniques*, in *Methods in enzymology*. 1986, Elsevier. p. 742-766.
170. Nguyen, H.M., M.A. Rocha, K.R. Chintalacharuvu, and D.O. Beenhouwer, *Detection and quantification of Panton–Valentine leukocidin in Staphylococcus aureus cultures by ELISA and Western blotting: Diethylpyrocarbonate inhibits binding of protein A to IgG.* Journal of immunological methods, 2010. **356**(1-2): p. 1-5.
171. Goding, J.W., *Use of staphylococcal protein A as an immunological reagent.* Journal of immunological methods, 1978. **20**: p. 241-253.
172. Shaw, L., E. Golonka, J. Potempa, and S.J. Foster, *The role and regulation of the extracellular proteases of Staphylococcus aureus.* Microbiology, 2004. **150**(1): p. 217-228.
173. Novick, R.P., *Autoinduction and signal transduction in the regulation of staphylococcal virulence.* Molecular microbiology, 2003. **48**(6): p. 1429-1449.
174. Lee, J.S., T. Groothuis, C. Cusan, D. Mink, and J. Feijen, *Lysosomally cleavable peptide-containing polymersomes modified with anti-EGFR antibody for systemic cancer chemotherapy.* Biomaterials, 2011. **32**(34): p. 9144-9153.

175. Wang, Y. and Y.-L. Hsieh, *Immobilization of lipase enzyme in polyvinyl alcohol (PVA) nanofibrous membranes.* Journal of Membrane Science, 2008. **309**(1): p. 73-81.

176. Tanihara, M., Y. Suzuki, Y. Nishimura, K. Suzuki, Y. Kakimaru, and Y. Fukunishi, *A novel microbial infection-responsive drug release system.* Journal of pharmaceutical sciences, 1999. **88**(5): p. 510-514.

177. Suzuki, Y., M. Tanihara, Y. Nishimura, K. Suzuki, Y. Kakimaru, and Y. Shimizu, *A novel wound dressing with an antibiotic delivery system stimulated by microbial infection.* Asaio Journal, 1997. **43**(5): p. M858.

178. Chatzispyrou, I.A., N.M. Held, L. Mouchiroud, J. Auwerx, and R.H. Houtkooper, *Tetracycline antibiotics impair mitochondrial function and its experimental use confounds research.* Cancer research, 2015. **75**(21): p. 4446-4449.

179. Schnappinger, D. and W. Hillen, *Tetracyclines: antibiotic action, uptake, and resistance mechanisms.* Archives of microbiology, 1996. **165**(6): p. 359-369.

180. Sheehan, J., P. Cruickshank, and G. Boshart, *A Convenient Synthesis of Water-Soluble Carbodiimides.* The Journal of Organic Chemistry, 1961. **26**(7): p. 2525-2528.

181. Montalbetti, C.A. and V. Falque, *Amide bond formation and peptide coupling.* Tetrahedron, 2005. **61**(46): p. 10827-10852.

182. Valeur, E. and M. Bradley, *Amide bond formation: beyond the myth of coupling reagents.* Chemical Society Reviews, 2009. **38**(2): p. 606-631.

183. Anderson, G.W., J.E. Zimmerman, and F.M. Callahan, *The use of esters of N-hydroxysuccinimide in peptide synthesis.* Journal of the American Chemical Society, 1964. **86**(9): p. 1839-1842.

184. Bell, D.R., *Treatment of amoebiasis.* Tropical doctor, 1973. **3**(3): p. 140-143.

185. Mitscher, L.A., *Tetracycline, aminoglycoside, macrolide, and miscellaneous antibiotics.* Burger's Medicinal Chemistry and Drug Discovery, 2010.

186. Carpino, L.A., H. Imazumi, B.M. Foxman, M.J. Vela, P. Henklein, A. El-Faham, J. Klose, and M. Bienert, *Comparison of the Effects of 5-and 6-HOAt on Model Peptide Coupling Reactions Relative to the Cases for the 4-and 7-Isomers.* Organic letters, 2000. **2**(15): p. 2253-2256.

187. Brewer, C.F. and J.P. Riehm, *Evidence for possible nonspecific reactions between N-ethylmaleimide and proteins.* Analytical Biochemistry, 1967. **18**(2): p. 248-255.

188. Veronese, F.M., *Peptide and protein PEGylation: a review of problems and solutions.* Biomaterials, 2001. **22**(5): p. 405-417.

189. Patterson, J. and J.A. Hubbell, *Enhanced proteolytic degradation of molecularly engineered PEG hydrogels in response to MMP-1 and MMP-2.* Biomaterials, 2010. **31**(30): p. 7836-7845.

190. Galler, K.M., L. Aulisa, K.R. Regan, R.N. D'Souza, and J.D. Hartgerink, *Self-assembling multidomain peptide hydrogels: designed susceptibility to enzymatic cleavage allows enhanced cell migration and spreading.* Journal of the American Chemical Society, 2010. **132**(9): p. 3217-3223.

191. Brinckerhoff, L.H., V.V. Kalashnikov, L.W. Thompson, G.V. Yamshchikov, R.A. Pierce, H.S. Galavotti, V.H. Engelhard, and C.L. Slingluff, *Terminal modifications inhibit proteolytic degradation of an immunogenic mart-127–35 peptide: Implications for peptide vaccines.* International journal of cancer, 1999. **83**(3): p. 326-334.

192. Kutscher, M., *Novel Approaches to Antimicrobial Therapy of Pneumonia Using Antibiotics and Therapeutic Antibodies.* 2016.

Appendix

9. Appendix

9.1 List of abbreviations

ACN	Acetonitrile
Af	Aminofluorescein
AP	Leucine aminopeptidase
APMA	4-Aminophenylmercuric acetate
au	Arbitrary units
BOC	*tert*-Butoxycarbonyl
Cf	Carboxyfluorescein
CHD	Chelocardin
CL:	Cleavable linker
CTC	Chlorotrityl Chloride resin
Da	Dalton
DBCO	Dibenzylcyclooctyne
DCM	Dichloromethane
Dex	Dextran
DIC	*N,N'*-Diisopropylcarbodiimid
DIPEA	*N,N*-Diisopropylethylamine (or Hünings Base)
DMF	Dimethylformamide
EDC	1-Ethyl-3-(3-dimethylaminopropyl)carbodiimide
EDTA	Ethylenediaminetetraacetic acid
FITC	Fluorescein isothiocyanate
FMOC	Fluorenylmethoxycarbonyl amino acid protecting group
FPLC	Fast protein liquid chromatography
GFP	Green Fluorescent Protein
HBTU	2-(1*H*-benzotriazol-1-yl)-1,1,3,3-tetramethyluronium hexafluorophosphate
HOBt	1-Hydroxybenzotriazol
HPLC	High-performance liquid chromatography
LC-MS	Liquid chromatography-Mass spectrometry
MALDI	Matrix-assisted Laser Desorption/Ionization
MIC	Minimum inhibitory concentration
MRSA	Methicillin resistant *Staphylococcus aureus*
MSSA	Methicillin susceptible *Staphylococcus aureus*
NHS	*N*-Hydroxysuccinimide
NP	Nanoparticle
PECA	Polyethylcyanoacrylate
PEG	Polyethylene glycol
PLGA	Poly(lactide-co-glycolic) acid
PVA	Polyvinyl alcohol
rpm	Rotations per minute
SAB	*Staphylococcus aureus* bacteremia
SPPS	Solid Phase Peptide Synthesis
TCA	Trichloroacetic acid
TFA	Trifluoroacetic acid
tris	Tris(hydroxymethyl) aminomethane
UV	Ultraviolet
UHPLC	Ultra-high performance liquid chromatography
v/v	Volume concentration
w/v	Weight concentration
WHO	World Health Organization

9.2 List of Figures

Figure 1	Main reasons for bacterial antibiotic resistance development
Figure 2	Tridimensional structure of S. aureus zinc metalloproteinase aureolysin.
Figure 3	Chemical structure of tetracycline analogue chelocardin
Figure 4	Minimum inhibitory concentrations for chelocardin against different pathogens
Figure 5	Study design for the development of a bioresponsive antibiotic release system
Figure 6	MALDI-TOF spectrum of C3 protein originated peptide sequence and ÄKTA chromatogram
Figure 7	MALDI-TOF spectrum of insulin originated peptide sequence and ÄKTA chromatogram
Figure 8	MALDI-TOF spectrum of plasminogen originated peptide sequence and ÄKTA chromatogram
Figure 9	Chromatogram of C3 sequence cleavage assay with aureolysin
Figure 10	Chromatogram of C3 sequence cleavage assay with MMP-8
Figure 11	Chromatogram of C3 sequence cleavage assay with MMP-1
Figure 12	Chromatogram of insulin sequence cleavage assay with aureolysin
Figure 13	Chromatogram of insulin sequence cleavage assay with MMP-8
Figure 14	Chromatogram of insulin sequence cleavage assay with MMP-1
Figure 15	Chromatogram of plasminogen sequence cleavage assay with aureolysin
Figure 16	Chromatogram of plasminogen sequence cleavage assay with MMP-8
Figure 17	Chromatogram of plasminogen sequence cleavage assay with MMP-1
Figure 18	Cleavage percentage of peptide sequences after one hour incubation with aureolysin, MMP-8 and MMP-1
Figure 19	Structure of plasminogen originated peptide sequence
Figure 20	Time course of aureolysin and trypsin activity
Figure 21	Specific enzymatic activity comparison for aureolysin and trypsin
Figure 22	Overview of indirect ELISA
Figure 23	Standard curve of aureolysin detection by serial dilution of α-aureolysin primary antibody
Figure 24	Plasminogen cleavage by aureolysin
Figure 25	Plasminogen sequence cleavage efficiency [%] as a function of aureolysin concentration
Figure 26	Overlay of chromatograms after aureolysin digestion
Figure 27	Plasminogen sequence cleavage [%] as a function of time
Figure 28	Mass spectrum of resulted fragment after incubation of plasminogen based linker sequence with aureolysin
Figure 29	Strategy representation of antibiotic physical incorporation into hydrogel
Figure 30	Structures of PVA functionalized with maleimide groups and PEG-link
Figure 31	Fluorophore diffusion fractions over the time for hydrogel formulations
Figure 32	Constant rates for fluorophore diffusion from different formulations of hydrogel
Figure 33	Chromatogram of l-thiol-Plasminogen peptide sequence
Figure 34	Mass spectrum of l-thiol-plasminogen peptide sequence
Figure 35	Chromatogram of d-thiol plasminogen peptide sequence after one hour incubation with aureolysin
Figure 36	Mass spectrum of d-thiol-plasminogen peptide sequence
Figure 37	Fluorophore diffusion fractions over the time for hydrogel formulations
Figure 38	GFP release over time of different hydrogel formulations
Figure 39	Schematic depiction of the new release strategy
Figure 40	Chromatogram of Cf-thiol-plasminogen peptide sequence
Figure 41	Mass spectrum of Cf-thiol-plasminogen peptide sequence
Figure 42	Overlay of Cf-thiol plasminogen sequences chromatograms before and after 1 h incubation of aureolysin
Figure 43	Fluorescence chromatograms overlays of hydrogel incubation with and without aureolysin and peptide incubation and hydrogel incubation with aureolysin
Figure 44	Representation of using plasmatic aminopeptidases as a bioresponsive tool for the complete release of antibiotic in case of a bacterial infection
Figure 45	Mass spectrum of KVYL peptide
Figure 46	Mass spectrum of KVYL-Af peptide
Figure 47	Fluorescence chromatogram of KVYL-Af peptide
Figure 48	Basal aminopeptidase concentrations in human plasma
Figure 49	Complete release of fluorophore by aminopeptidase
Figure 50	Aminofluorescein release over time by aminopeptidase
Figure 51	Chromatograms of full release of Af after 15 and 30 min incubation with aminopeptidase
Figure 52	Schematic depiction of linker synthesis strategy followed by conjugation to tetracycline via HATU/HOBt coupling
Figure 53	Chromatogram of N3-plasminogen peptide sequence with protecting groups
Figure 54	Mass spectrum of N3-plasminogen peptide sequence with protecting groups

List of Figures (continued)

Figure 55	Chromatogram of N3-plasminogen peptide sequence with protecting groups after conjugation with CHD
Figure 56	Mass spectrum of N3-plasminogen peptide sequence with protecting groups coupled to CHD
Figure 57	Chromatogram of N3-plasminogen CHD peptide sequence with (grey line) and without PG
Figure 58	Mass spectrum of N3-plasminogen peptide sequence without protecting groups coupled to CHD
Figure 59	ÄKTA chromatogram of PEG-linker-CHD construct purification
Figure 60	Mass spectrum of PEG-Plasminogen-CHD construct
Figure 61	Chromatograms of PEG-linker-CHD construct before and after incubation with aureolysin
Figure 62	Release profile of CHD from PEG-linker-CHD release system after incubation with aureolysin
Figure 63	Strategy of constructing 4-armed CHD release system
Figure 64	Mass spectrum of 4-armed PEG and 4-armed PEG-DBCO conjugate
Figure 65	Mass spectrum of first click attempt between 4-armed PEG-DBCO and linker-CHD
Figure 66	Mass spectrum of second click attempt between 4-armed PEG-DBCO and linker-CHD
Figure 67	Cleavage rates for free and PEGylated linker-CHD systems after incubation with aureolysin
Figure 68	Polydispersity index (PdI) of PEGylated CHD release systems after incubation in aureolysin buffer at 37 °C

9.3 List of Tables

Table 1	Non-ideal properties of drugs and their therapeutic implications
Table 2	Peptide sequences synthesized in this work.
Table 3	Hydrogel formulations
Table 4	Peptide sequences as candidates for aureolysin dependent cleavable linker.
Table 5	Intermediate amino acids - aminofluorescein fragments formed by aminopeptidase activity, until the complete release of the fluorophore

9.4 Publications and presentations

Publications

Schilling, K.; Amstalden, MC., Meinel, L.; Holzgrabe, U. Impurity profiling of l-asparagine monohydrate by ion pair chromatography applying low wavelength UV detection, **(2016) Journal of Pharmaceutical and Biomedical Analysis 131, 202-207**

Moll, H.; Fite, RF.; Good, L.; Amstalden, MC.; Chindera, K.;Kamaruzzaman, NF.; Schultheis, M.; Röger, B.; Hecht, N.; Oelschlager, T.; Meinel, L.; Lühmann, T. Pathogen- and Host-Directed Antileishmanial Effects Mediated by Polyhexanide (PHMB), **(2015) Plos Neglected Tropical Diseases 9 (0004041)**

Congresses

Amstalden, MC.; Rayad, AA., Müller, R.; Lühmann, T.; Meinel, L. Bacterial protease responsive antibiotic delivery, **Controlled Release Society Chapter Meeting 2017, Marburg, Germany (oral presentation)**

Amstalden, MC.; Rayad, AA., Müller, R.; Lühmann, T.; Meinel, L. Bacterial protease responsive antibiotic delivery, **JungChemiker Forum 2016, Würzburg, Germany (poster presentation)**

Acknowledgements

10. Acknowledgements

Firstly, I want to sincerely thank my advisor Prof. Dr. Dr. Lorenz Meinel for the privilege of accepting me to do my PhD in his research group. His profound knowledge and outstanding scientific skills were of a valuable importance for the accomplishment of this work. I will be always grateful for his efforts and patience throughout this journey.

I would also like to thank PD Dr. Tessa Lühmann for her guidance and scientific support. I highly appreciate her insightful comments and encouragement, as well as for pushing me to widen my research from various perspectives.

I thank Prof. Dr. Rolf Müller from Helmholtz Institute for Pharmaceutical Research Saarland for the harmonious collaboration concerning the Chelocardin release system. This acknowledgement is also extended to his research group, in particular to Dr. Antoine Abou Fayad and Dr. Jennifer Herrmann, for always supporting me during any questions I had during the development of our project.

I would like to acknowledge the financial support of the CAPES Foundation – Brazilian Federal Ministry of Education (Grant No. BEX 9414-13-4) during my entire PhD work.

Furthermore, I am highly grateful to Dr. Michael Büchner and Julianne Adelmann of the Organic Chemistry Department for their always efficient MALDI measurements and to Katharina Dodt and Johanna Siehler for performing the LC-MS measurement. Thanks to PD DR. Knut Ohlsen and Martina Selle for helping me with the immunoassays. I would also like to thank Georg Walther, Matthias Völker and Karl Vollmuth for always being helpful regarding technical issues. I am also thankful to all intern students who somehow helped me with this work and to all my colleagues outside the research group.

I would also like to thank all my PhD colleagues and other member of our team making my time in Würzburg memorable. Christine Schneider, Doris Moret and Dr. Sascha Zügner gave me a lot of support regarding administrative organization and student supervision. Thanks to Dr. Jennifer Ritzer for the help she gave me at the beginning of my work. Thanks to Alexandra Braun and Marcus Gutmann for always having time to discuss my issues, whether they were work related or not. Also, I would like to thank Dr. Anja Balk, Dr. Christoph Steiger and Joel van Dorp for the friendship we developed inside the group and Klaus Schilling for becoming a true friend at the institute.

Thanks to Christine and to her late husband Fritz Dinkelmeier, for trusting me and giving me the opportunity of finding a place in Würzburg to call home, as well as for the friendship we developed throughout the time.

Thanks to all of my close friends in Brazil, Germany and in other parts of the world for every laugh, deep conversations and good times we shared at some moment of our lives.

I want to thank my parents and my brothers Martin and Ignacio for their unconditional support and encouragement, not only during the elaboration of this work but during my entire life. Thank you for all the things you made possible and for always believing in me. I wouldn't be here if it weren't for you.

Finally, I would like to thank my dearest friend Dr. Ludwig Höllein for giving me every day the strength and motivation to finish this journey. You are one of the most amazing people I ever met and it's an enormous honor to be your friend.

Muito obrigada a todos,

Cecilia Amstalden